



Research Institute for Advanced Computer Science  
NASA Ames Research Center

IN-60  
43063

# On the Suitability of the Connection Machine for Direct Particle Simulation *P17A*

Leonard Dagum

RIACS Technical Report 90.26

June 1990

(NASA-CR-188863) ON THE SUITABILITY OF THE  
CONNECTION MACHINE FOR DIRECT PARTICLE  
SIMULATION (Research Inst. for Advanced  
Computer Science) 179 p CSCL 09B

N92-10293

Unclas  
G3/60 0043063



# On the Suitability of the Connection Machine for Direct Particle Simulation

Leonard Dagum

The Research Institute of Advanced Computer Science is operated by Universities Space Research Association, The American City Building, Suite 311, Columbia, MD 244, (301)730-2656

---

Work reported herein was supported by the NAS Systems Division of NASA and DARPA via Cooperative Agreement NCC 2-387 between NASA and the University Space Research Association (USRA). Work was performed at the Research Institute for Advanced Computer Science (RIACS), NASA Ames Research Center, Moffett Field, CA 94035.



©Copyright by Leonardo Dagum 1990  
All Rights Reserved



## Abstract

This work examines the algorithmic structure of the vectorizable Stanford particle simulation (SPS) method and re-formulates the structure in data parallel form. Some of the SPS algorithms can be directly translated to data parallel, but several of the vectorizable algorithms have no direct data parallel equivalent. This requires the development of new, strictly data parallel algorithms. In particular, a new sorting algorithm is developed to identify collision candidates in the simulation and a master/slave algorithm is developed to minimize communication cost in large table look up.

Validation of the method is undertaken through test calculations for thermal relaxation of a gas, shock wave profiles, and shock reflection from a stationary wall. In addition to these test calculations, a large scale two dimensional simulation for the flow about a double ellipse geometry is presented and compared to the results for same calculation performed with the fully vectorized SPS method on the Cray 2.

This investigation provides a quantitative measure of the performance of the Connection Machine for direct particle simulation. The massively parallel architecture of the Connection Machine is found quite suitable for this type of calculation. However, there are difficulties in taking full advantage of this architecture because of the lack of a broad based tradition of data parallel programming. An important outcome of this work has been new data parallel algorithms specifically of use for direct particle simulation but which also expand the data parallel diction.





## Acknowledgements

The acknowledgements part of a dissertation traditionally is the only place where the author can escape the objective high ground and let the subjectivity of emotions rule his writing. Glad of the opportunity, let me begin by expressing the gratitude I owe Professor Donald Baganoff for his guidance throughout the course of this work. Don is an outstanding instructor and a visionary thinker, and to work for such as he is an experience to be cherished. But words cannot do justice to emotion, so rather let me express my feeling by drawing on the commonality that must certainly exist amongst all who have completed doctorates, thus to remind you of the special relation that develops between a Ph.D. advisor and his graduate student.

Research is not usually conducted in a vacuum, and I could not have conducted this work without the help of innumerable people in the Stanford and Ames research communities. At Stanford I thank Jeff McDonald, an invaluable source for *all* information; Mike Woronwicz, for his insights on particle-surface interactions; Brian Haas, for his help with multiple species and chemistry; Mike Fallavollita, who kept me afloat on the ethernet; and Marc Goldberg, for his unbounded knowledge of statistics. At NASA Ames I thank Bill Feiereisen for providing me with the geometry and results for the double ellipse calculation, and Forrest Lumpkin who provided me with yet more results for test calculations. I also would like to thank Chris Lewis, for many valuable discussions on the Connection Machine, and John Krystynak, who first started me on the road to Paris.

An equally important aspect of fruitful research has been a stimulating social environment. Needless to say I am tremendously indebted to my parents *por el amor y apoyó que siempre me dieron*, my two brothers, Paul and Alex, and numerous friends, especially Joanna Meek, with whom I discovered California.

This work was supported in part by the National Aeronautics and Space Administration (NASA) under grant NAGW-965 and grant NCA2-313, and by DARPA under Cooperative Agreement NCC2-387 between NASA and the Universities Space Research Administration (USRA). Generous computer resources were made available by the Numerical Aerodynamic Simulation division of NASA and by the Research Institute for Advanced Computer Science (RIACS).



# Contents

	Page
<b>Abstract</b> . . . . .	iv
<b>Acknowledgements</b> . . . . .	v
<b>List of Figures</b> . . . . .	ix
<b>1 Introduction</b> . . . . .	1
1.1 Motivation for Direct Particle Simulation . . . . .	1
1.2 Motivation of Current Investigation . . . . .	3
<b>2 The Connection Machine Computer Architecture</b> . . . . .	5
2.1 Data Parallel Versus Vectorizable . . . . .	5
2.2 Virtual Machine Architecture . . . . .	9
2.2.1 Virtual Processor Sets and Virtual Processor Ratios . . . . .	10
2.2.2 Communication . . . . .	11
2.3 I/O Subsystems . . . . .	12
2.3.1 Mass Storage System . . . . .	12
2.3.2 Graphics System . . . . .	13
2.4 General Router Communication Performance . . . . .	14
2.4.1 Router Performance as a Function of Message Length . . . . .	15
2.4.2 Effect of Router Contention on Communication . . . . .	18
<b>3 Implementation on the Connection Machine</b> . . . . .	22
3.1 Mapping Data to Virtual Processors . . . . .	23
3.2 Selection of Collision Partners . . . . .	26
3.2.1 Identifying Collision Candidates . . . . .	27
3.2.2 Selecting Collision Partners . . . . .	28
3.2.3 Collision Partner Selection on the Connection Machine . . . . .	30
3.3 Collision Algorithms . . . . .	31
3.3.1 Degree of Freedom Mixing Collision Algorithm . . . . .	32
3.3.2 Implementing the Degree of Freedom Mixing Collision Algorithm . . . . .	34
3.3.3 Direction Cosine Decomposition Collision Algorithm . . . . .	35
3.3.4 Extension to Inelastic Collisions . . . . .	38
3.3.5 Collisions on the Connection Machine . . . . .	45
3.4 Sampling Macroscopic Quantities . . . . .	47

<b>4</b>	<b>Sorting Algorithms On the Connection Machine</b>	51
4.1	Sorting for Particle Simulations on Sequential or Vector Machines	52
4.2	The Radix Sort	60
4.3	Sorting Using Multiple Grids	64
4.3.1	Algorithm for a Single Grid	64
4.3.2	Using Multiple Grids	66
4.3.3	Factors Affecting Performance of the Algorithm	68
4.3.4	Using a Single Grid Effectively	72
4.4	Sorting by Merging Ordered Subsets	73
4.4.1	Two Fundamental Observations	73
4.4.2	The Merged Ordered Subsets Sorting Algorithm	73
4.4.3	Maintaining Statistical Independence	78
4.4.4	When Assumptions Fail	84
4.4.5	Performance and Extension to Three Dimensions	85
<b>5</b>	<b>Implementing General Boundary Conditions</b>	87
5.1	Representation of Physical Space	88
5.1.1	Faceted Geometry Approximation	88
5.1.2	Storage of Geometry Table	91
5.1.3	Definition of a Geometry Space	91
5.1.4	Master and Slave VP Sets	98
5.2	Models for Particle-Surface Interaction	100
5.2.1	Specular Reflection	101
5.2.2	Diffuse Reflection With Surface-Driven Energy Exchange	103
5.2.3	Diffuse Reflection With Gas-Driven Energy Exchange	105
<b>6</b>	<b>Active Flow Visualization Through the I/O Subsystems</b>	108
6.1	Visualization Technique	108
6.1.1	Mechanism for Visualization	108
6.1.2	Implementation of Visualization Mechanism	110
6.2	Visualization Strategies	111
6.2.1	In Real Time	111
6.2.2	Through Play Back	112
6.3	Extension to Three Dimensions	114
<b>7</b>	<b>Results</b>	117
7.1	Relaxation of Internal Energy Modes	117
7.2	Normal Shock Wave Structure	121
7.3	Shock Reflection	125
7.3.1	Ideal End Wall	127
7.3.2	Isothermal End Wall	134
7.4	Double Ellipse in Hypersonic Flow	140
7.5	Performance	147

<b>8 Multiple Species and Chemistry</b> . . . . .	152
8.1 Reaction Fundamentals . . . . .	152
8.2 Implementing Multiple Species . . . . .	154
8.3 Implementing Chemical Reactions . . . . .	157
8.3.1 Reaction Mechanics . . . . .	157
8.3.2 Creation and Destruction of Particles . . . . .	160
8.3.3 Estimated Cost . . . . .	161
<b>9 Concluding Remarks</b> . . . . .	162
8.1 Summary . . . . .	162
8.2 Conclusions . . . . .	163
<b>References</b> . . . . .	165



## List of Figures

Figure		Page
2.1	Schematic of the Connection Machine architecture . . . . .	6
2.2	Communications performance as function of message length . . . . .	16
2.3	Effect of router contention on communications performance . . . . .	20
3.1	Representation of particle data amongst virtual processors . . . . .	25
3.2	Two dimensional scattering process involving hard spheres . . . . .	37
3.3	Schematic of communications for sampling macroscopic quantities . . . . .	50
4.1	Schematic of steps in DSMC sort algorithm . . . . .	55
4.2	Schematic of collision candidate pairing algorithm . . . . .	56
4.3	Schematic of radix sort algorithm . . . . .	62
4.4	Using a single grid to compute cell density and cell base index . . . . .	65
4.5	Using a single grid to rank the particles . . . . .	66
4.6	Layout of a multi-grid . . . . .	67
4.7	Using a multi-grid to rank the particles . . . . .	68
4.8	Maximum radius of motion over one time step . . . . .	74
4.9	Schematic of the merged ordered subsets sorting algorithm . . . . .	77
4.10	One possible mapping of nine sources to the merging grid . . . . .	80
4.11	Two deterministic shuffling algorithms . . . . .	83
5.1	The faceted body approximation . . . . .	89
5.2	Definition of physical space and geometry space . . . . .	93
5.3	Indirect mapping between geometry space and geometry table . . . . .	95
5.4	Direct mapping between geometry space and geometry table . . . . .	97
5.5	Specular reflection of particle from a stationary plane . . . . .	102
7.1	Relaxation of internal degrees of freedom in a diatomic gas . . . . .	119
7.2	Shock wave structure at Mach 10 in a perfect diatomic gas . . . . .	123
7.3	Shock wave structure at Mach 10 with $Z_{rot} = 1.0$ . . . . .	124
7.4	Shock wave structure at Mach 10 in nitrogen. . . . .	126
7.5	Temperature and density profiles for incident shock wave . . . . .	129
7.6	Temperature and density profiles for reflected shock wave . . . . .	130

7.7	Temperature, density, and momentum flux histories at ideal end wall	132
7.8	Temperature and density profiles for incident shock wave . . . . .	137
7.9	Temperature, density, and momentum flux histories at cold end wall	139
7.10	Density contours in Mach 25 flow over double ellipse geometry . .	142
7.11	Density along stagnation streamline . . . . .	143
7.12	Temperature contours in Mach 25 flow over double ellipse geometry	144
7.13	Temperature along stagnation streamline . . . . .	145
7.14	Velocity field for Mach 25 flow over double ellipse geometry . . . .	146
7.15	Velocity along stagnation streamline . . . . .	147
7.16	Performance of the simulation as function of virtual processor ratio	149
8.1	Flow chart for collision process with inclusion of chemical reactions	159



# Chapter 1

## Introduction

Of increasing interest to NASA and the fluid mechanics community in general has been the development of accurate and efficient methods to treat hypersonic rarefied flow problems. The renewed interest in hypersonic flight is lead by research activity in the design of two new classes of vehicles: hypersonic aeroplanes, of which the National Aero-Space Plane (NASP) will be the first prototype, and Aero-Assisted Space Transfer Vehicles (ASTV), of which the Aero-Flight Experiment (AFE) will be the first prototype. The great difficulty and expense associated with reproducing the flight conditions for these vehicles in ground-based testing facilities must by necessity be alleviated through computational simulation. This increased reliance on computational simulation demands efficient and effective methods to be developed and implemented on today's supercomputers.

### 1.1 Motivation for Direct Particle Simulation

The hypersonic rarefied flow regime is distinguished from other flow regimes by a high Mach number (typically greater than 5) and a high Knudsen number (typically greater than 0.01). The Knudsen number,  $K_n$ , gives a measure of the degree of rarefaction and is defined as

$$K_n \equiv \frac{\lambda}{L_{ref}} \propto \frac{M}{Re} \quad (1.1)$$

where  $\lambda$  is the local mean free path for molecules in the fluid and  $L_{ref}$  is a reference length in the flow. The Knudsen number can also be related to the Mach and Reynold's number as given in equation (1.1).

As the Knudsen number becomes large the continuum description of the gas, as given by the Navier–Stokes equations, begins to break down. Specifically, the constitutive relations which describe the gas and are required to close the set of conservation equations can no longer be applied. Two separate paths have been followed in the computational simulation of hypersonic rarefied flows. One path has been to extend the continuum description into the rarefied regime through the use of higher order closure relations as described by Burnett (1935). This procedure initially met with limited success because the computational solution of the resulting set of equations, known as the Burnett equations, was unstable for all but the most modest Mach numbers. Not until the work of Fisco (1989) were solutions of these equations available for hypersonic Mach numbers. More recently Lumpkin (1990) was able to extend Fisco's work to diatomic gases and resolve some inconsistencies in the procedure for monatomic gases as presented by Fisco.

The continuum path is an attractive one because of the strong foundation in fluid mechanics with the use of continuum methods. By far the majority of problems in fluid mechanics are best described with a continuum formulation and the field is rich with mathematical methods for solving problems described in this manner. However the strength of mathematical tradition alone should not preclude consideration of more physically based methods of simulation. The alternative path then is to accept the molecular nature of the gas in the rarefied regime and perform a direct particle simulation.

The direct particle simulation assumes a gas can be described by a collection of simulated molecules, or particles, and thus completely avoids any need for differential equations explicitly describing the flow. By accurately modelling the microscopic state of the gas the macroscopic description is obtained through the

appropriate integration. The primary disadvantage of this approach is that the computational cost is relatively large. Therefore, although the molecular description of a gas is accurate at all densities, a direct particle simulation is competitive only for low densities where accurate continuum descriptions are difficult to make.

## 1.2 Motivation of Current Investigation

The most common method of direct particle simulation in current use is the direct simulation Monte Carlo (DSMC) method. The DSMC method was originated by G. A. Bird in 1963 and has evolved over 27 years into a powerful tool for the analysis of rarefied gas flows. It has a rich history of providing accurate flow descriptions in this difficult regime, however the method was originated before the advent of supercomputers and is best suited for implementation on a dedicated minicomputer (Bird (1980)). Many of the algorithms in the DSMC method are not efficient on vector-oriented or massively parallel computers. With such computers there is a distinct advantage to be gained by using the Stanford particle simulation (SPS) method (Baganoff and McDonald (1990)). The algorithms in the SPS method are specifically designed to make efficient use of current vector computer architectures. Part of the motivation of the current work was to investigate the applicability of the SPS method on a massively parallel computer architecture like that of Thinking Machines' Connection Machine.

The current direction for supercomputer architectures is towards increased parallelism as a means of overcoming the physical and technological limits with uniprocessor systems. Multi-processor architectures are often classified by *grain size*, and although no single or perfect definition of grain size exists it loosely describes node size or complexity. Coarse-grain systems have relatively few but very complex processors whereas fine-grain systems have many very simple processors. The simplest step toward parallelism is through coarse-grain parallel architectures. An example is the Cray Research line of supercomputers which went from a single processor in the Cray 1 to four processors in the Cray 2 and most recently up to

8 processors in the Cray Y-MP. At the research frontier of parallel architectures are fine-grain systems. These are massively parallel architectures with thousands of processors working concurrently on a single computation. There are clear indications that the future of supercomputing lies at least in part with massively parallel architectures, therefore it is appropriate and timely to investigate the suitability of this architecture for direct particle simulation.

The Connection Machine serves as a useful test bed for this study; its massive parallelism is supported by a very general communication network which is absolutely necessary for supporting the random motion of the particles. The massively parallel architecture provides a computational performance greater than any vector-oriented computer, however in most applications of practical interest there is also a price in communications which must be assessed before the overall performance of the machine can be determined. Rather than judge the Connection Machine on absolute performance alone, this investigation takes a broader view and attempts to answer the question: "*What price for parallelism?*" This question is answered in three steps. The first step is to determine the cost of communication in the problem. This is the cost of communication relative to computation and is a value which should remain constant regardless of the size of problem or machine. The second step is to judge this cost in an absolute sense through a performance comparison of the Connection Machine with a vector computer, in this case the Cray 2. This gives a quantifiable answer to the price for parallelism. The third step introduces a less quantitative element. This step is to judge the effort required to program the Connection Machine compared to programming the Cray 2. By carrying out these three steps a full view of the Connection Machine is obtained and the suitability of this machine for direct particle simulation may be accurately judged.

# Chapter 2

## The Connection Machine Computer Architecture

This chapter is meant to highlight the architectural features of the Connection Machine which distinguish it from conventional computers. Emphasis is given to those attributes which either help or hinder the implementation of a direct particle simulation on this machine. To some extent the precise technical description of the machine is de-emphasized in favor of the more abstract architectural model which should remain accurate over future models of this machine.

### 2.1 Data Parallel Versus Vectorizable

The Connection Machine is most often characterized as a massively parallel computer. In the largest configuration currently available there are 65536 processors each with 32 kB of memory. The processors are referred to as *data processors* because they store no part of the program and act on their stored data under the control of a front end computer. The front end computer serves to carry out scalar calculations and issue *data parallel* instructions to the Connection Machine. Figure 2.1 is a schematic of the architecture. Between the data processors and the front

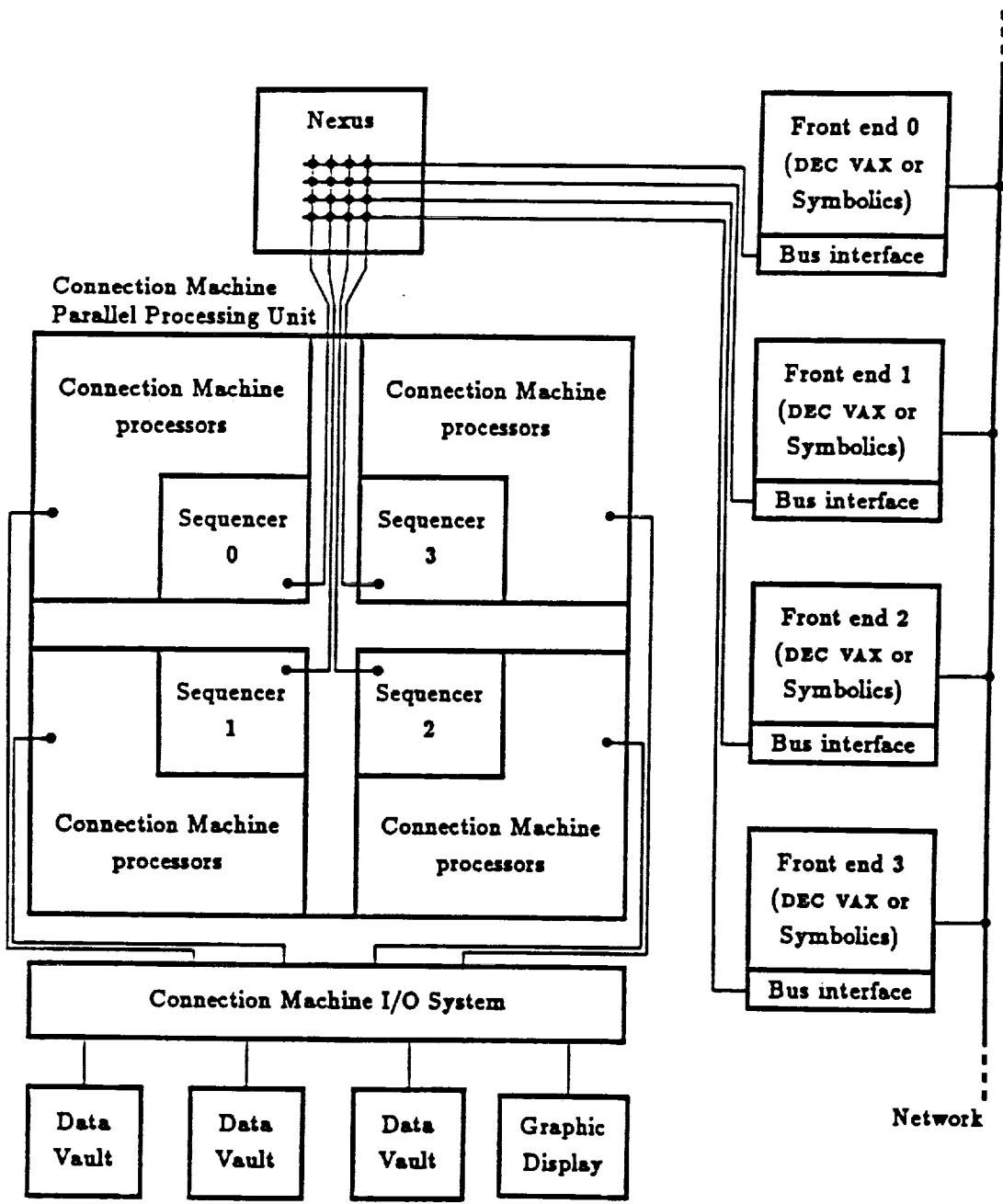


Figure 2.1 Schematic of the Connection Machine architecture.

end is a *sequencer* whose purpose is to broadcast data parallel instructions from the front end to the Connection Machine processors. In mapping a problem to this architecture the data must be distributed amongst the processors such that one processors is associated with each data element.

Algorithms suited for this type of architecture are known as *data parallel* algorithms (Hillis and Steele (1986)) because the parallelism is fine-grained and exists only across the data. In other words, the steps in the algorithm are meant to be carried out in parallel across large sets of data rather than in parallel through multiple threads of control, as is the case in a *control parallel* algorithm. More commonly this distinction is made in characterizing different parallel architectures. The Connection Machine is characterized as a Single Instruction Multiple Data stream (SIMD) machine as opposed to a Multiple Instruction Multiple Data stream (MIMD) machine (Flynn (1972)). However, the architectural classification is somewhat broader than the algorithmic one and the SIMD model includes vector architectures. In this sense the algorithmic classification is more specific and data parallel algorithms can be applied only to massively parallel architectures in the same way that *vectorizable algorithms* can be applied only to vector architectures.

The distinction between data parallel and vectorizable algorithms is subtle but very important for the context of this thesis. In many cases vectorizable algorithms can easily be translated to data parallel algorithms, however it is not true that *all* vectorizable algorithms can be put in data parallel form. Chapter 5 presents an example of this which is especially important in a direct particle simulation.

The difference between what is vectorizable and what is data parallel has to do with the *degree of independency* required of the data. If we define a quantity,  $\Lambda$ , as the minimum distance between dependent data elements of a data set, then the degree of independency,  $I$ , can be defined as

$$I = \frac{\Lambda}{N} \tag{2.1}$$

where  $N$  is the total number of data elements in the data set. Clearly, a data parallel algorithm can operate only on a data set with  $I \equiv 1.0$ ; there can be *no* dependencies between any of the elements in the data set on which an instruction is to operate. Therefore in solving a problem with a data set of  $N$  elements, if  $\Lambda < N$  it becomes necessary to restrict instructions to operate on just  $N'$  elements such that  $\Lambda = N'$  so  $I(N') = 1.0$ .

In a vectorizable algorithm there can be no dependencies between the data elements of a vector. If the vector length is  $V$  then the algorithm can be applied to any data set with  $I \geq V/N$ . There are then two ways of making the comparison between vectorizable and data parallel algorithms; one can consider how data parallel algorithms can be made vectorizable or one can consider how vectorizable algorithms can be made data parallel.

To vectorize a data parallel algorithm typically requires looping over the  $N'$  elements of a single data parallel instruction with  $N'/V$  repetitions of the equivalent vector instruction. Therefore in problems where  $N' \gg V$  one finds that a massively parallel architecture carrying out the data parallel algorithm will have significantly better performance than a vector architecture carrying out the vectorizable algorithm. The current high level of interest in the scientific computing community for massively parallel architectures is directly related to this point. For many scientific problems, not only is  $N' \gg V$  but also  $N'$  is a constant fraction of, or equal to,  $N$ , the total number of data elements in the problem. In such a situation the issue of *scalability* becomes important. Vector machines have maintained relatively constant vector lengths (typically  $V = 64$ ) throughout their development and improvements in performance have come about primarily through faster clock speeds and memory access times. The performance associated with vector machines is due to pipelining the operations such that optimally one operation is performed every clock cycle in every functional unit. For this reason increasing the vector length does not usually improve performance. Consider then a problem which scales linearly with  $N$ . If one doubles the problem size from  $N$  data elements to  $2N$  data elements, a vector machine will require double the number of instructions and must operate at twice the clock speed to solve the problem in the same amount of time. On the other hand, a massively parallel architecture will require the same number of instructions but will need double the number of processors to solve the problem in the same amount of time. Since the massively parallel architecture depends on the scalability of a single processor to create a machine with  $N$  processors, it seems likely that scaling up to  $2N$  processors is a simpler task than doubling the clock speed of the vector machine.



Now consider what is required to make data parallel a vectorizable algorithm. Typically this will involve determining  $N'$  for the data set of the problem and replacing  $N'/V$  repetitions of the vector instruction with a single data parallel instruction operating on  $N'$  elements. Therefore in problems where  $N' \approx V$  one finds that massively parallel architectures have significantly poorer performance than vector architectures. Consider for example a Connection Machine with 65536 processors and a vector machine with vector length 64. If  $N' = 64$  then on the Connection Machine one will have to repeat the data parallel instruction 1024 times with different sets of 64 processors. Although feasible, this would be tremendously time consuming because the individual processors of the Connection Machine are rather slow and the performance of the machine depends on employing large numbers of these processors concurrently. Therefore the vectorizable algorithm for this data set could not be converted directly to a data parallel algorithm without a great loss in performance. In such a situation it becomes necessary to replace the vectorizable algorithm with an alternative data parallel algorithm. An important result of the current work has been identifying such instances for the vectorized direct particle simulation and arriving at suitable replacement data parallel algorithms.

## 2.2 Virtual Machine Architecture

As seen from the previous section, an important property for a massively parallel architecture is scalability. The property of scalability must exist at both the hardware and the software level. On the Connection Machine hardware scalability is supported through the sequencers which connect the front end computer to the Connection Machine data processors (see Figure 2.1). A single Connection Machine system can have up to four sequencers each broadcasting to either 8192 or 16384 processors depending on the installation. A single user can be connected to 1, 2, or 4 sequencers such that in the larger configuration the user can employ 16384, 32768, or 65536 processors for the calculation. Usually the number of processors affects only the size of problem that can be handled.

The hardware scalability is enhanced in the software by which a user programs the machine. The software presents to the user an abstract version of the Connection Machine consisting of *virtual processors*. Each physical processor is made to simulate some greater number of virtual processors (or VP's as they are often referred to) and a program can assume any appropriate number of virtual processors are available for the calculation. In simulating virtual processors, a physical processor divides its memory evenly amongst the virtual processors and repeats each instruction once for every virtual processor. Therefore the number of virtual processors is limited by the amount of memory in a physical processor. Also, there cannot be fewer virtual processors than physical processors. Note that in the remainder of this thesis the terms processor and virtual processor will be used interchangeably, and the term physical processor will be used to specify the hardware element.

### **2.2.1 Virtual Processor Sets and Virtual Processor Ratios**

To implement a data parallel algorithm on the Connection Machine it is necessary to associate one virtual processor with each element of the data set. The set of all virtual processors associated with a data set is known as a *virtual processor set*, or *VP set*. VP sets are allocated dynamically therefore their size (the number of virtual processors in the set) may be made to fit conditions in the calculation. The number of VP sets in a single calculation may vary although only one VP set may be active at any time.

The *virtual processor ratio*, or *VP ratio*, is the ratio of virtual processors to physical processors in a VP set. Because virtual processors are created through binary division of a physical processor's resources, the VP ratio must always be a power of two. In simulating virtual processors each physical processor will execute an instruction a number of times equal to the VP ratio, therefore the machine performs very differently at different VP ratios. There is an essentially linear relation between VP ratio and execution time for VP ratios greater than about 4.

At VP ratios less than or equal to 4 there is a marked deviation from linearity.

This is due to the overhead associated with broadcasting an instruction to the physical processors. For lower VP ratios the time required by the physical processors to execute an instruction becomes comparable to the time for the instruction to arrive from the front end. Therefore the processors may be idle for a significant fraction of the calculation awaiting instructions from the front end. At higher VP ratios the time to broadcast an instruction becomes insignificant compared to the time to execute the instruction; if all the virtual processors are active for the calculation then the overhead in broadcasting the instruction is amortized over the greater amount of work carried out for the instruction.

Occasionally there arise situations where an instruction must be carried out over a VP set where not all the virtual processors are active but in each physical processor the *same* virtual processors are active. For example, the first virtual processor of each physical processor in a VP set may be the only one active for the instruction. In such a situation the use of *field aliasing* becomes profitable. Without describing the mechanics of this operation, let it suffice to say that field aliasing allows the physical processor to execute an instruction at a lower VP ratio (that is, repeating the instruction over a fewer number of virtual processors) than is associated with the data on which the instruction is to operate. Therefore in this example the instruction could be executed at a VP ratio of 1 (that is, only once by each physical processor) although the variable affected by the instruction resides in a VP set of VP ratio greater than 1.

### 2.2.2 Communication

The Connection Machine supports two mechanisms for interprocessor communication. The more general mechanism for communication employs the *router*, a hardware device which allows any processor to communicate with any other processor in the machine. Because of its generality, communication of this sort can be relatively slow. A less general but much faster mechanism for communication employs the *NEWS grid*. The NEWS grid is a software construction. Processors are organized into an  $n$ -dimensional grid and communication is allowed only

between immediate neighbors in the grid. The initials NEWS stand for the four directions North, East, West, and South in a two dimensional grid. Because the communication pattern is fixed it can be optimized for speed. Such optimization is not restricted to  $n$ -dimensional grid communication and most recently it has become possible to optimize any general communication pattern which is to remain fixed throughout a calculation. However, no such compiler optimization exists for general communication with a dynamically changing pattern.

The discussion in the previous subsection concerning the execution time as a function of VP ratio is most accurate for operations which take place within each virtual processor independently of other virtual processors. Operations which perform communication have a more complicated and therefore less predictable behavior. Nonetheless there is essentially a linear relation between VP ratio and execution time for VP ratios greater than about 4 so long as the other variables controlling communications performance are fixed. A later section analyzes in some detail those variables controlling the performance of general router communication.

## 2.3 I/O Subsystems

The fine-grained parallelism inherent to the Connection Machine architecture also extends to the I/O subsystems. This parallelism allows very high bandwidth links to exist between the data processors of the Connection Machine and external I/O devices. Two I/O devices in particular deserve special attention: the mass storage system, known as the *Data Vault*, and the graphics system.

### 2.3.1 Mass Storage System

The Connection Machine data processors may be connected to one or more mass storage systems, or DataVaults, each capable of storing up to 20 GB of data. The DataVault stores data in an array of 39 disk drives with 32-bit words spread across 32 drives and an additional 7 bits of Error Correcting Code (ECC) stored in the

remaining 7 drives. Failure of any one of the 39 drives does not prevent reading of stored data since the ECC allows the detection and correction of any single bit error.

The data processors send and receive data via I/O controllers. Up to eight I/O controllers may be configured in a system, each allowing transfer rates of 40 MB per second for a maximum combined rate of 320 MB per second. Each I/O controller connects to 8k physical processors through 256 I/O data lines. Each Connection Machine chip contains 16 physical processors and is connected to one I/O data line, therefore 8k physical processors are connected to 512 I/O lines. The controller can connect simultaneously to only 256 of these and must treat its 8k processors as two banks of 4k each. A bank will pass 256 bits in parallel to its associated I/O controller and parity checking of each byte adds another 32 bits to each data transfer. An I/O controller can buffer 512 such transfers in its own internal memory. The I/O controllers are connected to the DataVault through the Connection Machine I/O bus which is 80 bits wide (64 data bits, 8 parity bits, and 8 control bits) so the I/O controller has to multiplex and demultiplex between the 256-bit words of its internal buffer and the 64-bit bus.

### **2.3.2 Graphics System**

The Connection Machine graphics system consists of a frame buffer and a high-resolution color monitor. The frame buffer is a single module which resides in the Connection Machine backplane in place of an I/O controller. Because it is connected directly to the backplane rather than through the I/O bus the framebuffer can receive data from the Connection Machine processors at rates up to 256 MB per second.

The framebuffer contains a large video memory to store the raster image data. There are 28 planes of memory, each plane providing one bit per pixel and able to describe  $2^{21}$  (over two million) pixels. The 28 planes are divided into 4 buffers; the red, green, and blue buffers each have 8 planes and the "overlay" buffer has 4 planes. There are three color lookup tables (red, green, and blue) each with 259

entries of 8 bits. The first 256 entries map the colors for the corresponding red, green, or blue buffer and the last 3 entries map the overlay buffer.

To generate the analog video signal for the monitor the framebuffer requires 24 bits of data per pixel. These 24 bits per pixel are taken from the three color lookup tables. Two alternate schemes are possible: each color lookup table may independently supply an 8-bit entry thus allowing  $2^{24}$  possible colors for every pixel, or each color lookup table may supply the same 8-bit entry thereby allowing only  $2^8$  or 256 possible colors for every pixel.

The first scheme is known as "24-bit mode" and has the advantage of allowing a choice from  $2^{24}$  colors for simultaneous display. However this mode requires 24 bits of data per pixel to be transferred from the Connection Machine for each displayed image. On the other hand the second scheme, known as "8-bit mode", requires only 8 bits of data per pixel. Of course only 256 different colors can be displayed simultaneously in this mode but there exists an additional advantage. In 8-bit mode the framebuffer supports double buffering of output data, therefore data may be displayed from one buffer while a new image is being written to another buffer. Once the other buffer is completely loaded it can be switched with the displayed buffer in a synchronized manner such that the change appears instantaneous and the viewer never sees parts of two different images at the same time.

The overlay buffer is useful for creating independent or temporary images to be overlaid on the display. This allows the main image to be changed without having to repeat static portions of the display such as text or visual aids.

## 2.4 General Router Communication Performance

Because of the random nature of particle motion in a particle simulation, and because many of the algorithms to be implemented rely on table look ups which require cross VP set communication, it is often necessary to use the router for general communication between processors. The performance of router

communication is a complex function dependent on many variables and is difficult to predict for any given application. This section identifies two variables which strongly affect router performance and which are especially important in the context of a particle simulation. Some of these issues are touched upon in Myers and Adams (1988) but are developed more fully here for the present purposes.

#### **2.4.1 Router Performance as a Function of Message Length**

Communication time in parallel computers is usually assumed to be a linear function of message length. On the Connection Machine the relation is not as straightforward. Figure 2.2 shows the normalized cost for router communication as a function of message length. The normalized cost is defined as the total time for communication divided by the time to send one 32 bit word. The curve was determined by measuring the time required for all the processors in a VP set to send a message to a different processor with a random address in the VP set. This test differs from the one performed by Myers and Adams (1988) in two ways: the Hamming distance between a sending and receiving processor is not fixed, and the test was performed for VP ratios greater than one. It was desired here to in some ways mimic the router communication most often required in a particle simulation, therefore Hamming distance was not fixed. Myers and Adams correctly observe a sharp improvement in communication performance when the Hamming distance is less than five thereby constricting communication to be between processors on the same chip. Since the Hamming distance can rarely be controlled in a particle simulation it was desired to arrive at a relation averaged over a distribution of Hamming distances thereby removing it as a factor.

The other difference from Myers and Adams, that is the use of VP ratios greater than one, is only partly an effort to reproduce conditions of interest in a particle simulation. More important is the fact that at lower VP ratios the front end computer begins to affect the performance and the measurements become difficult to interpret. Generally, for VP ratios greater than four the VP ratio has a linear effect on performance and can be removed from consideration by using the similarity construct

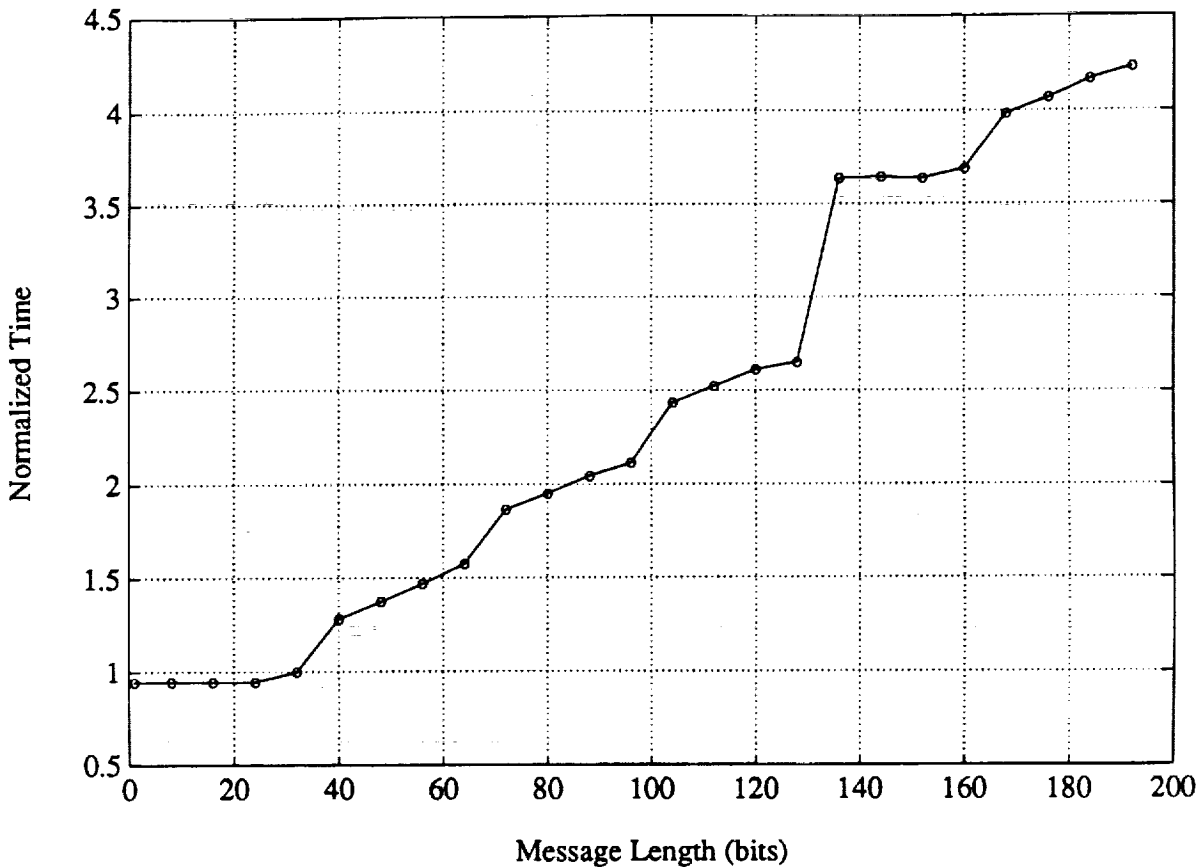


Figure 2.2 Communication time is linear as a function of message length only when the length is an integer number of 32 bit words. There is an additional overhead for sending fractional words.

$$T = \frac{t}{VPR} \quad (2.3)$$

where  $t$  is the measured time and  $VPR$  is the VP ratio.

Two very important features of figure 2.2 deserve discussion. The first is the “staircase” shape of the curve and related to this the indication that for message lengths less than 32 bits the communication time is essentially constant. This is somewhat unexpected since the Connection Machine processors are bit serial and one would expect a linear relation between communication time and message length measured in bits not in words. However, from this figure one can conclude that the router operates on 32 bit words unlike the processors which operate on single bits and have memories that are bit addressable. It is very important to



understand this difference between the way processors treat data and the way the router treats data. Because the processors are bit oriented it is tempting to believe that the same is true of the router and that one could achieve substantial improvements in communication performance by reducing message lengths to the minimum number of bits necessary. However it is obvious from the figure that message lengths consisting of "fractional" words introduce an additional overhead to the communication time, therefore in designing algorithms which require general router communication it is best to consider sending messages of lengths evenly divisible by 32. In relation to this it is especially important to realize that sending a single bit through the router will require the same amount of time as sending a whole word. This is unfortunate since often it is desirable to reduce router contention (discussed in the next section) by sending flags to processors which need not participate in the communication. However such an operation incurs a heavy overhead penalty and rarely is profitable.

The second feature of figure 2.2 which should be noted is the sharp rise of the curve for message lengths greater than 128 bits. Again this is contrary to what one would expect. That is, the relation between communication time and message length was found to be linear for lengths consisting of whole words and one would expect it to remain linear regardless of the number of words in the message. Unfortunately this is not true, and it is clear from figure 2.2 that the router has a maximum message length of 128 bits. If this length is exceeded the router will simply buffer the excess bits until it can repeat sending the message with the extra bits. Consequently the overhead for sending a message gets repeated if the message length is greater than 128 bits. This maximum message length, not surprisingly, corresponds exactly to the maximum integer length on the Connection Machine which also is 128 bits.

The overhead in sending a message through the router is approximately equal to half of the cost of sending a single word. If the message length is an integer number of 32 bit words, then the cost of communication using the router is given by

$$C = 0.52L + 0.48\lceil L/4 \rceil \quad (2.4)$$

where  $C$  is the normalized cost, that is the total communication time normalized by the time to send a single word, and  $L$  is the message length measured in words. Equation (2.4) is just a linear fit to the curve of figure 2.2 when only whole words are considered.

#### 2.4.2 Effect of Router Contention on Communication

Contention for hardware resources can occur in all computer architectures and algorithms should be designed to avoid or limit this as much as possible. For example, on vector oriented computers such as the Cray 2 contention most often arises as memory bank conflicts, that is the memory system is unable to keep pace with the processor which must then wait idle as the memory system services the memory request. A similar situation exists on the Connection Machine, here contention most often arises in the message routing hardware. There is a router node for every 16 physical processors (or PE's for physical elements), which make up a chip. Therefore if more than one of these needs to send a message through the router there will be contention. This type of contention will be referred to as *router node contention* in order to distinguish it from *router network contention* which is discussed below. Myers and Adams (1988) observe a linear relation between the number of PE's communicating off-chip and the time for communication, this is the expected result for router node contention. There is an initial overhead for setting up the communication after which there is a fixed cost for every message sent, hence the relation is linear. This observation has limited application in the current context of a particle simulation since rarely is the communication pattern so regular. One possible application is in the case of look up tables where it is known *a priori* that some entries will be required more often than others. Here one should consider the possibility of spreading the more common entries amongst the greatest number of router nodes in order to minimize node contention.

Router network contention refers to the contention which arises in the router

network from heavy network traffic. Router network contention can be reduced by limiting the number of processors which actually need to communicate, this is generally more feasible in a particle simulation than is the direct reduction of router node contention. It is important to realize that the two types of contention are essentially decoupled. In other words, it is possible for all the processors served by a particular node to require router service, however once that node has sent all the messages the transit time is faster because there is less traffic in the network. Overall then there is an improvement in communication performance even though for that node there was no reduction in node contention.

It was desired to test the effect of router network contention in order to better understand what advantage there exists in limiting it. The test conditions were similar to those of the previous section in that message destinations were random and the test was performed for VP ratios greater than four. However the test here consisted of measuring the communication time, as the fraction of active processors in the VP set was reduced. Furthermore the active processors always occupied continuous addresses in the VP set. For example if there were 64k processors in the VP set and only one quarter of these were active then they would have had addresses from 0 to 16383. Note that if one wanted to test the effect of router node contention as described above then for the same example every fourth processor in the VP set would have been active, that is processors 0, 3, 7, . . . , 65535.

The results of this test are presented in figure 2.3. Once again it is possible to use a similarity construct to eliminate the effect of changing the VP ratio. The cost also has been normalized by the maximum time for a given VP ratio, therefore the curve in figure 2.3 is true for all VP ratios greater than four. The normalized cost,  $C$ , is defined as  $C = T/t_{max}$  where  $T$  is defined in (2.3) and  $t_{max}$  is the communication time measured with all the processors active. Note that the plot in figure 2.3 is logarithmic in both axes; the abscissa corresponds to the base 2 logarithm of the fraction  $F$  of processors active for the communication.

The interesting feature in figure 2.3 is that the curve is not linear. Consider for now just the portion of the curve for  $\log_2(F)$  greater than  $-9$ . This portion of the curve is steepest near  $-1$  and levels off as it approaches  $-9$ . Clearly then, the greatest

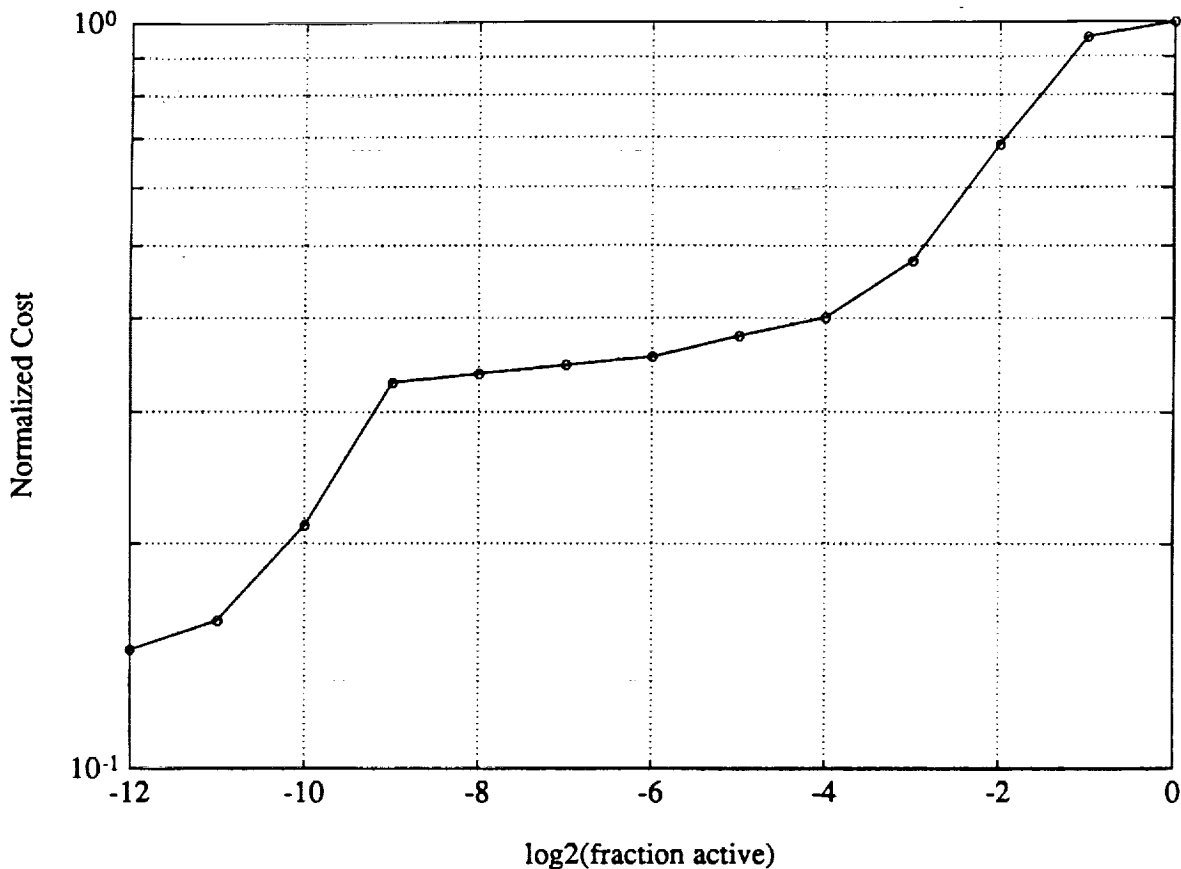


**Figure 2.3** Router network contention has a non-linear effect on the communication cost. The best improvement in performance is observed in the initial reduction in network traffic. The dramatic drop in communication cost when the fraction active is reduced beyond  $\frac{1}{16}$  is due to the reduction in router node contention which has a linear effect on communication cost.

improvement in performance occurs in the initial reduction of network traffic, that is when the fraction of processors active for the communication is reduced to one quarter or one eighth of the total. Beyond that there is only limited improvement in performance and router network contention is not a dominant factor.

The dramatic drop in the curve for  $\log_2(F)$  less than  $-9$  is simply the effect of reducing the router node contention. There are 16 physical processors per node, therefore for 8192 physical processors (the number used for this test) there are 512 router nodes. Once the fraction  $F$  is reduced to  $\frac{1}{512}$  the only remaining active processors are all in the same node and any further reductions will result in decreased node contention.

From figure 2.3 it should be evident that contention plays a very important role in determining the performance of router communication. There can be up to an order of magnitude improvement by reducing both node and network contention, and it can be quite profitable to design algorithms to take advantage of this.



## Chapter 3

# Implementation on the Connection Machine

The initial, and therefore fundamental, question to be addressed in implementing the direct particle simulation method (and in general any method) on the Connection Machine is that of mapping the data to the processors. All the succeeding algorithms used in implementing the method will depend on how the data is distributed amongst the processors and careful attention must be given to this question. Once a mapping has been determined it is possible to consider designing algorithms for the implementation.

A single time step of the direct particle simulation method is comprised of five events which include:

- 1) collisionless motion of particles
- 2) enforcement of boundary conditions
- 3) pairing of collision partners
- 4) collision of selected collision partners
- 5) sampling of macroscopic flow quantities

The first two events are concerned with the translational motion of the particles. The next two events are concerned with the collision of particles and the last event

concerns the realization of the solution from the flow simulation. This chapter considers the implementation of the last three events and defers the first two to Chapter 5.

### 3.1 Mapping Data to Virtual Processors

A key issue in the implementation of a particle simulation on the Connection Machine is the mapping of data to virtual processors. Two approaches may be taken—one can map computational cells to individual processors or one can map individual particles to individual processors. Note that the term processor refers to virtual processor and not to physical processor. Consider the cells-to-processors mapping first. Such a mapping is appealing for its apparent simplicity, however if such a mapping is implemented it must be dynamically load balanced, otherwise the calculation will suffer from inefficient hardware utilization and wasteful memory management. Without load balancing, computations are slowed to the rate of the most populated cell and the memory assigned to each processor must be great enough to accommodate the highest density of particles encountered in the simulation. Assuming there is sufficient memory to accommodate the particles in these cells, one will find throughout most of the calculation a great number of processors will be idle with large parts of their memory unused. Therefore to reduce these inefficiencies it is necessary to remap the cells to the processors as the calculation progresses.

Consider then how one would remap the cells to load balance the problem. The simplest scheme is to allow each processor to represent an integer number of cells, therefore data for particles in a cell cannot be spread across processors. This scheme does not produce a perfect load balance but has the advantage of being relatively straightforward to implement. Unfortunately, not allowing particle data to be spread across processors immediately fixes a maximum cell number density that can be accommodated by a processor. The amount of memory associated with each physical processor (usually 8 kB) is sufficiently limited that conditions can often exist where the cell number density is too great for the associated data to be



stored in a single processor. Therefore this scheme is too restrictive and would not be generally useful.

A more general scheme would allow each processor to represent any number of cells including fractions, such that data for particles in a cell could be spread across processors. Clearly this scheme would lead to a perfect load balance and would not be subject to the restrictions of the first approach. However, implementing such a scheme is much more difficult. In particular consider that an explicit mapping of the cells to the processors would have to exist in a distinct VP set such that as particles move from one cell to another the processors could know where to send the particles' data by consulting the mapping. This mapping would have to be consulted by each processor once for each different cell to which its particles had moved. In addition, there would be some difficulty with obtaining information for the cells when the particles in a cell are distributed across processors. These difficulties are not insurmountable, however they unnecessarily complicate the implementation and there is no clear advantage to be gained by employing such a mapping.

The alternative approach of mapping particles to processors is the one taken here. It eliminates the concern regarding load balancing by virtue of assigning a distinct processor to the element in the finest grain parallel decomposition of the problem. However, the problem solution still requires a connection between the particles and the cells, that is, the particles need to know of other particles in the same cell. This is accomplished by arranging the data such that adjacent processors in the one dimensional VP set created for the data set are representing particles in the same cell in physical space (see figure 3.1). Note that the data for particles is allowed to spread across physical processors but the virtual processor abstraction makes this transparent. This mapping makes the programming simpler because the object represented by each processor is consistent across all processors. In other words, the data stored in each processor is always associated with a single particle. This is quite different from the cells-to-processors mapping discussed above where the data stored in a processor could be associated with some variable fraction of a cell or more than one cell. Furthermore, the particles-to-processors mapping allows the calculation to proceed at a much higher VP ratio which is a distinct advantage

0	1	2	3	4
position	position	position	position	position
velocity	velocity	velocity	velocity	velocity
energy	energy	energy	energy	energy

**Figure 3.1** Representation of particle data amongst the Connection Machine processors. Each virtual processor stores the data for a single particle in a one dimensional virtual processor set. Neighboring processors in this set represent particles in the same cell in physical space.

over the cells-to-processors mapping.

There are three advantages to be gained by going to a higher VP ratio. The first is in the reduced time in communication. As the VP ratio increases there is a corresponding decrease in the relative time spent in communication because more of the virtual processors tend to be on the same chip and therefore less use is made of the router. The second advantage is in the sequencing of instructions from the front end to the Connection Machine. There is a fixed overhead associated with this step which is amortized over more virtual processors with higher VP ratios. This overhead is what accounts for the difference between the real time and the `CM_time` reported by the Connection Machine timer. The `CM_time` corresponds to the amount of time the Connection Machine processors are busy and can be substantially lower than the real time elapsed for the computation (as measured by the front end computer) when the VP ratio is low and the time spent in broadcasting the instruction from the front end becomes a substantial fraction of the total. The final advantage to be gained from higher VP ratios is in improved floating point performance. With a higher VP ratio the pipelines in the floating point accelerators can be kept full and floating point calculations proceed at their fastest rate.

In further discussing the present implementation of a particle simulation, it is useful to make clear the distinction between the particles and the processors which simulate them. For the diatomic gas molecules of the model used, the physical state of a particle is completely defined by its position, its translational velocities, and its internal energy, i.e.  $\mathbf{x}_i$ ,  $\mathbf{u}_i$ ,  $E_{rot}$ ,  $E_{vib}$ . The present implementation is two dimensional, therefore this representation requires seven distinct values. However, it is useful and necessary for the processors to store more information than just the physical state of the particles. The additional information stored by the processors includes the cell index, and depending on the particular collision algorithm either a five element permutation vector (or permutation sequence), or a two element vector of distributed random numbers. The cell index is a distinct index value that identifies the cell occupied by the particle. The two dimensional grid of cells is mapped to one dimension such that only a single value is necessary to identify a particular cell. The extension to three dimensions is straightforward. The permutation vector is a permutation of five numbers, 0 through 4, used in the degree of freedom mixing collision algorithm to re-order the relative velocity components. The stored random numbers are used in the alternative direction cosine decomposition collision algorithm which is most efficiently implemented by storing a table of random direction cosines to be used in the algorithm. The table is distributed across the processors such that one row of the table is split between two consecutive processors. This is done to minimize the storage requirements. Since two particles participate in a collision, the look up values necessary for the collision can be stored across two processors.

### 3.2 Selection of Collision Partners

Having decided upon a mapping of the data to the processors, it is appropriate to consider the ramifications of this decision on the algorithms to be implemented. The first algorithm to be considered here is the selection of collision partners. This is a two step process which requires first identifying collision candidates, and then from

these selecting colliding partners. It is important to distinguish between candidates for collision and actual partners in a collision. Collision candidates are sampled randomly from the particles in the same discrete volume of space in the simulation. The selection of collision partners is made by considering the interactive potential of the sampled collision candidates.

### 3.2.1 Identifying Collision Candidates

To identify collision candidates and for sampling macroscopic quantities from the flow solution, it is necessary to introduce a grid of cells associated with discrete regions in the simulated space. Since particles occupying the same cell are neighboring particles in physical space, these then are considered collision candidates.

McDonald and Baganoff (1988) argue for small, geometrically simple and similar cells on the basis that a simple and regular grid reduces much of the overhead in identifying collision candidates and more easily allows vectorization. Furthermore, small cells allow greater resolution of macroscopic flow gradients. These can be important even in low density regions of the flow, (for example in the recirculation region in the wake of a blunt body (Woronowicz and McDonald (1989)) and it is not sufficient to assume low density regions do not require small cells. Smaller cells do, however, lead to fewer particles per cell which correspondingly reduces confidence in distributions sampled from within the cells. Therefore it is important with the present method to be able to handle larger numbers of particles than are typically considered with other methods, and indeed this has been a principal focus in the development of the SPS method.

These considerations lead to a rectangular grid of cells of unit normal width; the cells are cubic in three dimensions and square in two dimensions. Special attention must be given to the fractional cells created by boundaries defining the body in the simulation. In order to account for the fractional cell volume being considered, an adjustment must be made in the rule used for selecting collision partners. Furthermore, the normal vector to the body must be known in each cell in order to properly reflect the particles from the surface. Feiereisen and McDonald (1989)

have developed a method useful for defining complex three dimensional geometries within a regular grid of cubic cells and have applied it to the full simulation of an ASTV. The isothermal or adiabatic boundary conditions of Woronowicz and McDonald (1989) can be incorporated into any geometry defined in this manner.

### 3.2.2 Selecting Collision Partners

With the set of collision candidates identified, it is necessary to select suitable collision partners. The most common approach has been the "time counter" approach used in the DSMC method, where pairs of molecules within a cell are randomly chosen and collided until the asynchronous cell time exceeds the global simulation time (cf. Bird (1976)). Pryor and Burns (1988) describe a vectorized implementation of this method but clearly it suffers a strong dependence on the number of cells in the simulation. At best this method can be parallelized only across cells and thus is strongly influenced by statistical fluctuations in the cell populations. More recently Bird introduced the "no time counter" method (Bird (1989)) which specifies the number of candidate pairs to be sampled from each cell and assigns a probability of collision to each pair. However this method is equally unsuitable for implementation on the Connection Machine because the sample of candidate pairs is of variable and predetermined size in each cell. Therefore it is difficult to generate the necessary sample for each cell in a data parallel fashion.

Nanbu (1980) introduces the idea of a probability of collision which he applies unconditionally to decide on a collision and then on a conditional basis to select a collision partner. This approach has a better theoretical foundation by virtue of being derivable from the Boltzmann equation, however it has the drawback of being an  $O(N^2)$  calculation. Ploss (1987) shows how Nanbu's scheme can be implemented as  $O(N)$  and vectorized thus yielding performance comparable to Bird's scheme. However, both Ploss's and Nanbu's scheme conserve only the mean energy and momentum of a cell and therefore the total energy and momentum of an individual colliding pair is allowed to vary. This can lead to greater statistical fluctuations in a solution, as shown by Bird (1989). In addition, an extension of this method to

chemically reacting flows does not exist and the development of such an extension is questionable.

Baganoff and McDonald (1990) introduce a selection rule based on a collision probability which allows a fine grained parallelization while conserving energy and momentum in a collision. In this approach, a probability of collision is computed for each pair of collision candidates and collisions are carried out in accordance with this probability. This probability is applied to individual candidate pairs independent of the cell as a whole. Consequently, like Ploss's scheme, the selection rule can be parallelized across particles.

The derivation begins with the general expression for the bimolecular collision rate but without the usual assumption of thermodynamic equilibrium. By transforming the equation into the center of mass frame of reference it is possible to arrive at an expression for the total number of collisions per unit time in a unit volume. It is then a simple matter to convert this expression into a probability of a given pair of particles undergoing a collision in a unit volume in unit time. If the volume under consideration is different from unity then the probability must be scaled accordingly. For an inverse-power law potential,  $\alpha$ , the collision probability within a unit volume is given by

$$P_s = \left(\frac{n}{2S}\right) \left(\frac{n}{n_\infty}\right) D(2/\alpha) \left(\frac{\bar{C}_\infty}{g}\right)^{4/\alpha} \left(\frac{g\Delta t}{\sqrt{2}\lambda_\infty}\right) \quad (3.1)$$

where  $n$  is the local number density,  $S$  is the number of pairs of collision candidates or sample size,  $g$  is the relative speed of the pair,  $\Delta t$  is the time step,  $\lambda$  is the mean free path,  $\bar{C}$  is the mean thermal speed, and the subscript  $\infty$  refers to free stream reference conditions. The quantity  $D(2/\alpha)$  is given by

$$D(2/\alpha) = \left(\frac{\pi}{2}\right)^{2/\alpha} / \Gamma(2 - 2/\alpha). \quad (3.2)$$

McDonald (1990) further extends this expression to account for multiple species. Typically, a value of  $S = \frac{n}{2}$  is used in a simulation. Fixing  $S$  in this manner allows the calculation of  $P_s$  to be made and applied to each collision pair independent of

any other collision pair, thus eliminating the data dependencies which would prevent a data parallel decomposition. Note that the sample size,  $S$ , is not dictated by equation (3.1), but rather is dependent on the particular implementation. Therefore there is greater freedom in choosing an algorithm for sampling candidate pairs from the simulation, although care must be taken to ensure the chosen algorithm creates a sufficiently large sample size such that the probability of selection does not exceed one for any collisions.

### 3.2.3 Collision Partner Selection on the Connection Machine

The selection of collision partners on the Connection Machine is exacerbated by the two scales of granularity inherent to the problem. Once the particles have been moved and all the boundary conditions enforced, each particle computes its current cell index. In order to identify collision candidates it is necessary to access all particles occupying the same cell. This requires sorting the particles in some manner such that particles with the same cell index can be identified. The sorting algorithm is described in Chapter 4, the object of the sort is to move the data for the particles in a cell into neighboring virtual processors thereby allowing access to cell information.

What the sort achieves for the algorithm is the perfect dynamic load balancing one would desire in a cells-to-processors mapping. Since each particle is assigned to a virtual processor, the amount of processing power and memory allocated to a given cell in the simulation is directly proportional to the number density of the cell. Because this value changes on every time step, it becomes necessary to dynamically reallocate the resources on every time step, and this is accomplished through the sorting process.

A further requirement of the sort is to change the order of particles within a cell between time steps. This is necessary because collision candidates are identified on an "even/odd" basis, i.e. all even numbered particles within a cell are eligible for collision with their odd numbered neighbor. This proves to be a very efficient arrangement because, for virtual processor ratios greater than 1,

candidate pairs are never split across physical processors hence communication time is minimized for the collision. However, it is important that candidate partners change between time steps otherwise the situation arises where the same partners collide repeatedly leading to correlated velocity distributions. This is discussed more fully in Chapter 4.

Collision partners are selected from the candidate pairs by applying the selection rule given by equation (3.1). This requires specific knowledge of the cell density which can be best obtained on the Connection Machine by making use of the `CM_scan` functions (Thinking Machines Corporation (1989)).

### 3.3 Collision Algorithms

Having identified a set of colliding pairs of particles, it then becomes necessary to perform the collision mechanics. It should be clear at this point that the method is statistical in nature therefore collision outcomes are determined on a probabilistic rather than deterministic basis. The purpose is to account for the exchange of energy between particles in a statistical sense and thus neglect the details of the particle trajectories. This is consistent with the collision selection rule which reproduces the correct collision rate for cells in the simulated flow without examining individual particle trajectories to determine if interaction would be possible.

This section concerns itself with two distinct collision algorithms. The first of these, the Degree of Freedom Mixing (DFM) collision algorithm, was first developed by Baganoff (1987) and McDonald and Baganoff (1988) and further analyzed by McDonald (1990) and by Feiereisen(1990). The second of these, the Direction Cosine Decomposition (DCD) collision algorithm was first introduced by McDonald (1990) as a method for vectorizing the collision mechanics of hard sphere interactions. As discussed by McDonald (1990), the DFM algorithm is an attempt at reducing the operation count in performing collisions but at the expense of more memory references. The alternative DCD algorithm requires greater computational effort but less memory references and therefore will run faster on high performance



machines such as the Cray 2 (which was of concern to McDonald) where processor speed is much faster than memory speed. On the Connection Machine the choice of collision algorithm does not have much impact on the overall performance of the simulation for the simple reason that collisions require only a small fraction (less than 10%) of the total computational time. The implementation of both algorithms is described, however the current implementation employs the DCD algorithm because of its stronger theoretical foundation and greater generality.

### 3.3.1 Degree of Freedom Mixing Collision Algorithm

The algorithm presented here is that developed by McDonald and Baganoff (1988) and considers collisions between perfect diatomic molecules of equal mass. The outcome of a collision of two particles is, for each particle, a new velocity and internal energy subject to the constraints of conservation of linear momentum and energy. In this model, rotational energy is accounted for by a rotational velocity vector  $\mathbf{r}$  such that

$$E_{rot} = \frac{1}{2}m(\mathbf{r} \cdot \mathbf{r}). \quad (3.3)$$

For a diatomic gas,  $\mathbf{r}$  has two components (corresponding to the two degrees of freedom in rotation) and the translational velocity  $\mathbf{u}$  has three components (corresponding to the three degrees of freedom in translation). Conservation of energy can then be written as

$$E_{tot} = E'_{tot} \quad (3.4)$$

or

$$\begin{aligned} |\mathbf{u}_{rel}|^2 + |\mathbf{r}_{rel}|^2 + |\mathbf{u}_{mean}|^2 + |\mathbf{r}_{mean}|^2 = \\ |\mathbf{u}'_{rel}|^2 + |\mathbf{r}'_{rel}|^2 + |\mathbf{u}'_{mean}|^2 + |\mathbf{r}'_{mean}|^2, \end{aligned} \quad (3.5)$$

where

$$\mathbf{u}_{rel} = \frac{\mathbf{u}_i - \mathbf{u}_j}{2} \quad (3.6)$$

$$\mathbf{r}_{rel} = \frac{\mathbf{r}_i - \mathbf{r}_j}{2} \quad (3.7)$$

$$\mathbf{u}_{mean} = \frac{\mathbf{u}_i + \mathbf{u}_j}{2} \quad (3.8)$$

$$\mathbf{r}_{mean} = \frac{\mathbf{r}_i + \mathbf{r}_j}{2} \quad (3.9)$$

and the prime indicates a post-collision value (these equations correspond to eqs. 16–21 of McDonald and Baganoff (1988)). Conservation of linear momentum can be written as

$$\mathbf{u}_{mean} = \mathbf{u}'_{mean}. \quad (3.10)$$

Then, by assuming

$$\mathbf{r}_{mean} = \mathbf{r}'_{mean} \quad (3.11)$$

the two conservation equations can be combined as a single equation

$$|\mathbf{u}_{rel}|^2 + |\mathbf{r}_{rel}|^2 = |\mathbf{u}'_{rel}|^2 + |\mathbf{r}'_{rel}|^2. \quad (3.12)$$

Equation (3.12) forms the basis of the collision algorithm. One begins by computing the relative and mean pre-collision velocity components for each collision partner. It is important to note that for the isotropic scattering of a hard sphere collision, any post-collision values that satisfy (3.12) are valid. Computationally, the simplest way to arrive at five values that satisfy (3.12) is to use the same pre-collision values calculated by eqs. (3.6) and (3.7). By re-ordering these values in a random fashion and assigning each element a random, equally-probable sign, one arrives at a valid and completely new post-collision relative velocity vector. The post-collision velocity vector for the particles is now easily obtained. For the first particle the new relative velocity is added to the mean velocity and for the second particle the relative velocity is subtracted from the mean velocity. By randomly selecting both a sign and a permutation there are  $5!2^5 = 3840$  possible outcomes for a collision.

The collision conserves both energy and linear momentum however, as with all probabilistic particle simulations, there is no conservation of the angular momentum of the rotors within a collision. Since fluid vorticity is not dependent on particle angular momentum, it is still possible to resolve vorticity in a flow (Woronowicz and McDonald (1989)).

Of concern with this collision algorithm is the bias introduced in the calculation of the post-collision state. If the scattering were perfectly isotropic then the angle

between the pre- and post-collision relative velocity vectors would show a sine distribution. However, because this algorithm selects the post-collision relative velocity from components of the pre-collision relative velocity, there is a preference for angles of  $0^\circ$ ,  $60^\circ$ ,  $90^\circ$ ,  $120^\circ$ , and  $180^\circ$ . This biasing is most marked when the algorithm is applied to monatomic particles which have only three degrees of freedom therefore only  $3!2^3 = 48$  possible outcomes for a collision. Nonetheless, even with monatomic particles this collision algorithm reproduces the correct density and temperature profiles across a normal shock wave and shows deviations from the correct results only in the actual velocity distribution within the shock (Feiereisen (1990)).

### 3.3.2 Implementing the Degree of Freedom Mixing Collision Algorithm

The essential issue that needs to be addressed in the implementation of this algorithm on the Connection Machine is that of re-ordering the relative velocity components to arrive at the post-collision state. On the Connection Machine this is done by using a permutation vector which is stored in each processor. There are two permutation vectors available per colliding pair of particles. Which one gets used is inconsequential, however to maintain statistically random collision outcomes it is desirable for particles to have different permutation vectors in succeeding time steps. The standard algorithm for creating random permutations is given by Knuth (1973) and an adaptation of this is implemented here. The approach taken is to initialize the particles with random permutations and generate new permutations by performing random transpositions on the existing permutation. A random transposition is the operation of arbitrarily switching the order of two randomly selected elements in the permutation sequence. Consider a permutation  $p$  with  $n$  elements. If  $p_j$  is the  $j^{th}$  element of  $p$  then transposition of the  $j^{th}$  element with the first element produces the new permutation  $p'$ .

Aldous and Diaconis (1986) prove that  $n \log(n)$  transpositions of this type are required to generate a new, statistically uncorrelated permutation. For the present purposes, at each time step a single random transposition of a particle's permutation

vector is performed. It follows that 10 time steps are required before a particle has a completely new permutation vector. Since individual particles collide less frequently than every time step, a particle may undergo several transpositions between collisions. Furthermore, the collision algorithm is only loosely bound to the randomness of the permutation since randomization of the outcome is enhanced by random partner selection. For these reasons a single transposition per time step is found sufficient to ensure unbiased outcomes. This has been substantiated through the correct reproduction of normal shock wave density profiles using just a single random transposition of the permutation vector.

Because there no inter-processor communication is required one expects this algorithm to perform well, however it should be pointed out that more work must be performed in the implementation than what is immediately obvious. This is because the Connection Machine is a SIMD machine and this algorithm assumes a MIMD behavior. Specifically, each processor is storing a different permutation vector which is used to dictate which component of the relative velocity vector is to be used in computing the collision outcome. Because the processors can receive only a single instruction, to process a single outcome component requires considering each of the five possibilities for the permutation element with only those processors storing the element under consideration active. The Connection Machine software does provide a faster means for accessing array elements specified by a per-processor index however it requires the array to be stored in a "sideways" fashion to allow parallel access to the bits of the array. Because this algorithm requires only one parallel access per element of the array, the overhead in converting the array to this sideways storage overcomes the advantage of the faster access and this feature of the software is not employed.

### **3.3.3 Direction Cosine Decomposition Collision Algorithm**

The Direction Cosine Decomposition collision algorithm was first introduced by McDonald (1990) for treating hard sphere elastic collisions in a vectorized manner which can be efficiently extended to inelastic collisions. Elastic and inelastic here

refer to the kind of energy exchange allowed in the collision. Elastic collisions allow energy exchange only between translational degrees of freedom whereas inelastic collisions allow energy exchange between translational *and* internal degrees of freedom. This section considers just the algorithm for elastic collisions and defers the treatment of inelastic collisions to the following section.

Hard sphere interactions are characterized by isotropic scattering. This means that in a two dimensional scattering process (see figure 3.2) the post-collision relative velocity vector,  $\mathbf{g}'$  is uniformly distributed on a circle and in three dimensions the distribution is uniform over a sphere. As has been shown by Bird (1980, 1983), isotropic scattering can still be used in simulating other interaction potentials because the scattering angle distribution does not have any observable effects on the solution of gas dynamic problems. This leads to a simplified model for treating inverse power law potentials, the “variable hard sphere” (VHS) model first introduced by Bird (1980). This model combines the hard sphere scattering law with a variable cross section which, in the SPS method, is simulated by using the the selection rule given by equation (3.1).

As discussed above, the isotropic scattering of two colliding particles requires specifying a post-collision relative velocity vector sampled from a distribution of vectors which is uniform over a sphere. For an elastic collision the magnitude of the relative velocity vector must remain constant in order to satisfy conservation of momentum and energy. Therefore if  $g$  is the relative speed, then the post-collision relative velocity  $\mathbf{g}'$  is given by

$$\mathbf{g}' = g\mathbf{n} \quad (3.13)$$

where  $\mathbf{n}$  is the direction cosine vector. In three dimensions  $\mathbf{n}$  has three components,  $n_x, n_y$ , and  $n_z$ , and requires two angles,  $\chi$  and  $\epsilon$ , to specify completely. The angle  $\chi$  is the scattering angle in the scattering plane and the angle  $\epsilon$  just specifies the orientation of the scattering plane (see figure 3.2). Clearly  $\epsilon$  must be uniformly distributed in the range  $[0, 2\pi]$  and may be selected as  $2\pi R_1$  where  $R_1$  is a uniformly distributed random fraction in the range  $[0, 1]$ . The scattering angle  $\chi$  must be in the range  $[0, \pi]$  and distributed such that  $n_x$  is uniform over  $[-1, 1]$ . Since  $n_x = \cos\chi$

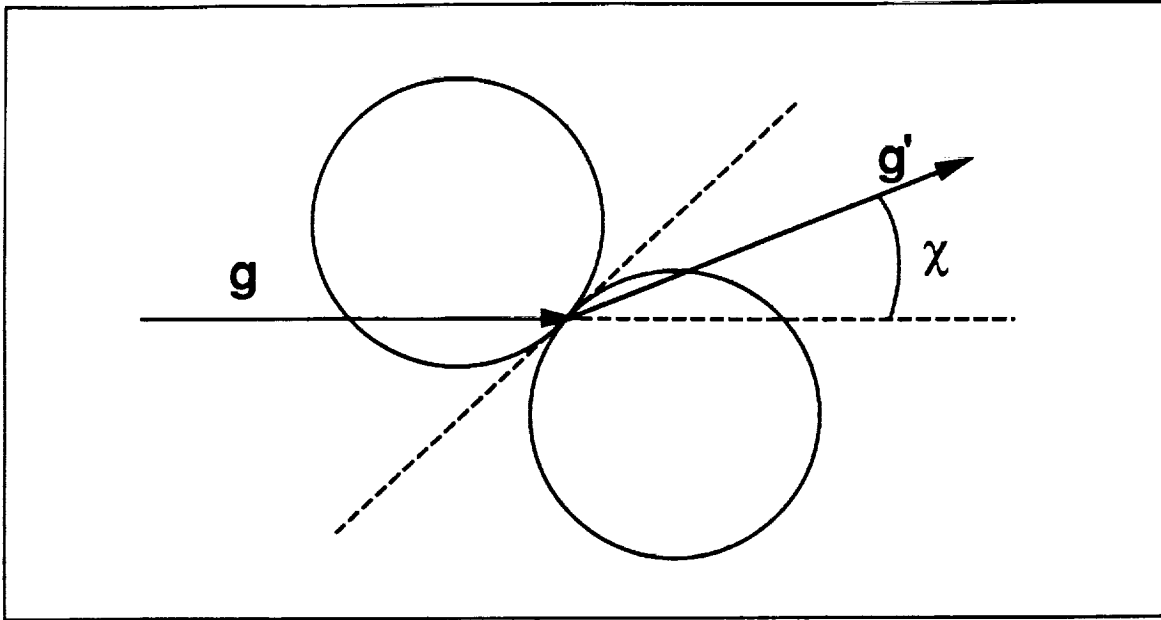


**Figure 3.2** Two dimensional scattering process involving hard spheres. This is equivalent to the three dimensional process viewed in the scattering plane.

we must have  $\cos\chi = 2R_2 - 1$  where  $R_2$  is another random fraction. Therefore a valid direction cosine vector can be determined by selecting

$$\begin{aligned}
 \epsilon &= 2\pi R_1 \\
 \cos\chi &= 2R_2 - 1 \\
 \sin\chi &= \sqrt{1 - \cos^2\chi}
 \end{aligned}
 \tag{3.14}$$

and then computing

$$\begin{aligned}
 n_x &= \cos\chi \\
 n_y &= \sin\chi \cos\epsilon \\
 n_z &= \sin\chi \sin\epsilon.
 \end{aligned}
 \tag{3.15}$$

The DCD algorithm differs from standard isotropic scattering collision algorithms in its treatment of (3.14) and (3.15). In the standard approach (cf. Bird (1976)), equations (3.14) and (3.15) are computed directly for each collision thus allowing essentially an infinite number of different possibilities for the direction

cosine vector. However, in the DCD approach a fixed number of direction cosine vectors are calculated once and stored in a table during the initialization stage of the simulation. This corresponds to discretizing the sphere over which direction cosine vectors are distributed; the granularity of the discretization is controlled by the number of entries generated in the table. When a collision is performed a vector is chosen randomly from the table and used in (3.13) to compute the collision outcome.

### 3.3.4 Extension to Inelastic Collisions

The term inelastic collision is used to mean that translational energy is not necessarily conserved over the collision and does not imply any loss in total energy. Any change in translational energy is accounted for by a corresponding change in internal energy which in this work includes energy in both rotation and vibration. Models for treating inelastic collisions are of two types: *impulsive models*, which attempt to incorporate the inelasticity directly into the collision dynamics, and *phenomenological models*, which account for inelasticity as a relaxation phenomenon and retain the hard sphere collision dynamics.

Impulsive models suitable for a particle simulation include the 'rough-sphere' model (Bird 1970) and the 'loaded-sphere' model (Melville 1972). Neither of these models is completely satisfactory, both being excessively artificial. Bird's rough sphere model inadequately represents diatomic molecules as having three rotational degrees of freedom rather than two. Melville's loaded sphere model is restricted to 'hard' interactions with no control over the effective relaxation time. More advanced impulsive models exist but these are generally excessively demanding of computing time and unsuitable for a particle simulation.

The limitations of impulsive models has led to almost exclusive use of phenomenological models for particle simulations. Of these the most widely employed is the Borgnakke-Larsen model (Borgnakke and Larsen (1975)). The model requires the specification of a fraction  $\phi$  of collisions to be treated as fully inelastic and the remaining fraction  $1 - \phi$  as completely elastic. Elastic collisions are treated

in a manner similar to that presented in the previous section. Inelastic collisions are treated by assuming a diffusion of energy between the colliding particles and an equilibrium gas. More specifically, the fraction of the total collision energy which belongs as relative-translational energy after the collision is determined by sampling from the corresponding distribution for this fraction in an equilibrium gas. Therefore a gas out of thermal equilibrium will be driven to an equilibrium state but in a manner that satisfies detailed balance.

The basis of the Borgnakke-Larsen model lies in the application of the appropriate distribution for determining the post-collision energy balance. The appropriate distribution is just the equilibrium distribution and can be derived analytically. Begin with the equilibrium relative speed distribution for colliding pairs (cf. Bird (1976))

$$F_{coll}^{\circ}(g)dg \propto g^{1-4/\alpha} g^2 \exp\left(-\frac{m^*}{2kT}g^2\right)dg \quad (3.16)$$

where  $\alpha$  is the exponent in the inverse-power law potential,  $m^*$  is the reduced mass for the colliding particles, and the superscript on  $F$  indicates equilibrium. Introducing a non-dimensionalized relative energy defined by

$$\epsilon_{rel} = \frac{\frac{1}{2}m^*g^2}{kT} \quad (3.17)$$

the distribution (3.16) can be written as a function of relative energy so

$$F_{coll}^{\circ}(\epsilon_{rel})d\epsilon_{rel} \propto \epsilon_{rel}^{1-2/\alpha} \exp(-\epsilon_{rel})d\epsilon_{rel} \quad (3.18)$$

The non-dimensionalized total collision energy,  $\epsilon_{coll}$ , is just given by

$$\epsilon_{coll} = \epsilon_{rel} + \epsilon_{int}. \quad (3.19)$$

Now define  $\mathcal{F}$  as the fraction

$$\begin{aligned} \mathcal{F} &= \frac{\epsilon_{rel}}{\epsilon_{coll}} \\ &= \frac{\epsilon_{rel}}{\epsilon_{rel} + \epsilon_{int}}. \end{aligned} \quad (3.20)$$



The equilibrium distribution for  $\mathcal{F}$  can be obtained from (3.18) by introducing the distribution function for the total internal energy in the collision. The distribution function for the internal energy of a single molecule is given by (Hinshelwood (1940))

$$F^\circ(\epsilon_{i,1})d\epsilon_{i,1} \propto \epsilon_{i,1}^{(\zeta_i/2-1)}d\epsilon_{i,1} \quad (3.21)$$

where  $\epsilon_{i,1} = E_{i,1}/kT$  and  $\zeta_i$  is the internal degrees of freedom. The total internal energy in the collision is simply  $E_{int} = E_{i,1} + E_{i,2}$ . The distribution function for the total internal energy may be obtained by considering the joint probability distribution for a particular value  $E_{i,1}$  of internal energy in molecule 1 and  $E_{i,2} = E_{int} - E_{i,1}$  in molecule 2. Integrating for all values of  $E_{i,1}$  up to  $E_{int}$  gives

$$F^\circ(\epsilon_{int})d\epsilon_{int} \propto \epsilon_{int}^{<\zeta_i>-1} \exp(-\epsilon_{int})d\epsilon_{int} \quad (3.22)$$

where  $<\zeta_i> = (\zeta_{i,1} + \zeta_{i,2})/2$  is the mean number of internal degrees of freedom. The product of (3.18) and (3.22) gives the joint probability of a collision with relative translational energy  $\epsilon_{rel}$  and internal energy  $\epsilon_{int}$ . Using (3.22) to eliminate  $\epsilon_{int}$  from the result and noting that  $\epsilon_{coll}$  is constant then gives

$$F^\circ(\epsilon_{rel}, \epsilon_{coll})d\epsilon_{rel} \propto \epsilon_{rel}^{1-2/\alpha} (\epsilon_{coll} - \epsilon_{rel})^{<\zeta_i>-1} d\epsilon_{rel}. \quad (3.23)$$

By substituting  $\mathcal{F} = \frac{\epsilon_{rel}}{\epsilon_{coll}}$  one may write

$$F^\circ(\mathcal{F})d\mathcal{F} \propto \mathcal{F}^{1-2/\alpha} (1 - \mathcal{F})^{<\zeta_i>-1} d\mathcal{F} \quad (3.24)$$

which is the desired result. At each collision, a post-collision value  $E'_{rel}$  is determined by sampling from this distribution and computing

$$E'_{rel} = \mathcal{F}E_{coll}. \quad (3.25)$$

The relative speed  $g' = \sqrt{2E'_{rel}/m^*}$  can then be decomposed into a velocity using the algorithm of the previous section. The remaining internal energy is divided between the two particles according to the distribution (Bird (1980))

$$f'(\mathcal{G}) = \left\{ (\langle \zeta \rangle - 2)^{(\langle \zeta \rangle - 2)} / \left[ (\zeta_{i,1}/2 - 1)^{(\zeta_{i,1}/2 - 1)} (\zeta_{i,2}/2 - 1)^{(\zeta_{i,2}/2 - 1)} \right] \right\} \times$$

$$\left[ \mathcal{F}^{(\zeta_{i,1}/2 - 1)} (1 - \mathcal{G})^{(\zeta_{i,2}/2 - 1)} \right] \quad (3.26)$$

where

$$\mathcal{G} = \frac{E'_{i,1}}{E'_{i,tot}}$$

$$= \frac{E'_{i,1}}{E'_{i,1} + E'_{i,2}} \quad (3.27)$$

and where  $\zeta_{i,1}$  and  $\zeta_{i,2}$  are the equivalent number of internal degrees of freedom for molecule 1 and molecule 2 respectively.

Some points need to be noted in the algorithm thus far. Firstly, the sampling from distributions proceeds by the acceptance-rejection method therefore there is no need to know the constants of proportionality in the distributions. A rigorous but clear derivation of these distributions along with the constants of proportionality may be found in McDonald (1990) and the above is meant only as an outline of the origin of the model. Secondly, it should be noted that implicit in (3.24) and (3.26) is a temperature dependence. This arises in the determination of the degrees of freedom,  $\langle \zeta_i \rangle$  in (3.24) and  $\zeta_{i,1}$  and  $\zeta_{i,2}$  in (3.26). Since it is unfeasible to determine the macroscopic local temperature for use in determining these parameters, it becomes necessary to introduce a collision temperature  $T_{coll}$  defined from the relative translational energy as

$$T_{coll} = \frac{E_{rel}}{\frac{3}{2}k}. \quad (3.28)$$

This temperature can then be used to determine the degrees of freedom in the collision. Even when averaged over many collisions, (3.28) is not statistically equivalent to the macroscopic local temperature, however it is a good approximation and therefore a valid alternative.

It is important to realize that the “degrees of freedom” used in the model are based on a mathematical concept and do not reflect the physics being represented. The quantum-mechanical model for a molecule allows only an integer number of degrees of freedom but with partial excitation. The Borgnakke-Larsen model replaces this concept with one of fully excited *fractional* degrees of freedom, or using the terminology of McDonald (1990), *equivalent degrees of freedom*. This is not an important distinction when considering just rotational energy, which may be assumed to always be fully excited and therefore have two degrees of freedom. However no such assumption can be made with vibration which has a much higher characteristic temperature. Using the perfect harmonic oscillator model, the specific energy in vibration,  $e_{vib}$ , is given by (Vincenti and Kruger (1965))

$$e_{vib} = \frac{R\theta_{vib}}{\exp(\theta_{vib}/T) - 1} \quad (3.29)$$

where  $R$  is the gas constant defined by  $R = k/m$ ,  $T$  is the local equilibrium temperature, and  $\theta_{vib}$  is the characteristic temperature for vibration. This last is defined by

$$\theta_{vib} = \frac{h\nu}{k} \quad (3.30)$$

where  $h$  is Planck’s constant,  $\nu$  is the classical frequency of vibration for the oscillator, and  $k$  is Boltzmann’s constant. The number of equivalent degrees of freedom is determined by assuming a specific energy of  $\frac{1}{2}RT$  for every fully excited degree of freedom, therefore

$$\zeta_{vib} = \frac{e_{vib}}{\frac{1}{2}RT}. \quad (3.31)$$

The rate of relaxation of internal modes is specified by the fraction  $\phi$  of collisions that are to be treated as fully inelastic. Usually, suitable values for  $\phi$  are derived empirically, although the reciprocal of  $\phi$  can be related to the collision number  $Z$  by (Pullin (1978))

$$Z_{rot} = \frac{8(2 + \zeta) 1}{5\pi \phi} \quad (3.32)$$

where  $\zeta$  is the number of internal degrees of freedom. Nonetheless it is customary to define the collision number in a particle simulation strictly as the reciprocal of  $\phi$  and the rest of this work adopts that convention.

It is usually necessary to specify different relaxation rates for rotation and vibration corresponding to the different collision numbers for these modes. This requires defining at least two different types of inelastic collision, one which allows no vibrational energy transfer in the exchange and one other which does allow vibrational energy exchange. If the second type of inelastic collision allows rotational exchange as well, in other words all types of energy may be exchanged, then the definition of collision numbers must be slightly modified as

$$\begin{aligned} Z_{rot}^* &= 1 / \left( \frac{1}{Z_{rot}} - \frac{1}{Z_{vib}} \right) \\ Z_{vib}^* &= Z_{vib}. \end{aligned} \quad (3.33)$$

Most implementations of particle simulations which use the Borgnakke–Larsen model have fixed values for the collision numbers. This is not completely realistic as it is well known that collision numbers are a function of temperature. Parker (1959) gives an approximate expression for the rotational collision number with temperature dependence in agreement with the more rigorous treatment of Lordi and Mates (1970). These considerations have been incorporated into the Borgnakke–Larsen model by Pullin (1978). More recently Boyd (1989) included expressions for a temperature dependent probability for both rotational and vibrational energy transfer and made a comparison against a model with a fixed probability for internal energy exchange. Boyds' calculations reveal only a small effect on the important macroscopic flow quantities although most likely this is due to the type of flow considered. Chapter 7 presents calculations for a double shock flow where a temperature dependent exchange probability is crucial for reproducing the experimentally observed behavior.

The primary disadvantage of the Borgnakke–Larsen method is the excessive computational cost required in sampling from complex distributions defined analytically like (3.24) and (3.26). There is also some question to the validity of the non-physical concept of equivalent degrees of freedom and certainly there is question with extending the method to more complex vibrational representations than the harmonic oscillator. These disadvantages are overcome in the model proposed by McDonald (1990). McDonald uses a Borgnakke–Larsen representation for rotational energy which is accurately modelled as fully excited with two degrees of freedom. However vibration is represented by a discrete distribution corresponding to the quantum states such that it is possible to use an uneven spacing between energy levels to model an anharmonic oscillator, although in the work of McDonald and in the present work the harmonic oscillator model is retained.

The use of the Borgnakke–Larsen model for strictly a two degree of freedom system leads to a greatly simplified treatment of rotationally inelastic collisions. For rotationally inelastic collisions  $\zeta_{i,1} = \zeta_{i,2} = 2$  and therefore all temperature dependence is eliminated in (3.24). Consequently, the distribution for  $\mathcal{F}$  is the same everywhere in the flow and can be pre-computed and stored in a table for easy access. The post-collision energy balance is determined by randomly selecting an entry from the table and using it in (3.25). The division of total rotational energy between the two molecules is also greatly simplified since the distribution function (3.26) which specifies the division reduces to a uniform distribution in the range  $[0,1]$  for this case. Clearly there is a great computational advantage to be gained by restricting use of the Borgnakke–Larsen model to only translation–rotation energy exchanges.

A completely new approach is taken for collisions involving vibrational energy exchange. It is noted that both rotation and vibration are two degree of freedom systems, the difference being that rotation can be accurately modelled by a continuous Boltzmann distribution whereas vibration requires a discrete distribution. The discretization relates to the quantization of the energy levels which for a harmonic oscillator is given by

$$E_{vib,i} = (i + \frac{1}{2})h\nu \quad i = 0, 1, 2, \dots \quad (3.34)$$

To arrive at a post-collision vibrational state is then simply a matter of discretizing a continuous Boltzmann distribution at the appropriate temperature. Such a distribution is available from the rotational energy. Using the rotational energy of the colliding particles as the sample guarantees the correct temperature since the particles are representative of the local conditions, however attention must be given to ensuring statistical independence between the energy modes. The post-collision vibrational state may be obtained by truncating  $E_{rot}$  as

$$q'_{vib} = \left\lfloor \frac{E_{rot}}{\Delta E_{vib}} \right\rfloor \quad (3.35)$$

where  $q'_{vib}$  is the post-collision quantum number for the vibrational state of the molecule and  $\Delta E_{vib} = h\nu$  is the spacing between quantized energy levels. This equation assumes equally spaced energy levels consistent with the harmonic oscillator model however it can be easily modified to accommodate the arbitrarily spaced energy levels of an anharmonic model.

McDonald suggests an iterative procedure for applying (3.35) to ensure the necessary statistical independence is maintained. An iteration consists of first using (3.35) with the molecule's own rotational energy to determine the vibrational state, then determining the new rotational state using the remaining collision energy in the restricted Borgnakke-Larsen model. Less than three iterations are found sufficient for convergence even in highly non-equilibrium situations.

### 3.3.5 Collisions on the Connection Machine

In this section we discuss the implementation of a general collision algorithm on the Connection Machine. The algorithm to be implemented is the direction cosine decomposition algorithm using the McDonald model for internal energy. This combination is preferred over the degree of freedom mixing collision algorithm because of its greater generality and stronger theoretical foundation. These

attributes become more important when considering the generalization of the implementation to include multiple species of reacting gases, a situation where the degree of freedom mixing algorithm has some serious limitations (McDonald (1990)).

The application of the necessary equations is straightforward and need not be discussed here. The issue which must be addressed is the storing of the necessary tables. At least two tables need to be stored to implement this algorithm, one for the three components of the direction cosine vectors and another for the distribution of the fraction  $\mathcal{F}$  of post-collision relative translational energy to total collision energy. For multiple species there must be a separate table of this fraction for each collision class, but for a single specie there is only one. For the single specie case there are then three table values to be obtained if the collision is elastic with a fourth value necessary if the collision is inelastic. Two alternatives exist for storing these tables: they can be stored in distinct VP sets or they can be stored in the same VP set as the particles. The first alternative utilizes the minimum amount of storage however it demands the use of the router to access the table entries. This is an undesirable situation because the communication time becomes excessive. A significant fraction of all the particles undergo collision on every time step and if their representative processors are all required to get information from random locations in a relatively small VP set there will be serious router contention and this should be avoided.

The second alternative is the better one to use. Here the two tables are made of equal length and distributed amongst the processors representing the particles. Storage requirements can be reduced by having each processor store only half of a table entry. In other words, if there are four values to be stored in a table entry then the first two are stored in an even-addressed processor and the last two are stored in the succeeding odd processor. Since collision pairs are created as even-with-odd this guarantees a full table entry is available for a collision with only NEWS communication required for access.

It is still necessary to ensure each colliding pair is provided with a random table entry. The motion of particles through the simulation space leads to processors representing different particles over the course of a calculation, therefore it can

be argued that the colliding pair represented by two processors changes between time steps and to any particular pair the table entry will effectively be random. However it is undesirable for the same collision dynamics to occur repeatedly in the same region of the flow. Once steady state has been reached, the number densities of the cells remain relatively constant and the particles in a given cell will tend to be represented by the same group of processors. Therefore if the table entries stored by the processors remain unchanged over the course of the simulation, then the collision dynamics performed in a cell will tend to be repeated leading to unwanted statistical dependencies between time steps. This problem is relieved by shifting the table entries "upwind" on every time step, therefore processor  $P_k$  gets the table values from processor  $P_{k+2}$  and again only NEWS communication is employed. Upwind here is in the direction of decreasing NEWS address. Since the particles are sorted such that all the particles in a cell occupy consecutive NEWS addresses, and since the cells are mapped to one dimension in row major order, it follows that the processors with the higher addresses will represent particles further downstream for a given row of cells. Of course by this definition upwind for the processor representing the first particle in a row of cells will indicate the processor representing the last particle in the row below it. This is still acceptable for our purposes.

### 3.4 Sampling Macroscopic Quantities

The grid of cells used to identify collision candidates serves also in sampling macroscopic quantities from the flow field. These quantities are collected in each cell from the distribution of particles within that cell. Once steady state has been reached it is possible to time average the macroscopic quantities of interest, thereby reducing the statistical uncertainty of just a single measurement. Because there is some correlation in macroscopic quantities between successive time steps, the statistical independence of samples of a given quantity can be improved if they are collected less frequently. Since sampling of the solution can take up a significant



fraction of the time step when many quantities are to be measured, there can be a performance advantage in sampling less frequently than every time step.

The process of sampling the solution is straightforward but can be expensive because of communication time. A separate VP set, which will be referred to as the *sampling VP set*, is created to store the running averages. There is one virtual processor in the sampling VP set for every cell in the simulation. Little calculation is necessary to create the samples, most often only a sum of all the values in a cell is required, although averages of second moments of the velocity distribution (e.g.  $u^2$  or  $v^2$ ) also require some multiplication. The time to perform these calculations is always small compared to the time required to send the values to their storage locations.

Two alternatives exist for sending the sampled results to the sampling VP set. The simplest approach is to send each value to be averaged directly to the sampling VP set using the `CM_send_with_add` instruction (Thinking Machines Corporation (1989)) such that the sampling VP set receives the sum of messages sent to the same destination. The Connection Machine instruction set (PARIS) includes a complete set of `send_with` type instructions that allow the combination of multiple messages sent to the same location. Some of the calculation required by these instructions gets carried out while the messages are *en route* to their receiving processor. The router is capable of detecting messages being sent to the same location and combining them at this time. The final calculation is carried out by the receiving processor which combines (in this case adds) the messages received with the value currently stored at the messages' destination address.

Using the `CM_send_with_add` as described saves on the cost of summing values across processors with `scan` instructions. However, because the `send_with` instruction has to be repeated once for every sampled quantity, the overhead in initiating the communication is repeated unnecessarily. More importantly, the communication is initiated from the VP set storing the particle data. The VP ratio of this VP set is very high and it is best to consider initiating the communications from the sampling VP set which has a much lower VP ratio. Therefore a better alternative is to use `scan` instructions to compute the desired averages in the cells

such that one processor for each cell stores all the quantities to be sent to the sampling VP set. These processors then send their self-address to the appropriate processors in the sampling VP set. Those processors in the sampling VP set which received an address can then *get* the sampled quantities in a single communications event. The schematic for the communications pattern is illustrated in figure 3.3. The advantage of this approach is that the bulk of the communications is initiated from the sampling VP set in a single instruction. This amortizes the overhead in initiating the communication and allows it to be carried out at the VP ratio of the sampling VP set thus proceeding much faster.

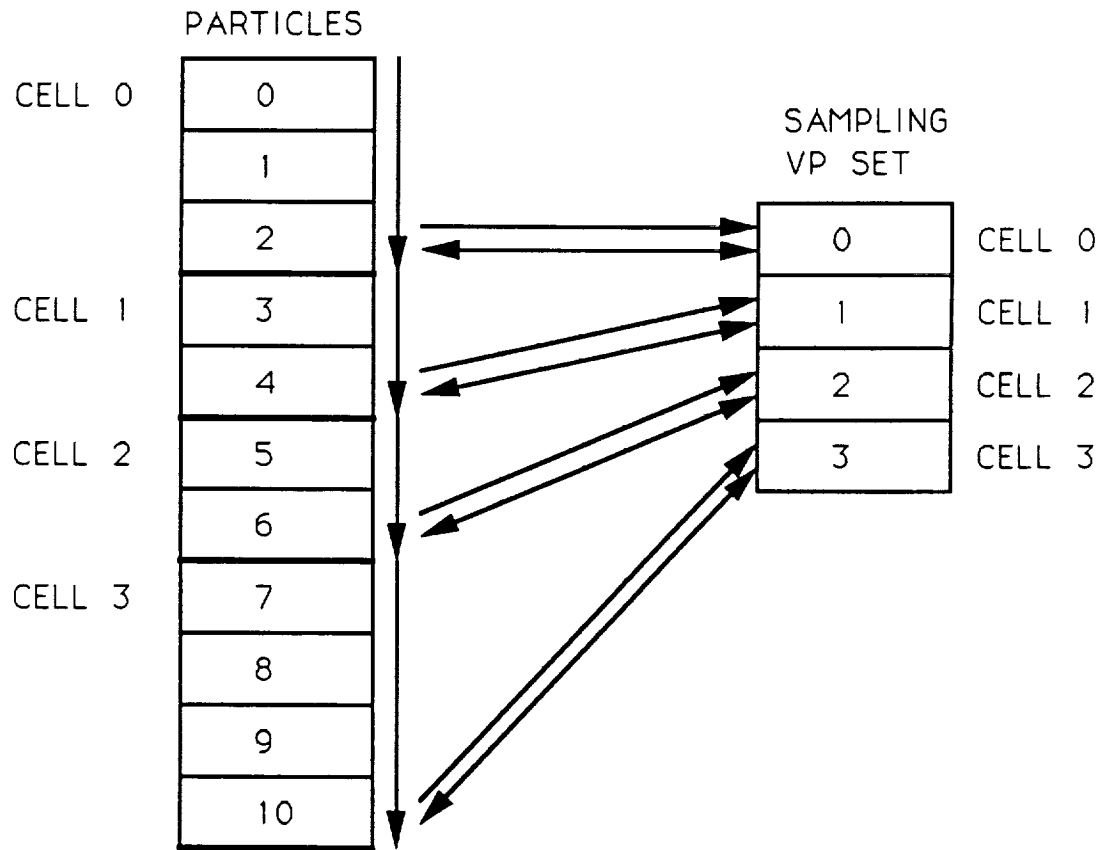


**Figure 3.3** Schematic of communications pattern for sampling macroscopic quantities from the simulation. Vertical lines with a single arrowhead are scan operations. Lines between VP sets represent general router communication. One arrowhead is used for a send instruction and two arrowheads are used for a get instruction.



# Chapter 4

## Sorting Algorithms On the Connection Machine

The selection of collision candidates in a particle simulation requires identifying particles occupying the same cell in physical space. In general this will involve a sorting operation which can take up a significant fraction of the computation. The amount of sorting required to some degree depends on the collision selection rule and its application to the candidate collision pairs. Baganoff and McDonald (1990) classify the application of the selection rule according to the role given to the sample of candidate pairs taken from a cell. If the sample size is left unspecified, such that one has the freedom of using whatever algorithm is most convenient for sampling candidate pairs from a cell, then the selection probability will be unconstrained and may exceed unity. However, because there is greater freedom allowed in the sampling of candidate pairs, the selection rule applied in this manner can be implemented with greater ease on different computer architectures. For this reason it is termed the *natural sample size* selection rule. The greater freedom afforded in choosing an algorithm for sampling candidate pairs is especially important on the Connection Machine because this is one of the algorithms which cannot be directly

translated from vectorizable to data parallel form.

The alternative application of a selection rule chooses a sample size which always ensures that the probability of selection is less than unity. The sample size is explicitly specified for each cell and therefore is coupled to the application of the selection rule. Consequently, there is very little freedom in the choice of algorithm for sampling candidate pairs from a cell, typically the particles must be fully sorted by order of their cell so that the correct number of pairs can be created in each cell. McDonald and Baganoff (1990) refer to this manner of application of the selection rule as the *constrained probability* selection rule. The first section of this chapter discusses in more detail the sorting used in implementing both the constrained probability and the natural sample size selection rules on sequential and vector computers. The remainder of the chapter then deals with the sorting necessary to implement the natural sample size selection rule on the Connection Machine.

## 4.1 Sorting for Particle Simulations on Sequential or Vector Machines

The first sort which will be discussed here is for the DSMC method which employs the constrained probability selection rule. In the DSMC method the particle indices are sorted such such that all the particles in a cell can be accessed through a continuous set of pointers in a cross-reference array. Then by knowing the cell density and the starting index in the cross-reference array for particles in the cell, one can identify the rest of the particles in the cell. Historically this type of a sorting operation has been required with the DSMC method because the time counter method for selection of collision partners employs an undetermined number of collision candidate pairs, therefore the sample size is tightly coupled with the process of selecting colliding pairs to the degree that candidate pairs are created as part of the selection process. However, with the constrained probability selection rule, or the no time counter (NTC) method as it is referred to by Bird (1989), the coupling of the sample size to the selection process is somewhat looser in that the sample size is specified before carrying out the selection process. Therefore it

would not be unreasonable to implement a particle simulation with the kind of sort employed by McDonald (1990) but using the constrained probability selection rule. Of course the scheme would fail if ever the sample size specified by the selection rule was greater than the sample size collected by the algorithm.

The sort operation here scales as  $O(N)$ , where  $N$  is the number of particles, rather than the  $O(N \log N)$  usually associated with sorting. The reason behind this is that the range of the elements to be sorted is known ahead of time so it is possible to create an array in which to sum up the number of occurrences of each element and use this to sort. More specifically, one can go through the table of particles once to create an array which stores the cell densities. Then, simply by computing the running sum of the cell densities one can create another array which stores a starting index for each cell. Finally, one goes through the table of particles a second time and adds the occurrence of each cell to the starting index for the cell and thus creates the rank for a particle. This sort cannot be fully vectorized although Boyd (1990) shows how it can be partially vectorized. Figure 4.1 is a schematic of the sorting process as performed by Boyd. The unvectorizable elements of this algorithm are the calculation of the cell densities and the counting of previous cell occurrences in the table of particles. The term "cell occurrence" is used to mean, for a particular particle, how many other particles before it in the table occupy the same cell. In other words it is an enumeration of the particles in a cell. If this enumeration is available in a separate array then the last part of the algorithm, which is the creation of the rank of each particle in the table and is called the "cross-reference array" by Bird (1976), can be vectorized. Therefore the algorithm proceeds as follows. First, in one pass through the table of particles, the particles in each cell are enumerated and the final count for each cell becomes the cell density. In the figure, the state of the cell density array is shown for every step of the enumeration. The next step in the algorithm involves computing an array of starting indices for each cell simply by carrying out the running sum of the cell densities. Finally, the rank of each particle is computed by adding a particle's enumeration to the starting index for its cell. The first step of this algorithm cannot be vectorized because it is impossible to ensure that two particles in a vector do not

also occupy the same cell. Note that the collision candidate matching algorithm of McDonald (1990) runs into the same problem in vectorization, and it will be shown that the same considerations that allow McDonald to fully vectorize his algorithm can be applied to the DSMC sort to fully vectorize it as well.

With the selection rule of Baganoff and McDonald (1990) the number of collision candidate pairs is fixed as a function of the cell density, typically one creates  $n/2$  pairs in a cell where  $n$  is the cell density. Therefore on a sequential machine there is no need to order the particles before creating pairs, one can simply go directly to creating a known number of pairs of collision candidates to be used in the collision routine. This is accomplished by going through the table of particles once and keeping track of every occurrence of a cell in a separate array. The separate array is a mapping in memory of the cells in physical space, and is referred to as the "space map" (McDonald (1990)). The space map will store either the index of a particle or a zero. Figure 4.2 is a schematic of this collision candidate pairing algorithm. One performs a single pass through the table of particles, and for each particle checks the appropriate element in the space map to see if another unpaired particle is in the same cell. If this is the case one creates a pair and zeroes the element in the space map. Otherwise the particle's index is stored in the space map as an unpaired particle. In figure 4.2 the state of the space map is shown for each step in the pairing process. Therefore it is possible to see how consideration of each particle in the table changes the state of the space map. Paired particle indices are stored at the time they are created in two arrays which are later used in the collision routine.

In the strictest sense this algorithm cannot be fully vectorized, however by allowing a very small and acceptable error McDonald (1990) is able to achieve full vectorization. The error which arises is the same error which prevents vectorization of the sorting algorithm used in the DSMC method, and occurs when two or more particles in a vector occupy the same cell. In this algorithm such a situation has two possible outcomes depending on the current state of the cell. If at the time the vector is being processed there are no unpaired particles in the cell, in other words the corresponding entry in the space map is zero, then only one of these particles will have their index written into the space map and the other one will essentially



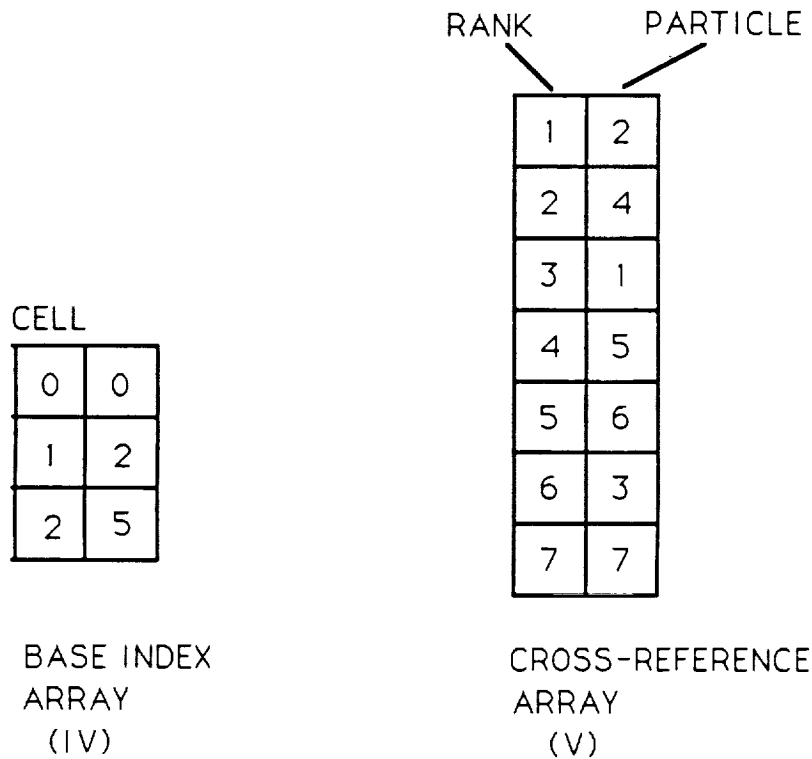
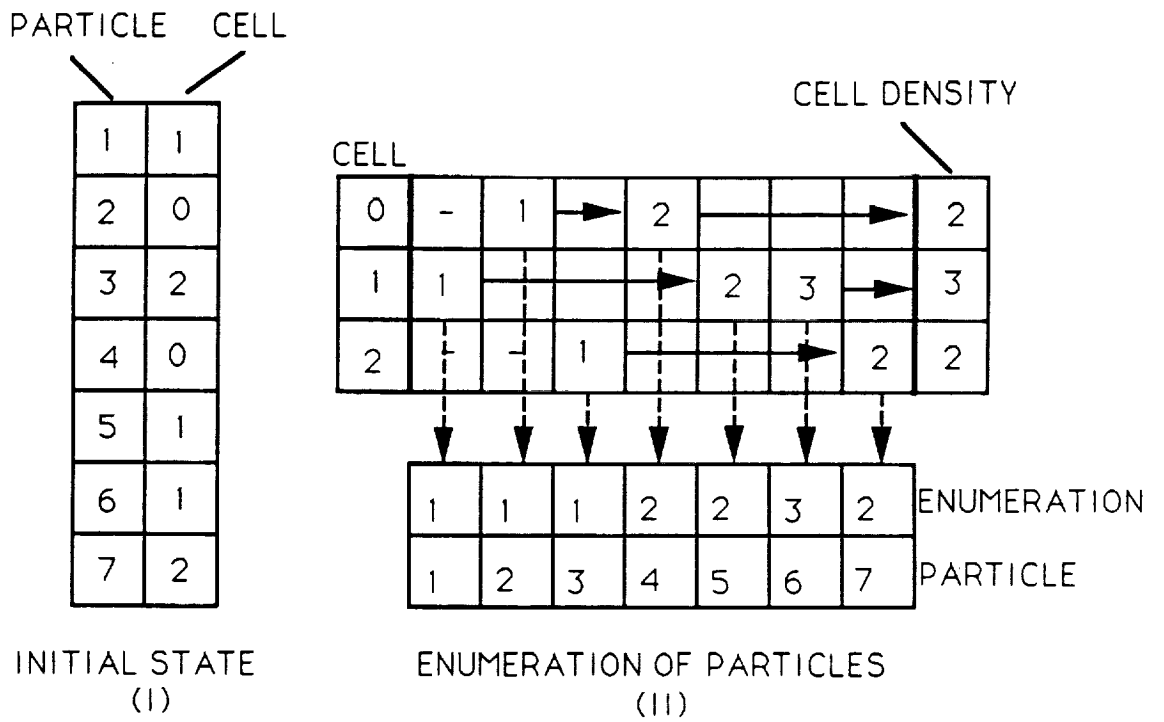


**Figure 4.1** Schematic of steps in the DSMC sort algorithm.

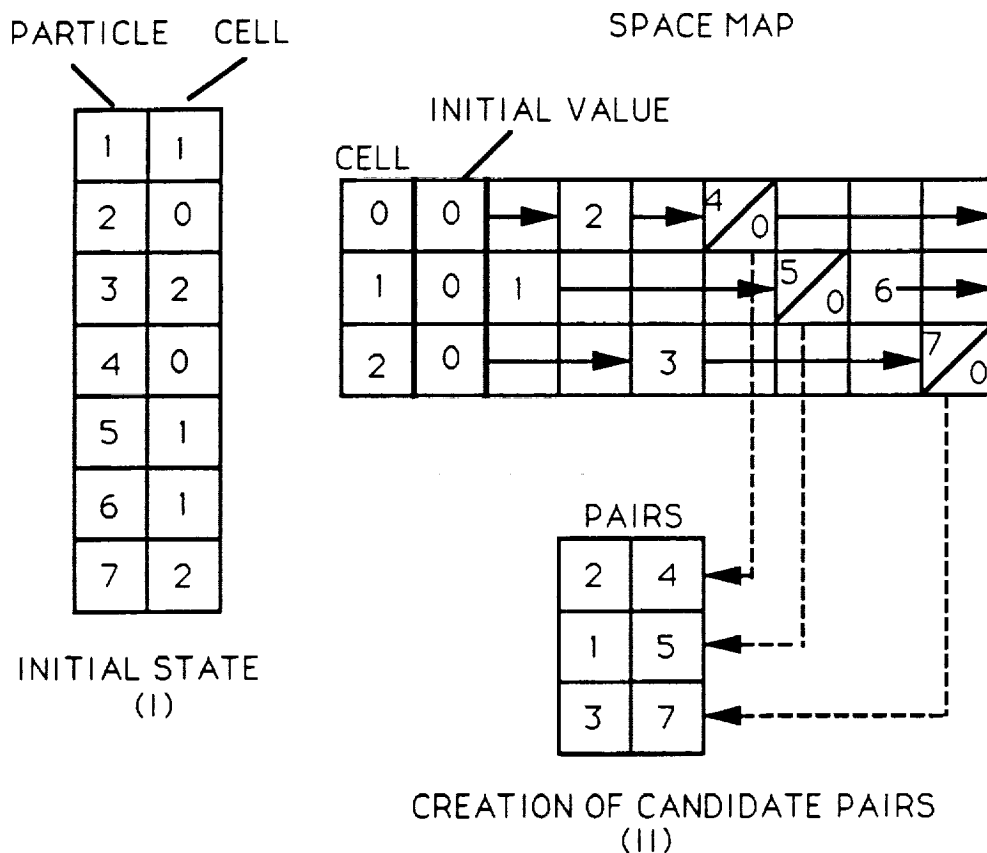


**Figure 4.2** Schematic of collision candidate pairing algorithm used in the vectorized Stanford particle simulation method. The end result is a list of candidate pairs of colliding particles.

be ignored as a candidate collision partner. This is not an error since the number of pairs created in a cell is counted and used in computing the probability of selection. However, if at the time the vector is processed there does exist an unpaired particle in the cell with its index stored in the space map, then this particle will get paired with both particles in the vector. This can lead to an implementation-dependent outcome for the collision of these particles. The collisions are carried out in a vectorized fashion, therefore if the same particle collides twice in a vector the outcome is unpredictable and very likely not to conserve momentum and energy. However, as indicated by McDonald (1990), the probability of the above occurrence

is very low because not only is it necessary for the two particles to have been in the same vector during the pairing process, but also the two pairs must be accepted for collision before an error is introduced. Furthermore, since the effect of this error is small the situation is quite acceptable.

It is possible in some degree to quantify the heuristic argument given above by deriving the probability of two or more particles in a vector occupying the same cell. To do this we must make the following assumptions:

(i) the cell populations are all identical.

(ii) particle indices are independent of the particle locations, therefore the indices can be thought of as randomly distributed amongst the particles.

The second of these assumptions is generally true, however the first is true only in the DSMC method where cell volumes are chosen to give a uniform cell population throughout the flow domain. For the cubic cells of unit width employed with the SPS method it is not possible to expect uniform cell populations, nonetheless one can proceed assuming (i) is true and then see how the result is affected when (i) does not hold.

Given the two assumptions above, one can find for any particle in the flow field the probability  $p$  that it occupies a particular cell  $c_j$  ( $j = 1, \dots, C_{tot}$ ) as

$$p = 1/C_{tot} \quad (4.1)$$

where  $C_{tot}$  is the total number of cells in the flow field. Conversely, the probability  $q$  that this particle *not* occupy a particular cell  $c_j$  is given by

$$q = 1 - 1/C_{tot}. \quad (4.2)$$

Now consider a group of  $N_{vec}$  particles, where  $N_{vec}$  is the number of elements in a vector (64 for the Cray 2). The probability of  $k$  particles in the group occupying the same cell is given by the binomial distribution

$$f(k) = \binom{N_{vec}}{k} p^k q^{N_{vec}-k} \quad (4.3)$$

where  $\binom{N_{vec}}{k}$  are the binomial coefficients defined as

$$\binom{N_{vec}}{k} = \frac{N!}{k!(N_{vec} - k)!} \quad (4.4)$$

The distribution is normalized so  $\sum_{k=1}^{N_{vec}} f(k) = 1$ . To determine  $P$ , the probability of two or more particles in a vector occupying the same cell, one must evaluate

$$\begin{aligned} P &= \sum_{k=2}^{N_{vec}} f(k) \\ &= 1 - f(0) - f(1) \\ &= 1 - q^{N_{vec}-1}(q + N_{vec}p). \end{aligned} \quad (4.5)$$

Substituting  $q = 1 - p$  gives

$$P = 1 - (1 - p)^{N_{vec}-1}(1 + (N_{vec} - 1)p). \quad (4.6)$$

Typically the number of cells  $C_{tot}$  is large so  $p \ll 1$  and

$$(1 - p)^{N_{vec}-1} \approx 1 - (N_{vec} - 1)p \quad (4.7)$$

and (4.6) simplifies to

$$\begin{aligned} P &\approx (N_{vec} - 1)^2 p^2 \\ &\approx \frac{(N_{vec} - 1)^2}{C_{tot}^2}. \end{aligned} \quad (4.8)$$

Now consider that in a moderate size simulation one may employ  $10^6$  particles and about  $5 \times 10^4$  cells. The probability of finding two particles in the same cell in a vector of 64 particles is then  $P = 1.6 \times 10^{-6}$ . One pass through the table of particles requires about 16000 vectors, therefore over 1000 time steps one would employ  $1.6 \times 10^7$  vectors and so one could expect  $1.6 \times 10^7 \times P \cong 25$  vectors to have two or more particles occupying the same cell.

The analysis above assumes that all cells have the same population therefore all particles are equally likely to occupy a particular cell. When the cell populations are not uniform then randomly chosen particles are more likely to be occupying the cells with greater population. Conversely, particles are less likely to be occupying cells with less population, therefore one can remove from consideration those cells with less population and employ the result in equation (4.8) but with  $C_{tot}$  adjusted to reflect the greater weight given to the more populated cells. In the typical simulation of the previous paragraph there were an average of 20 particles per cell. In the actual flow one would probably find some cells with no particles and some with 150 or more. In the worst case one would assume an average of 100 particles per cell is significant, therefore with  $10^6$  particles there are  $C'_{tot} = 10^3$  significant cells in the flow. Now over 1000 time steps there are 625 vectors which have two or more particles occupying the same cell. As a worst case this is still an insignificant amount considering that there are a million particles in the flow and the calculation has been carried out over a thousand time steps.

It is of interest now to consider what effect there would be in the DSMC method if the sorting algorithm there ignored the problem of two or more particles in a vector occupying the same cell. It is clear from the preceding paragraphs that such an occurrence is rare enough that ignoring it is acceptable so long as the result of such neglect is not catastrophic. First consider the effect on the calculation of the cell density. The cell density is the final result of enumerating the occurrences of a cell in the table of particles. If two particles in a vector occupy the same cell, then in processing that vector there will be two copies of the current cell count, each of which will be incremented by one. As a result the computed cell density will be less than the actual value by one. This is an insignificant error in view of the statistical nature of the simulation and the rarity of the occurrence as discussed above. McDonald (1990) allows precisely the same error in computing the cell density, as is necessary for allowing vectorization. The effect on the actual enumeration of the cell occurrences follows from this. If two particles in a vector occupy the same cell then they will both receive the same enumeration. In such a case, the two particles will receive an equal rank in the table, therefore in creating

the cross-reference array the same array element will receive two different values from the same vector. As a result, one of the particles will be ignored, and the cross-reference array will have one element left unwritten to. The latter could be useful as a check for this error. One could initialize the cross-reference array with an unused value such as  $-1$ , therefore any elements left unwritten after the sort will store this value. Later when the cross-reference array is used for creating candidate pairs it would be an easy matter not to allow any pairs which include particle  $-1$  as a partner.

On the Connection Machine it is not practical to employ either the DSMC sorting algorithm or McDonald's pairing algorithm. As discussed above, problems can arise if two or more particles in a vector also occupy the same cell, and equation (4.8) gives the probability of such an event occurring. On the Connection Machine the "vector length" is effectively as great as the active VP set, therefore there is a very high probability of two or more particles in a vector occupying the same cell. This is a situation where the relatively small vector length of the Cray 2 allows what is in the strictest sense a SISD algorithm to be carried out in a SIMD fashion. The discussion in section 2.1 explicitly applies to this situation. One could emulate a smaller vector length  $N_{vec}$  on the Connection Machine by looping through all the processors in the VP set with only  $N_{vec}$  processors active at a time. However, the meager performance of individual processors makes such a process very costly, and simply from a load balancing point of view it would be horribly inefficient regardless of the speed of individual processors. Consequently, on the Connection Machine one can virtually rule out as unfeasible any algorithm which requires almost SISD behavior over a large data set. Fortunately, alternative algorithms can be used and these are the topic of the remainder of this chapter.

## 4.2 The Radix Sort

The Connection Machine instruction set (PARIS) includes an instruction for finding the rank for each element in a disordered set of data. This is the

`CM_rank` instruction which is simply a radix sort algorithm written in microcode and supposedly optimized for performance. Hillis and Steele (1986) describe this algorithm for the Connection Machine. Sorting  $N$  elements with a maximum value of  $C_{tot}$  (the greatest value of a cell index in the current context) requires  $\log(C_{tot})$  passes through the  $N$  elements of the data set. Each pass considers a single bit of the sort key (the cell index in this case) beginning with the least significant bit and proceeding to the most significant bit. The elements with a zero bit are enumerated first, and the elements with a one bit are enumerated above these. Therefore if there are  $c$  elements with a zero bit they get assigned distinct integers  $y_k$  ranging from 1 to  $c$ . The remaining  $N - c$  elements with a one bit then get assigned distinct integers  $y_k$  ranging from  $c + 1$  to  $N$ . The values  $y_k$  are then used to permute the elements such that all the elements with a zero bit precede the elements with a one bit. By proceeding through the  $\log(C_{tot})$  bits of the sort key the set gets ordered.

Figure 4.3 is a schematic for this algorithm. Beginning with the same disordered data set of figures 4.1 and 4.2, two pairs of enumerations are carried out to sort the set. In this example the maximum key value is 2, therefore only two bits are required to represent all the key values. The first pair of enumerations is used to re-order the particle indices based on the value of the least significant bit in the cell index. The new order is shown in the figure and is labelled "rank[1]" to indicate it is the ranking after examining the first bit of the key. The second pair of enumerations uses the rank[1] values in re-ordering the indices and thus arrives at the rank[2] result which here is the final result since there are only two bits in the key.

It is worthwhile at this point to note the difference between a "ranking" algorithm and a "sorting" algorithm. A ranking algorithm returns the "rank" value for the elements of a set; in other words it returns the position that a particular element would take if the set were ordered. This is more general than a sorting algorithm which actually moves the disordered elements of the set into their ordered locations. Ranking is more efficient than sorting when the data to be ordered is much larger than the key that determines the ordering. In other words, if the elements of the disordered set are large, it is more efficient to first rank the elements and then move them to their ranked positions than to move the elements each time the

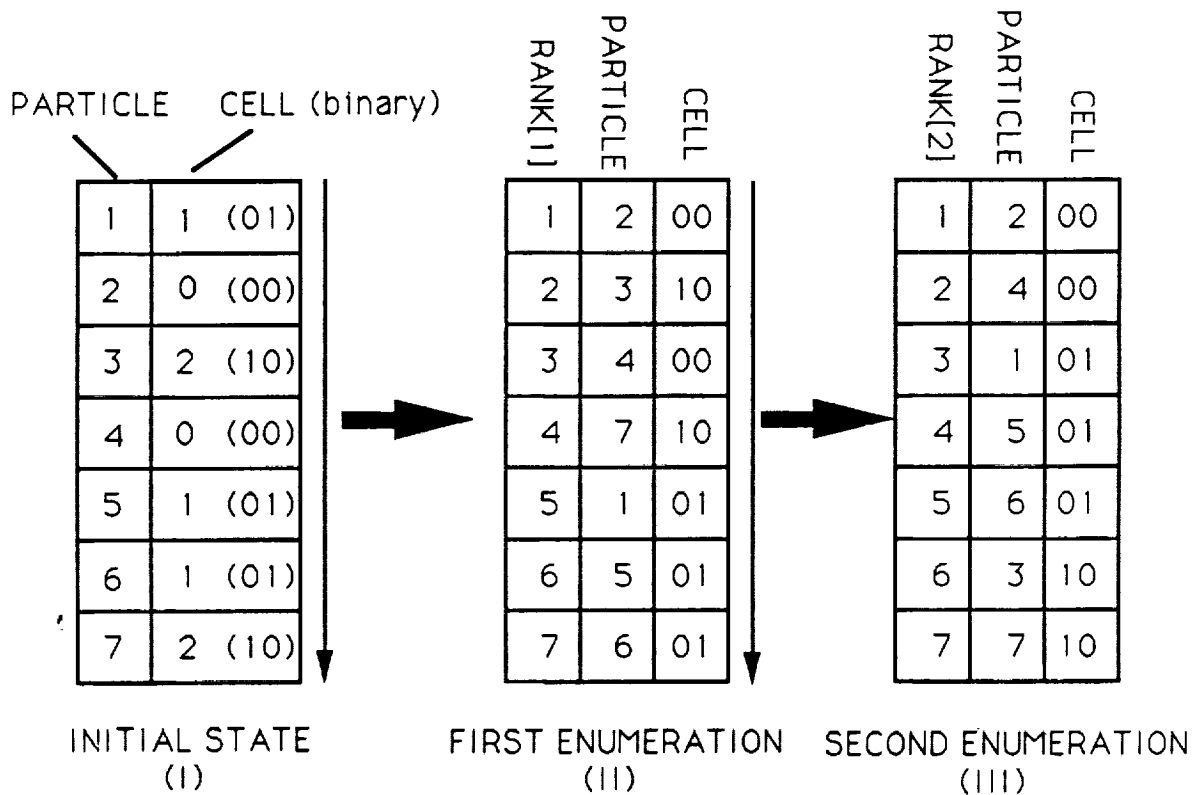


Figure 4.3 Schematic of radix sort algorithm for maximum key size of two bits.

sorting algorithm permutes the key.

On the Connection Machine each re-ordering of the data set requires a general router communications event in the form of a `CM_send`, therefore for the radix sort presented there must be two enumerations and one "send" per bit of the key. This ratio of enumerations to sends can be changed simply by examining more than one bit before re-ordering. In other words, one can look at two bits of the key and carry out four distinct enumerations before re-ordering, or one can look at three bits and carry out eight enumerations before re-ordering and so forth. In general  $2^j$  enumerations are required to re-order  $j$  bits. Therefore for every  $j$  bits in the key there will be  $2^j$  enumerations and one send. On the Connection Machine



enumerations are about 14 times faster than sends, therefore the cost of the radix sort is proportional to  $(2^j + 14)/j$  which is minimized for  $j = 3$ , in other words re-ordering 3 bits in the key at a time. It is interesting and perhaps surprising that the `CM_rank` instruction uses  $j = 2$  and it is possible to write a faster ranking routine in `PARIS` by using  $j = 3$ . Finally, it is worth noting that the sorting algorithm used in the DSMC method can be thought of as a special case of a radix sort which lets  $j$  be the maximum number of bits in the key and, because the range of the key is known precisely, allows the  $2^j$  enumerations to be performed in a single pass through the set as was described in section 4.1.

A final concern for the sorting algorithm is to maintain statistical independence between samples of collision candidate pairs taken from a cell over succeeding time steps. As was described in section 3.2.3, collision candidate pairs are identified on an even/odd basis, therefore the sorting algorithm must allow the order of particles within a cell to change if statistical independence is to be maintained. With the radix sorting algorithm a simple mechanism for accomplishing this is to concatenate a random sequence of bits to the least significant bit of the key, and then sort on this expanded key. A fixed number of bits are concatenated but their values are random, therefore sorting on the expanded key will restore the order of particles between cells while changing the relative ordering within cells. Unfortunately, expanding the key in this manner introduces additional bits to sort and there is a corresponding penalty in performance.

The radix sort algorithm as described scales as  $O(N \log(C'_{tot}))$ , where  $C'_{tot} = 2^k C_{tot}$  is the size of the expanded key when  $k$  bits are concatenated to the cell index. Each enumeration requires time proportional to  $N$  and the number of enumerations is proportional to  $\log(C'_{tot})$ . Therefore if this sort algorithm is used in a particle simulation, the computational time will scale linearly with the number of particles only if the total number of cells is held fixed. Since the number of cells in a simulation typically will be at least an order of magnitude smaller than the number of particles, the  $\log(C'_{tot})$  factor will not have a great effect on the scaling of the simulation for smaller problems. However it most certainly is a cause for concern with very large problems and the radix sort is not recommended for a

particle simulation other than for its simplicity and robustness.

### 4.3 Sorting Using Multiple Grids

Section 4.1 discussed in some detail the sorting algorithms used in particle simulations on sequential or vector machines. Common to all these algorithms is the representation of physical space by a data structure in memory with an individual element for each cell of physical space. Such a data structure will be referred to as a "grid". There is no architectural reason why a grid could not be used on the Connection Machine for sorting, however the current software does not allow the kind of communication necessary for effective use of just a single grid. Through the use of multiple grids this software limitation can be circumvented, and this section describes a sorting algorithm which uses multiple grids in an effective manner with the current software. The section ends by describing how sorting on a single grid could be made effective with the introduction of a new communications instruction.

#### 4.3.1 Algorithm for a Single Grid

To describe how sorting is performed on multiple grids, it is best to begin by describing how to sort using a single grid. On the Connection Machine the grid is implemented as a separate VP set with one processor for every element of the grid. In the following discussion, the processors representing the grid will be identified as "grid processors" in order to distinguish them from the processors representing the particles which will be referred to as "particle processors".

The rank of a particle can be determined from the sum of the base index for its cell and the particle's enumeration within the cell. The base index for a cell is easily obtained on a single grid as the running sum of the cell densities. Figure 4.4 is a schematic for the kind of communication required. Each particle processor uses the `CM_send_with_add` instruction to send a value of 1 to the grid processor for its cell. This instruction combines multiple messages going to the same destination by taking their sum, therefore the receiving processor receives only the sum of all

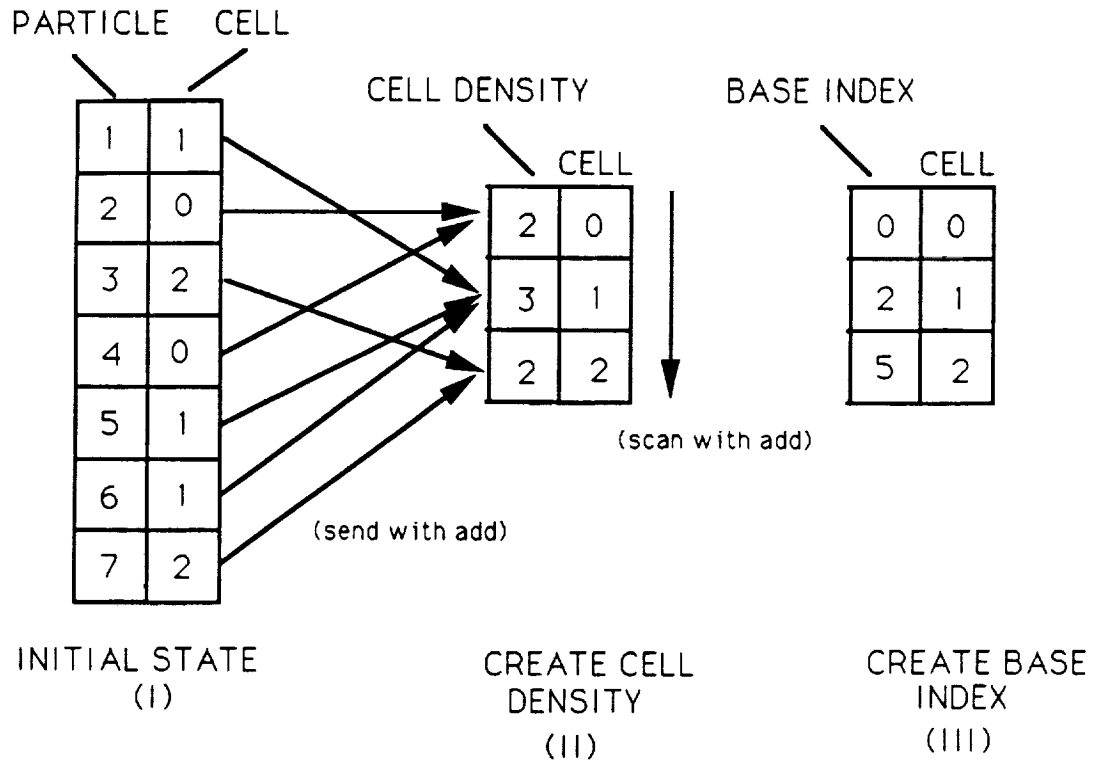


**Figure 4.4** Using a single grid to compute the cell density and the cell base index.

the messages sent to it. In this case the grid processors receive the cell density; the running sum of the cell densities can then be created by using the `CM_scan_with_add` instruction.

Enumerating the particles in a cell is an iterative process, figure 4.5 is a schematic for this part of the ranking algorithm. Each particle processor now uses the `CM_send_with_overwrite` instruction to send its self-address to the grid processor for its cell. This instruction ensures that one correct message is received from multiple messages sent to the same destination, which message gets received is unpredictable. This is a rather fortunate feature of the instruction since it provides, at no additional cost, the randomization of particle order within the cell which is required by the collision selection rule. Grid processors which receive messages return, to the particle processors, the current "base index" for the cell and then increment the base index by one. On the next iteration only those particle

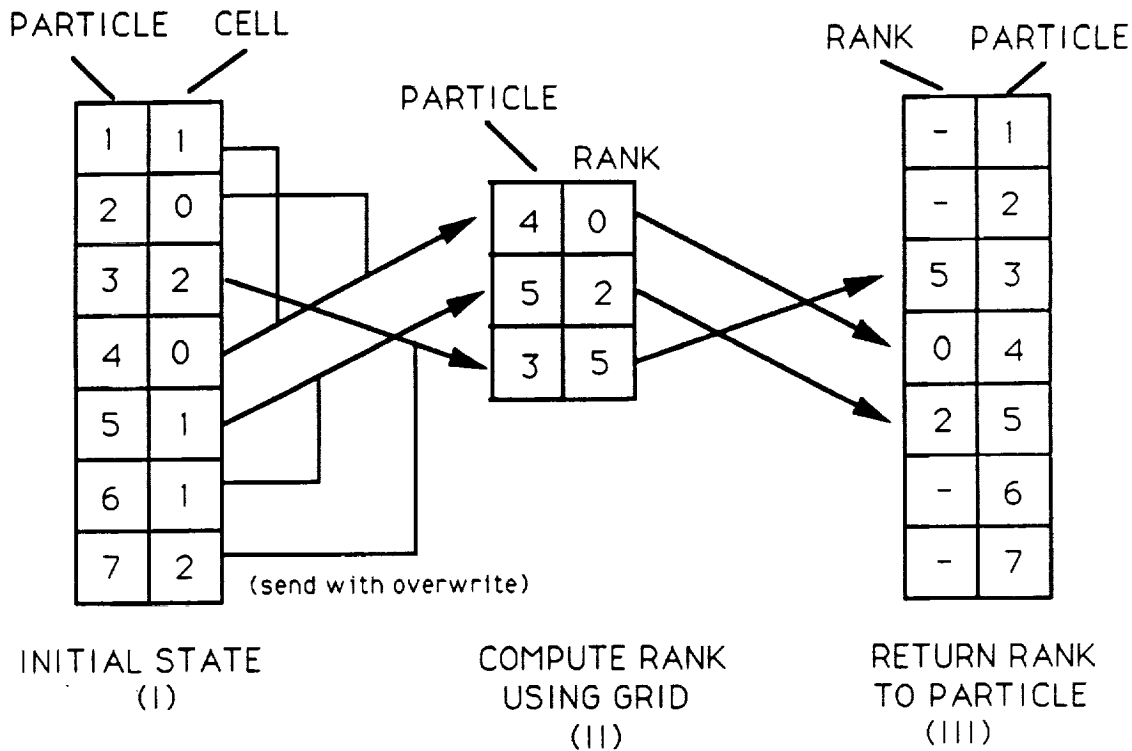
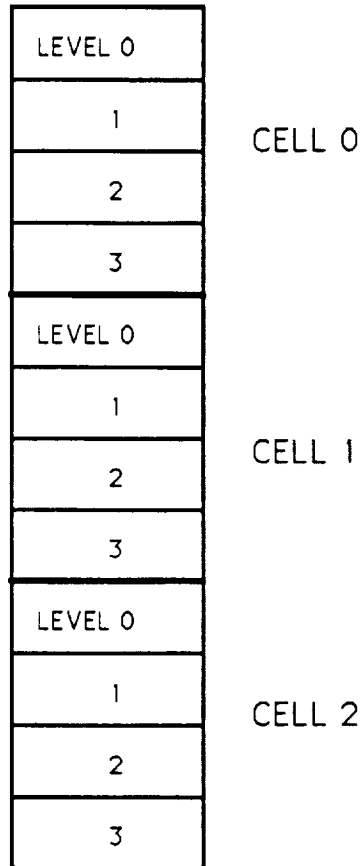


Figure 4.5 Using a single grid to rank the particles.

processors which did not receive a ranking from the grid participate. The process is repeated until all the particles have been ranked.

### 4.3.2 Using Multiple Grids

The number of iterations necessary to rank the particles with a single grid is equal to the greatest cell density in the flow. Since the cell density can become quite large the algorithm can be very inefficient and it is necessary to find some way of reducing the number of iterations. This is accomplished by employing multiple grids for the enumeration. The multiple grids are implemented in a single VP set as shown in figure 4.6 with the different levels for a given cell in the multi-grid occupying neighboring locations in the VP set. An iteration of the sorting algorithm employing a multi-grid is depicted in figure 4.7. Note that the multi-grid in figure 4.7 is somewhat unusual in that it has 3 levels. More typically the multi-grid will have a power of 2 number of levels like in figure 4.6, however in the interest of clarity



**Figure 4.6** Layout of a multi-grid. The different levels for a cell are neighboring processors in a VP set.

only 3 levels were depicted in this figure. A particle processor first randomly selects a level in the multi-grid, and then uses the `CM_send_with_overwrite` instruction to send its self-address to the grid processor for that level in its cell. Note that now the order of particles within a cell is randomized not only from the unpredictable nature of the `CM_send_with_overwrite` instruction but also through the random selection of a level in the multi-grid. Grid processors which receive messages are enumerated across the levels, and the enumeration is added to the base index for the cell to create a ranking. These processors then return the ranking to the particle processors and update the base index. On the next iteration only those particle processors which did not receive a ranking from the multi-grid participate.

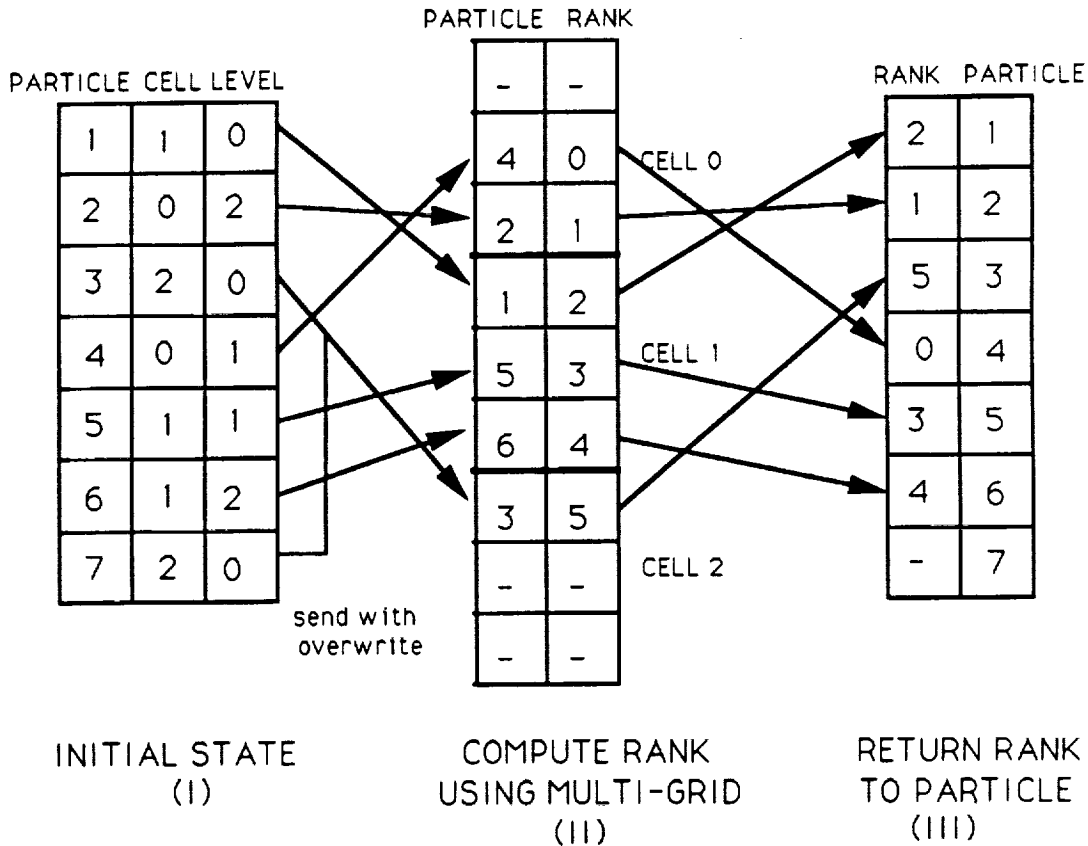


Figure 4.7 Using a multi-grid to rank the particles.

### 4.3.3 Factors Affecting Performance of the Algorithm

The performance of the algorithm is largely a function of the number of iterations. With multiple grids the number of iterations no longer is simply equal to the greatest cell density in the flow. The factors which affect the number of iterations now include the the number of levels in the multi-grid as well as the maximum cell density. A statistical analysis can be carried out to determine how these two parameters relate to the number of iterations. Begin by letting  $n$  be the cell number density and  $L$  be the number of levels in the multi-grid. If levels are selected randomly, then a single particle has a probability  $p = 1/L$  of being in a particular level and  $q = 1 - 1/L$  of not being in that level. Once again we can make use of the binomial distribution (equation (4.3)) to find the probability distribution

for  $n$  particles. For  $n$  particles we find the probability of  $k$  of these occupying the same level is given by

$$f(k) = \binom{n}{k} p^k q^{n-k}. \quad (4.3)$$

Therefore the probability of there being one or more particles in a level is

$$\begin{aligned} P &= \sum_{k=1}^n f(k) \\ &= 1 - f(0) \\ &= 1 - \left(1 - \frac{1}{L}\right)^n. \end{aligned} \quad (4.9)$$

Consider a particular cell and let  $n_0$  be the number density. After one iteration there are  $n_1 = n_0 - LP_0$  unranked particles remaining in the cell where  $P_0$  is just equation (4.9) evaluated for  $n = n_0$ . After two iterations there are  $n_2 = n_1 - LP_1$  unranked particles remaining in the cell where  $P_1$  is equation (4.9) evaluated for  $n = n_1$ . In general, after  $i$  iterations there are  $n_i = n_{i-1} - LP_{i-1}$  unranked particles remaining in the cell. Expanding this recursive relation gives

$$n_i = n_0 - L(P_0 + P_1 + P_2 + \dots + P_{i-1}). \quad (4.10)$$

The algorithm is converged when  $n_i = 0$  or,

$$\sum_{i=0}^I P_i = n_0/L. \quad (4.11)$$

Equation (4.11) substantiates what one may have guessed intuitively, namely that increasing the number of levels reduces the number of iterations. We can recover our result for a single level from (4.11) by setting  $L = 1$  so from (4.9)  $P = 1$  and we find, as before, that  $n_0$  iterations are required to converge. It is interesting also to determine how many levels would be required to converge in a single iteration. This can be done by setting  $P_0$  equal to  $n_0/L$  and solving for  $L$ . Doing this results in  $L = \infty$ , which of course must be the case since the algorithm chooses levels

randomly and it is impossible to guarantee with a finite number of levels that the same level is not chosen for two different particles. In general one can use (4.11) to predict how many iterations are required for convergence given some number of levels and particles to be ranked.

In practice it is found that reducing the number of iterations improves performance only to a point after which there is a drop in performance. This is due to the communications cost also being a function of the number of levels. For a greater number of levels, the VP set which stores the multi-grid becomes larger, therefore the cost of sending the rank value from the multi-grid to the particle processors increases. One could consider initiating all the communication from the particle processors, then the communication cost would be independent of the number of levels in the multi-grid. There are two reasons why that is not a profitable proposition. First, it entails the use of the `CM_get` instruction which has about double the overhead of `CM_send` and also uses an unpredictable amount of temporary storage which makes it very difficult to employ in any situation where memory is at a premium. This is quite a serious limitation especially in the current context where it is desired to use all the available temporary storage in order to create the largest multi-grid possible in order to minimize the number of iterations necessary to rank the particles. The second disadvantage in initiating all the communication from the particle processors is that it results in greater network traffic and greater router contention. Router contention has a great impact on the performance of this algorithm. After each iteration the number of particles left to rank decreases substantially, leading in the next iteration to a great reduction in router contention and consequently in the time to complete the iteration. If the grid processors are used to send the rank values back to the particle processors, then for that part of the iteration the network traffic is minimized since there are no redundant messages in the network. On the other hand if the particle processors are used to get the rank values from the multi-grid, then there must be a message sent for every particle processor which is active for the iteration. Not only does this lead to greater network traffic, it also creates more router node contention from grid processors which have two or more particle processors getting a value from them.



It is found for most situations that a multi-grid with twice as many virtual processors as there are particles in the simulation gives the best performance. The performance of the algorithm depends largely on the density distribution in the flow. A uniform flow density is the optimum condition for applying this algorithm. Such a situation only exists near the start of the simulation and the multi-grid sorting algorithm is found to take about half the time of the radix sort. Once the flow has reached steady state the density distribution is far from uniform, and the multi-grid sorting algorithm takes about 75% of the time of the radix sort. Fortunately, even in the most severe conditions density will maintain bounded values and sorting with a multi-grid is suitable for most flows. Consider that the stagnation region in a blunt body flow represents the most severe conditions one would expect to encounter in the simulation of an external flow. For diatomic molecules the jump in density across a shock wave is limited to six times the free stream density. There can be further increase in density within the stagnation region, most noticeably for an isothermal surface with a wall temperature significantly lower than the gas temperature in the stagnation region. In such a situation the wall tends to cool the gas and leads to a density gradient through the thermal boundary layer. However, even such a condition rarely leads to a density greater than ten times the free stream, and this is restricted to a thin layer of cells near the body. Consequently one can be fairly certain never to encounter cell densities greater than ten times the free stream value. That such a reasonable upper bound exists is important for guaranteeing the generality of this algorithm.

The above discussion is restricted to flow simulations without chemical reactions. When chemistry is introduced there are more degrees of freedom available for energy dissipation and the theoretical limit on the density jump across a shock wave becomes greater than six. It is conceivable then for the stagnation region to contain a large fraction of the particles in the flow. In such a situation it may prove profitable to sort the particles in two distinct sets. One could define a subspace of the physical domain to include the stagnation region, and create a multi-grid for this subspace with a much greater number of levels than would be possible for the full physical domain. The particles in this subspace would get ranked with this

multi-grid, then one would create the multi-grid for the full physical domain and rank the rest of the particles.

#### 4.3.4 Using a Single Grid Effectively

To use a single grid effectively for sorting the particles, it is necessary to introduce a new communications instruction. The instruction one would require would make the receiving processor simulate a stack or a queue. In other words, when multiple messages are sent to the same processor, the processor receives all the messages saving them in its own memory. It is possible that an instruction similar to this be made available in the near future, therefore it is worthwhile discussing how one could make use of it. Clearly with such an instruction one would only create a single grid, and begin as above by determining the density and base index for each cell. Next, all the particle processors would use this instruction to send their self address to the appropriate grid processor. The grid processors would then return to each particle processor the rank value, which would be the sum of the base index and the enumeration within the cell. The number of iterations required would be equal to the maximum cell density,  $n_{max}$ , divided by the maximum number of messages which could be received by the grid processors.

The communications related problem one encounters with this algorithm is in returning the rank values from the grid processors to the particle processors. In this algorithm the grid processors have to perform  $n_{max}$  send operations to return the rank values. Since these send operations are initiated from the grid VP set they are much faster than send operations initiated from the particle processors VP set. The concern here however is in load balancing. If the density distribution is perfectly uniform then  $n_{max} = n_{min} = N/C_{tot}$  and there is perfect load balancing. However when the density distribution is not uniform then  $n_{max} > N/C_{tot} > n_{min}$  and there is imperfect load balancing. Again it is possible to argue that density is a very "restrained" variable and the ratio  $n_{max}$  to  $N/C_{tot}$  is rarely more than 10. Furthermore the cost of router communication decreases as the network traffic lessens, therefore the extra cost in communications does not increase linearly with the ratio  $n_{max}$  to  $N/C_{tot}$ . Nonetheless this is cause for concern in the case of very

non-uniform density distributions and one would want to consider optimizations such as ranking the stagnation region separately or performing some load balancing in the grid before returning the rank values.

## **4.4 Sorting by Merging Ordered Subsets**

This section describes a very fast ranking algorithm with performance independent of the density distribution, and most suited for a two dimensional particle simulation. The algorithm proceeds by identifying ordered subsets in the full set of particles. The bulk of the work then involves the merging of these ordered subsets into a single ordered set.

### **4.4.1 Two Fundamental Observations**

There are two fundamental observations which can be made about the dynamics of a particle simulation and which can be used to design an efficient ranking algorithm for this problem.

(1) On every time step the particles begin and end in an ordered state. The disordering of the particles occurs through their motion from one cell to another. Furthermore, the nature of this motion is such that on one time step only about a third of the particles will change cells, therefore the set is never greatly out of order. In fact it is precisely for this reason that there is statistical dependence between even/odd pairings in succeeding time steps unless an effort is made to enhance the disorder (see section 3.2.3 or 4.4.3 ahead).

(2) The motion of the particles is such that to a very high probability if a particle moves out of its current cell it will move only into one of its two immediate neighboring cells in the direction of motion, that is, particles do not move more than two cell widths per time step (see figure 4.8).

### **4.4.2 The Merged Ordered Subsets Sorting Algorithm**

The merged ordered subsets sorting algorithm proceeds in the following manner.

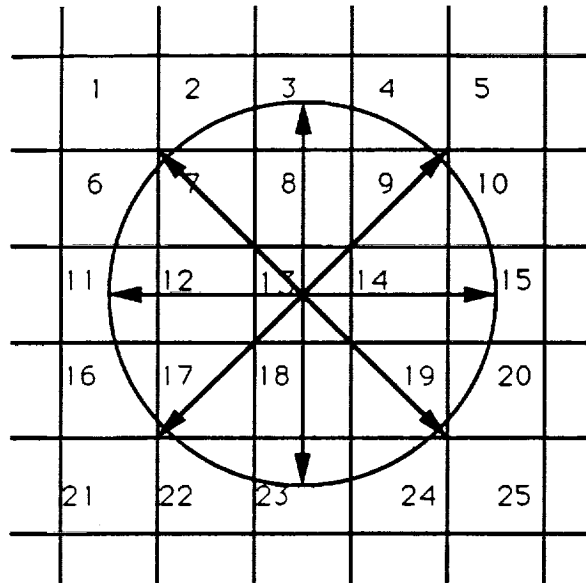


**Figure 4.8** The maximum radius of motion over one time step is to a very high probability less than two cell widths.

Making use of the first observation, at the beginning of the time step the particles are ordered and every processor is storing a value for its particle's current cell index. The particles then go through their motion after which a new value for the cell index must be computed. Both the old and the new values are stored, and now use is made of the second observation. It is convenient at this point to map the cell index into two dimensions and designate the pre-motion values by  $i, j$  and post-motion values by  $i', j'$ . Referring to figure 4.8 and assuming the second observation holds true, then it is obvious that a particle beginning in cell  $i, j$  has at most 25 different *and mutually exclusive* possibilities for its new cell location  $i', j'$ . (In three dimensions there are at most 125 mutually exclusive possibilities.) Conversely, if at the end of its motion a particle is occupying cell  $i', j'$ , there are at most 25 mutually exclusive possibilities for its previous cell position  $i, j$ . Therefore one can divide the set of particles into 25 distinct and ordered subsets based on the 25 distinct possibilities

for a previous cell location. In other words, because a particle in cell  $i',j'$  has 25 mutually exclusive possibilities for its previous cell location  $i,j$ , and because the particles were ordered in their previous cells, it follows that the order must be preserved in 25 mutually exclusive subsets. The problem thus has been reduced to one of identifying these 25 ordered subsets and merging them into just one set.

Identifying each subset is accomplished by simply comparing the previous cell position to the current one. Also at this time it is convenient to count the number of particles in each of the subsets. This is useful later for optimizing the merging step since often there are less than 25 active sources in a time step.

To merge the subsets it is necessary to identify the lowest numbered processor for every cell in each subset, and then enumerate in each subset the processors representing a cell (see figure 4.9). A one dimensional grid, referred to as the "merging grid" and distinct from the physical grid of the simulation, is created with size great enough to contain an element for all the cells in the non-zero subsets. In other words, if there are  $C_{tot}$  cells in the simulation and amongst all the cells  $N_s$  subsets are identified as active sources for the particles, then the merging grid must have at least  $N_s C_{tot}$  elements. Note that  $N_s$  is usually less than 25 and once steady state has been reached it almost always is equal to 9. In other words, active sources usually include just the cell itself and its 8 immediate neighbors. Therefore, although 25 possible sources must be checked, usually only 9 are active. Since  $C_{tot}$  is usually a power of 2, and since VP sets are restricted to powers of two, the greatest advantage occurs when  $N_s$  is 16 or less. If  $N_s$  is greater than 16 then the merging grid must have size  $32C_{tot}$ , but if  $N_s$  is 16 or less, then the merging grid will have size  $16C_{tot}$ . Therefore the merging grid is half the maximum size and any operations performed with the processors of this merging grid will require about half the time required in the larger sized grid.

The primary task for the merging grid is to compute the "global ending index" for every active cell in each active subset. This is just the greatest rank for the particles in a particular cell and subset. As in section 4.3, the `CM_send_with_add` instruction is used to determine the number density for every cell in each subset, then the `CM_scan_with_add` instruction is used to create a running sum of the

number density or the global ending index. Therefore the merging grid now stores the greatest rank in the merged list for the particles in the cell it handles. The particles in each subset can be ranked by subtracting their enumeration in their cell and subset from the global ending index supplied by the merging grid.

The grid result is obtained by the particle processors through the use of the `CM_get` instruction. In order to minimize router contention it is necessary to minimize the number of particle processors active for this step. There are at most  $N_s C_{tot}$  global ending indices, therefore at most  $N_s C_{tot}$  particle processors need to get a global ending index from the merging grid. In other words, one particle processor for each cell and subset needs to get a value from the merging grid. This value can then be copied across the rest of the particle processors in the cell and subset using the `CM_scan_with_copy` instruction. The lowest numbered processor for every cell in each subset was identified earlier in the algorithm and is used for this purpose.

Figure 4.9 is a schematic for the patterns of communication. Steps in the algorithm proceed from left to right across the page. In the first step the  $N_s$  active subsets are identified and the particles in each subset are enumerated with the enumeration re-starting at every cell. This requires  $N_s$  distinct pairs of scan operations, a pair for each set. The first scan is necessary to identify cell boundaries in a set and the second scan enumerates the particles in each cell. The next step of the algorithm requires all processors to send to the merging grid to create the cell number density. The global ending index is then created using a single `CM_scan_with_add`. Next, one processor in every cell in every subset gets its global ending index from the merging grid. This is depicted in the figure by an arrow with heads on both ends thus emphasizing the fact that this operation requires communication in both directions. Finally, this value is copied across the processors in the cell in each subset by using  $N_s$  distinct `CM_scan_with_copy` operations. Now the processors can compute their rank simply by subtracting their enumeration within the cell (step 1 of figure 4.9) from the global ending index computed in the merging grid.

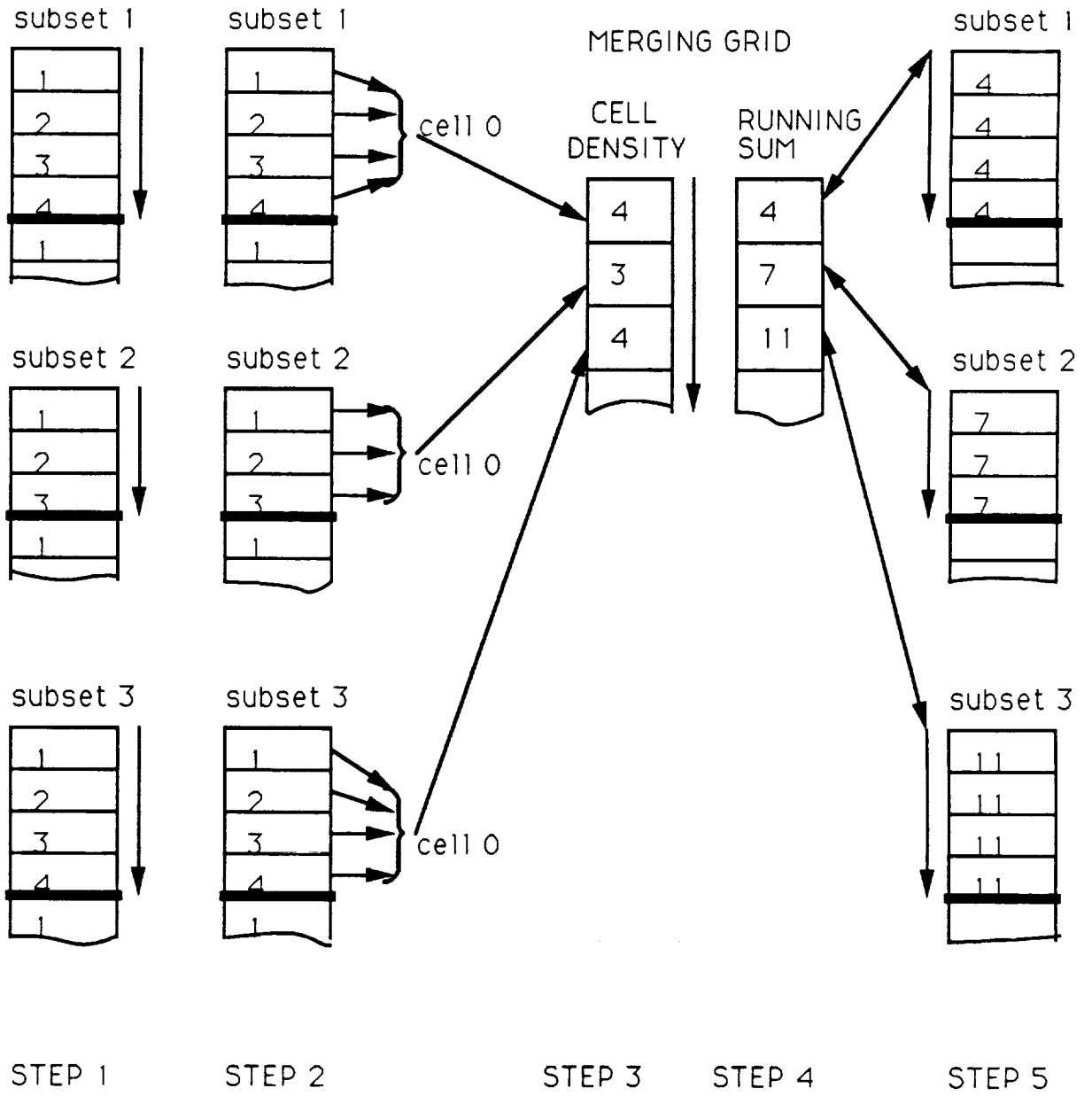


**Figure 4.9** Schematic of the communications pattern in the merged ordered sets sorting algorithm.

### 4.4.3 Maintaining Statistical Independence

It was claimed above that maintaining statistical independence of pairings between time steps is a concern of the simulation. In using the radix sort it was necessary to concatenate random bits to the end of the key and order the particles on this expanded key. The multi-grid sort inherently introduced mixing into the sorting operation by letting particle processors randomly select levels in the multi-grid. The merged ordered subsets algorithm maintains elements of randomization in two ways. The first of these comes about from the manner in which the  $N_s$  subsets are mapped to the merging grid; the second is a result of employing the merging grid to compute the global ending index as opposed to the global starting index for a cell and subset. It is shown in this section that these mechanisms for randomization are not sufficient and it is necessary to further enhance the randomization.

It is worthwhile at this point to analyze the requirements of statistical independence. More specifically, we would like to be able to answer the question "how many identical pairs can one expect between two successive time steps if at each time step the choice of candidate collision pairs is made independent of the previous time step?" This would allow us to gauge quantitatively whether a particular algorithm maintains statistical independence or not. For this purpose, consider an arbitrary cell and let  $n$  be the number of particles within it. One can create  $N = \binom{n}{2}$  different pairs from these particles. In a simulation one actually creates only  $k$  pairs where typically  $k = n/2$ . Clearly there are  $\binom{N}{k}$  different ways to choose  $k$  pairs from  $N$ . The probability of making any particular selection must be  $\binom{N}{k}^{-1}$ . Now consider the probability that in making two selections no two pairs are found common. Since the first selection takes  $k$  pairs out of the pool of available combinations, in the second selection only  $N - k$  pairs are available. So there are  $\binom{N-k}{k}$  ways of choosing  $k$  pairs without using any of the same pairs chosen in the previous selection. Therefore the probability that in the second selection there are no pairs from the first selection must be

$$P(0) = \frac{\binom{N-k}{k}}{\binom{N}{k}}. \quad (4.12)$$



Now consider the probability that in making two selections exactly one pair is common in both. The first selection takes  $N - (k - 1)$  pairs out of the pool, and there are  $\binom{k}{1}$  ways of choosing the one common pair from the  $k$  selected first. Therefore there are  $\binom{N - (k - 1)}{k - 1} \binom{k}{1}$  ways of choosing  $k$  pairs in the second selection with one pair common to the first selection. The probability that the second selection has one pair common to the first must then be

$$P(1) = \frac{\binom{N - (k - 1)}{k - 1} \binom{k}{1}}{\binom{N}{k}}. \quad (4.13)$$

This can be generalized to a probability distribution for finding  $i$  common pairs in two selections as

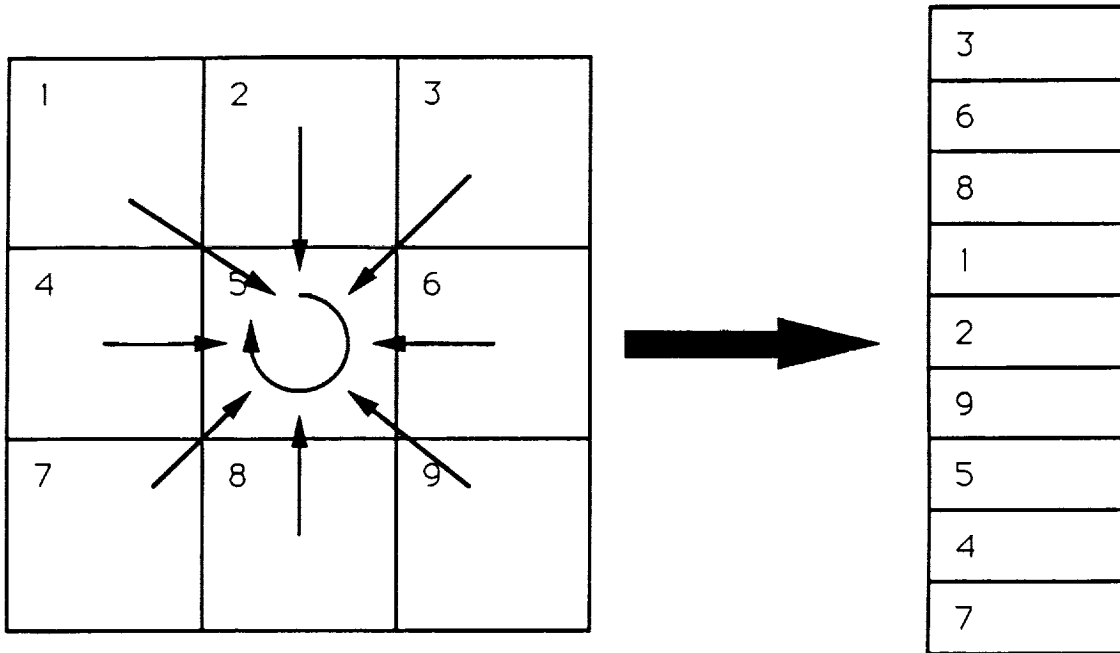
$$P(i) = \frac{\binom{N - (k - i)}{k - i} \binom{k}{i}}{\binom{N}{k}} \quad i = 0, 1, 2, \dots, k. \quad (4.14)$$

This series is known as the *hypergeometric series* and its mean is given by (cf. Guttman, Wilks and Hunter)

$$\mu = \frac{k^2}{N}. \quad (4.15)$$

Now substituting our values for  $k$  and  $N$  in terms of the cell density  $n$ , we find for large  $n$  the mean or expected value of the distribution goes to  $1/2$ . This can be interpreted to mean that if one were to count, over samples taken from many cells with large cell densities, the number of pairs common over two time steps, the average value would be  $1/2$  if the samples were selected independently.

Now consider the merged ordered subsets algorithm and how randomization is introduced there. In mapping the nine subsets to the merging grid there are  $N_s!$  different possibilities. Figure 4.10 illustrates one such possibility for  $N_s = 9$ . For this example, consider an arbitrary cell in the simulation and its nine mutually exclusive sources for particles, here numbered 1 through 9. Each of these sources has an element associated with it in the merging grid. The 9 elements together account for all the particles in the cell under consideration. It is clear that these 9



ARBITRARY CELL AND ASSOCIATED SOURCES

MERGING GRID

**Figure 4.10** One possible mapping of nine sources to the merging grid. In this situation, each cell has at most nine sources for incoming particles which taken for all the cells make up nine mutually exclusive ordered subsets of particles. There are  $9!$  different possibilities for mapping these sources to the merging grid.

sources can be mapped to the merging grid through any permutation of 9. By using a random, statistically independent permutation on every time step randomness is introduced to the outcome of the ranking. Once a permutation is chosen it is used in mapping all the cells at that time step. In other words the permutation is a front end array that gets applied in mapping the  $N_s$  ordered subsets of particles to the merging grid.

Unfortunately this does not completely remove the concern with maintaining statistical independence in even/odd pairings between time steps. Empirical measurements show that one can expect on average two thirds of the particles in the simulation to remain in their cells over one time step. Therefore of the  $N_s$  subsets identified as sources of particles in a particular cell, the greatest source is

the cell itself. Since the ordering is maintained within each subset, many of the particles in a cell can be expected to maintain the same neighbors in the NEWS grid between time steps. This is undesirable since collision candidate pairs are created from neighboring processors and for the collision selection rule to properly simulate the fluid mechanics it is absolutely necessary that the pairs created from the particles in a cell represent a *random* sample of all the different possible pairs which could be created.

The number of pairs created in a cell which are identical over two time steps depends on the particles that leave the cell between the first and the second time step. As an example consider the case of two particles leaving a cell which contained a total of four particles. If the two particles which leave were paired together as collision candidates in the cell, then the two remaining particles also were paired together and in the next time step, since their order is preserved, these two will again be paired together in the cell. Assuming as many particles enter the cell as leave, then half of the pairs created in the cell are identical over two time steps. Alternatively if the two particles which leave were not a pair, then they must have been paired with the two particles remaining in the cell. The two remaining particles, which were not paired together at that time step, will be paired together in the next time step, therefore in this situation none of the pairs created in the cell are identical over two time steps. This example can be made more general as follows. Consider a particular cell, let  $n$  be the cell density and let  $f$  be the fraction of particles which remain in the cell over the time step. If all of the particles which leave the cell were paired amongst themselves as collision candidates, then of the particles which remain all are paired identically over the two time steps. Again assuming the cell density is constant over the two time steps, then  $nf/2$  identical pairs are created. Alternatively if among the  $n(1 - f)$  particles which leave the cell none are paired amongst themselves as collision candidates, then  $nf - n(1 - f)$  particles remain which are paired identically over two time steps leading to  $n(2f - 1)/2$  identical pairs. Typically one can expect a result somewhere between these two extremes. If  $f = 2/3$ , then at worst one third of the pairs are identical and at best one sixth of the pairs are identical over two time steps.

This result is not very encouraging. The additional randomization in the method comes from reversing the order of enumeration of the particles in each cell and subset by using the global *ending* index in computing the rank. The rank is computed by subtracting the enumeration from this value. If the global ending index is odd, then evenly enumerated particles will get an odd rank and oddly enumerated particles will get an even rank. Consequently the pairing of particles, which is done as even-with-odd, will differ between the two time steps. This must occur on average in 50% of the cells, therefore for half of the cells the sample of collision candidate pairs is independent between time steps. Unfortunately, for the other half of the cells one can still expect between one third and one sixth of the pairs to be identical to those of the previous time step. This is far more than one would expect for statistically independent samples.

These results indicate that further randomization is required in this ranking algorithm. This additional randomization must be applied at two scales. Within a particular cell, there must be randomization in the order of the particles in each subset, and there must be randomization of the ordering across the subsets. The opportunity for accomplishing the first of these exists in the enumeration stage of the algorithm. The order of enumeration within each subset can be shuffled in a deterministic fashion at very little cost. The shuffling is performed by re-numbering the processors in a cell after the regular enumeration has been performed. Two shuffling algorithms are employed because each shuffling algorithm is deterministic and two applications of the same shuffle to a data set produces no change in the relative ordering. Alternating between two different shuffling algorithms ensures there is no correlation between samples taken two time steps apart.

Shuffling requires the particle processors to know the subset cell density. This is obtained through the use of the `CM_scan_with_copy` instruction. Figure 4.11 has a schematic for each of the two shuffling algorithms. In the first shuffling algorithm, the processors which previously had an even number are re-numbered continuously from 1 to  $n/2$  and the processors which previously had an odd number are re-numbered continuously from  $n/2 + 1$  to  $n$ . On the next time step when these processors are paired as even-with-odd the renumbering will effectively make pairs



basis of the direction of motion of the particles. For example, one subset will include all the particles which arrived at a new cell from the neighboring cell directly below. Therefore all those particles will tend to have positive  $v$  velocities regardless of how they are rearranged amongst themselves. Some correlation like this will exist in each of the subsets. In order to eliminate such correlations it is necessary to mix the order across subsets.

Of the two shuffles described above, it is clear that only the second one will allow mixing across subsets. The extension of this algorithm to shuffling across a complete cell is straightforward;  $n_{ev}$  becomes the number of even processors for the cell, as opposed to the number of even processors in a subset for the cell. The new numbering will then result in pairings between particles of different subsets in the cell. In a similar fashion the algorithm can be applied separately to the first and last half of the processors for the cell. By alternating between shuffling over the complete cell and shuffling the first and last halves separately, the pairing of collision candidates is made random. The effectiveness of these shuffling algorithms is investigated in Chapter 7 through calculations for thermal relaxation in a heat bath and for shock wave profiles. The results of these calculations could not be correct if the sample of candidate collision pairs taken from a cell is not random.

#### 4.4.4 When Assumptions Fail

The algorithm has been presented from a physical perspective and in the context of a generic cell in a generic time step. Two observations of the dynamics of the simulation were necessary for the algorithm to be valid. It is necessary now to discuss the situations where these observations do not hold true and the algorithm cannot be used.

The obvious situation for which the sort will fail occurs when particles move over more than two cells in one time step. The assumption that particles do not move more than two cell widths in one time step is true to a very high probability, however given the statistical nature of the simulation it is impossible to rule out the possibility of a particle not holding to this assumption. Therefore it is necessary to

trap such instances and switch to the multi-grid sort when they occur.

A more common situation is for the first observation to fail. The first observation claimed that the particles go from an ordered to a disordered state through their motion from one cell to another. This is not true at the upstream boundary of the wind tunnel where new particles must be introduced to maintain the free stream. However the introduction of new particles can be delayed an arbitrary number of time steps, therefore it is convenient to employ the multi-grid sort on those time steps where new particles are introduced and use the merged ordered subsets sort on the other time steps. The alternative is to treat the introduction of new particles as an edge effect and handle it separately. Since the new particles can be introduced in an ordered fashion the algorithm can be modified to handle this situation by performing an additional merging. In other words, after ordering the particles in the flow one introduces the new particles and merges these with the flow particles. The merging now involves only two ordered subsets and proceeds much faster than with  $N_s$  subsets.

#### 4.4.5 Performance and Extension to Three Dimensions

The performance of the merged ordered subsets algorithm depends to some degree on  $N_s$ , the number of subsets to be merged.  $N_s$  is usually 9, and for this case the merged ordered subsets algorithm takes about 45% of the time of the radix rank.

The performance of the algorithm scales linearly with the number of particles in the simulation. There is also some dependence of performance on  $C_{tot}$ , the number of cells, since this number determines the size of the merging grid to be used. However the fraction of work performed by the merging grid is decoupled from the fraction corresponding to the particles. Recall that the merging grid is used to perform one scan and one send operation. The time to perform these operations is dependent on  $C_{tot}$  and is independent of  $N$ , the number of particles. Therefore the algorithm can be characterized as scaling as  $O(N + C_{tot})$  although this should not be interpreted too literally since the time spent by the particle processors relative

to the grid processors is dependent on the particular problem.

The algorithm has been presented and discussed for only two dimensions. The extension to three dimensions is straightforward but does involve a loss in performance due to increased communications. In three dimensions there are at most 125 mutually exclusive sets instead of 25. Again one can expect for the vast majority of time steps only immediate neighbors will act as sources of particles in a cell, therefore in three dimensions 27 ordered subsets will usually be identified as opposed to 9 ordered subsets in two dimensions. The algorithm requires three scan operations with the particle processors per subset. In two dimensions these operations account for 55% of the time to rank. In the worst case, in three dimensions that fraction of the algorithm would triple in time so overall the new ranking algorithm would take about 2.1 times longer than for two dimensions. In addition, the merging grid would be twice as large in three dimensions and the time spent by the merging grid would double. Based on these linear extrapolations it is doubtful that the algorithm would be competitive. However the above discussion neglects to consider the smaller size of each subset in three dimensions and the corresponding effect of reduced contention in the enumeration of each subset. Therefore it is possible that in three dimensions the algorithm would remain competitive and it should not be ruled out for consideration until it has been implemented and tested as such.



## Chapter 5

# Implementing General Boundary Conditions

The discussion thus far has focused on the collision of particles amongst themselves, however of equal importance to a successful implementation of a particle simulation is also the collision of particles with the surfaces within physical space. The physics of this class of interaction is not as well understood as one would hope. Most models for particle–surface interaction assume a perfect crystal lattice for a scattering surface which interacts with incident particles through some interactive potential such as inverse power–law or Lennard–Jones (Goodman and Wachman (1976), Hurlbut (1986)). For purposes of a particle simulation the exact mechanics of these interactions need not be addressed. As with collisions between particles, the post–collision thermodynamic state can be sampled from an equilibrium distribution, however the post–collision position of a particle is more difficult to define. The situation worsens considerably when dealing with ablating surfaces. The present work considers only the case of neutral particles colliding with non–ablating surfaces and makes use of the models developed by Woronowicz (Woronowicz and McDonald (1989)). Reference is made to more complex particle–surface interactions as appropriate.

## 5.1 Representation of Physical Space

### 5.1.1 Faceted Geometry Approximation

Physical space is represented by the cartesian grid of cubical cells discussed in Chapter 3. Most problems of general interest involve the flow about some aerodynamic body, therefore it is usual to set up physical space to simulate a wind tunnel. Other configurations are occasionally of interest, for example a simple adiabatic mixer is useful for studying the relaxation of a gas into the equilibrium state or a standing shock configuration is useful for investigating the internal structure of a shock wave. These configurations are generally important only for developing or testing new collision models and have been implemented separately from the wind tunnel configuration specifically for these purposes.

Surfaces are defined within the grid of cells by planar segments, therefore a curved surface is approximated by a faceted geometry, as in figure 5.1. This is a good approximation if the radius of curvature of the surface is much greater than the dimension of the cell. Therefore in designing a geometry for a specific problem it is necessary to ensure that a sufficient number of cells are available to accurately represent the body. This is consistent with the paradigm under which the current method has been developed, that is one where computationally efficient algorithms allow greater numbers of particles, and therefore greater numbers of cells, to be employed in a simulation.

This faceted body representation was first introduced by McDonald and Baganoff (1988) and is a useful approximation which allows a great simplification both in the procedure for identifying particles which undergo boundary interaction and in defining the interaction for those particles. Each facet is defined by the equation of a plane

$$Ax + By + Cz + D = 0 \quad (5.1)$$

such that the unit normal to the plane is then  $\mathbf{n} = (A, B, C)$  and  $D$  is the displacement of the plane from some origin with a fixed position for all the facets.

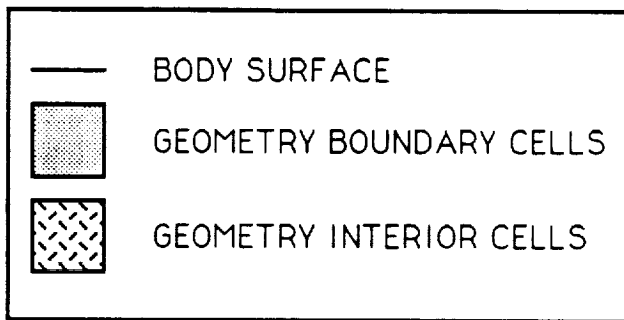
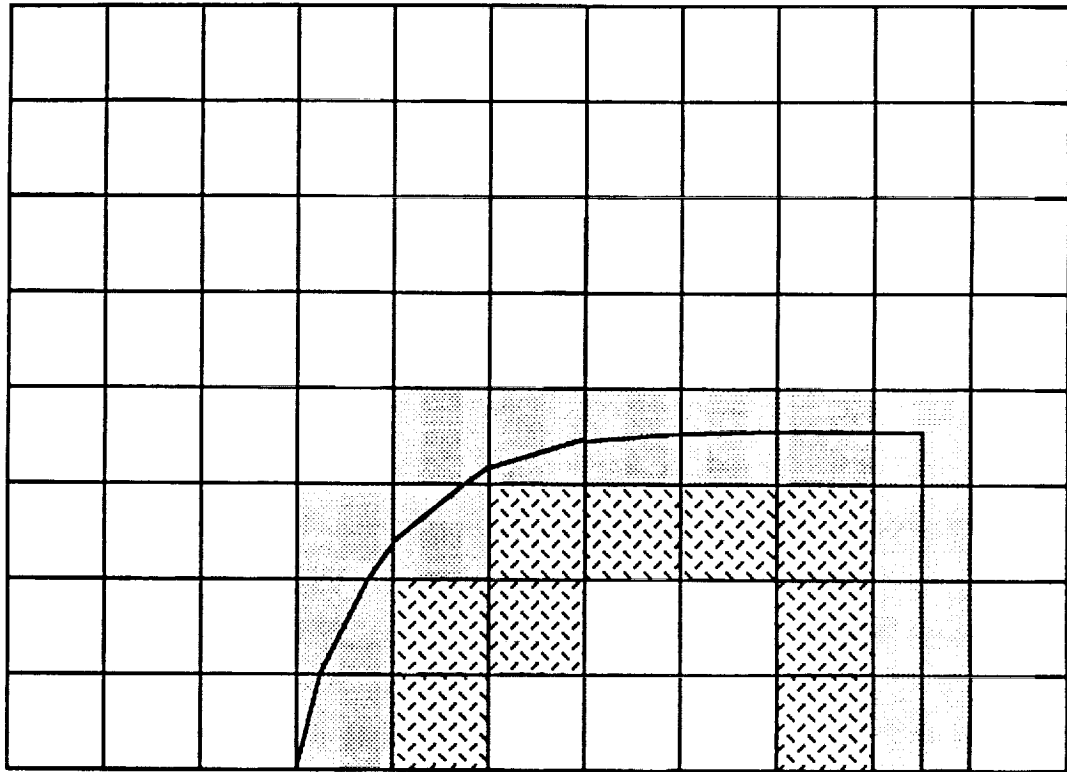


**Figure 5.1** The faceted body approximation. Curved surfaces are approximated by planar facets leading to a much simplified calculation for the boundary interaction. Cells which are intersected by the surface are unambiguously associated with a facet, however it is also necessary to associate some interior cells with a facet in order to handle particles with sufficient speed to travel beyond the boundary cells in one time step.

Each cell which gets intersected by a body surface must then have associated with it the parameters  $(A, B, C, D)$  representing the surface. It is also necessary for one or two layers of cells interior to the body to have associated with them these same parameters in order to capture any particles which had sufficient speed to cross the surface and travel to an interior cell. All cells associated with the geometry through these parameters will be termed *geometry cells*. It is a relatively straightforward procedure to determine which particles have moved behind the surface. For a particle  $i$  lying in a geometry cell the outward displacement,  $d_n$ , between the particle and the plane defining the facet is given by

$$d_n = Ax_i + By_i + Cz_i + D. \quad (5.2)$$

If  $d_n$  is negative then the particle must have moved behind the surface and the appropriate boundary interaction must be performed. There exists some ambiguity when particles have travelled to interior cells in that the interior cell will be associated with a single, particular, facet of the surface when in some instances it may be possible for a particle to have arrived at that cell by crossing a different facet from the one with which the cell has been associated. However, since the body surface must have a large radius of curvature with respect to a cell dimension, this introduces only a small and acceptable error.

A complete body definition must also include values for the fractional cell volumes,  $V$ , of the boundary cells. These must be used to adjust the selection rule (equation (3.1)) for colliding particles in these fractional cells. Therefore as a minimum, a body may be defined by a table of the values  $A, B, C, D$ , and  $V$  for all the surface cells and interior cells as necessary. For complex three dimensional bodies the task of determining these values can be carried out using a method devised by William Feiereisen and described in Feiereisen and McDonald (1989). On the Connection Machine only two dimensional problems are considered, primarily because the memory limitations make realistic three dimensional problems unfeasible. Consequently a full body definition requires only the values  $A, B, D$ , and  $V$  to be determined, and in describing the algorithms reference may be made to body segments instead of body facets.

On the Connection Machine the principal problem that must be resolved to efficiently implement body definitions of this type is again communications related. The following section describes in some detail how the communications time can be minimized in a manner that also optimizes the computational effort. The latter becomes especially important when the surface interactions to be modelled become complex.

### **5.1.2 Storage of Geometry Table**

The first issue which must be addressed in implementing this method is the storage of the geometry table. The problem of storage here is quite different from the one encountered in implementing the collision algorithm. The tables necessary for the collision algorithm represent distributions which must be accessed randomly. Since the collection of particles making up the simulation are themselves a distribution it makes sense to store the two in the same fashion. In fact the random motion of the particles is used to help ensure that entries taken from these tables represent random samples from the distributions. The geometry table, however, must be accessed in an ordered fashion and this randomizing mechanism is neither necessary nor useful. For this reason the geometry table must be stored in its own distinct VP set.

### **5.1.3 Definition of a Geometry Space**

Having decided upon a method of storage for the geometry information, the question now becomes how to access this information in an efficient manner. McDonald (1990) describes how this is done in a vectorized fashion in his PSim code on the Cray 2. In McDonald's implementation all the cells representing physical space get mapped to a three dimensional array which stores a pointer to the appropriate entry in the geometry table for each geometry cell and a null pointer for the rest of the cells. Therefore to get the geometry information it is necessary to access this array once for each particle in the simulation to determine if a particle is occupying a geometry cell and then use the pointers to obtain the

appropriate geometry table entry. It would be unreasonable to implement such a mechanism on the Connection Machine. The communications penalty would be great due to router contention from all the processors representing particles trying to access the table of pointers. In order to minimize such router contention it is useful to define within the simulation space a smaller rectangular subspace which is just large enough to wholly contain the body, as in figure 5.2. This subspace is termed the *geometry space* and only those particles occupying the geometry space are considered for boundary interaction. The purpose in defining such a subspace is to greatly reduce the communications traffic by making use of the fact that most bodies of interest will occupy only a small fraction of the physical simulation space, therefore one can easily remove a large fraction of the particles from consideration for boundary interaction. The only loss in generality is in the assumption of a wind tunnel configuration. That is, inlet and outlet conditions are hard wired to simulate a supersonic wind tunnel consequently the code can only be used in such a configuration. As discussed earlier in this chapter, other configurations are only of interest primarily in the development of new models and it is not unreasonable to implement specific codes just for this purpose.

Having defined a geometry space in this manner, it is necessary to map the geometry in that restricted space. The mapping used here is somewhat different from that employed on the Cray 2, again a result of reducing communication cost. On the Connection Machine, indirection can be used to reduce storage requirements as it is on the Cray 2 only by incurring a performance penalty in communications cost. If memory is at a premium then the extra cost of the indirect mapping may be warranted, otherwise it is best to use a direct mapping both for simplicity and in order to minimize communication cost. The following paragraphs describe first the indirect mapping and then the direct mapping.

In the indirect mapping, the geometry table is split into two, one table stores just the cell volumes for the geometry cells and the other stores the geometry values  $A$ ,  $B$ , and  $D$  for the interior and boundary cells. The two tables are stored in the same set of processors however indirection exists only for storing the second table and not in storing the first. Since there are usually less interior and boundary cells

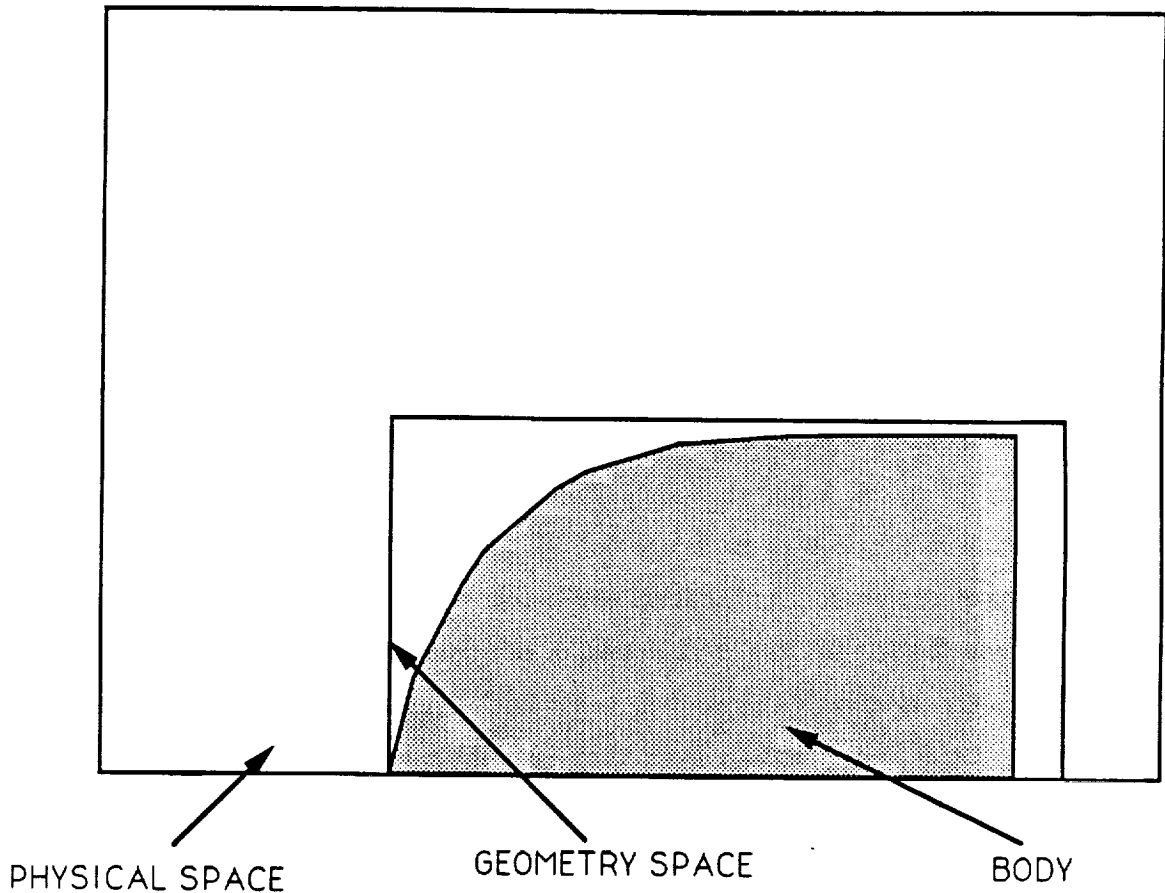


**Figure 5.2** Definition of physical space and geometry space in a wind tunnel configuration.

than there are geometry cells it is possible to save memory by storing each geometry value of the second table in a separate processor as in figure 5.3. This assumes that either the number of geometry cells or the number of virtual processors in the VP set is at least three times greater than the number of interior and boundary cells, which generally is a safe assumption given that VP sets cannot be created with VP ratio less than one.

There is a direct mapping between the cells in the geometry space and the table storing the cell volumes for these cells. In other words for every cell in the geometry space there is an entry in a table containing the corresponding cell volume. Processors representing particles in the geometry space can then access this table

directly to get the cell volume. Indirection arises when these processors need to get the surface geometry values stored in the second table. The pointers to the entries in the second table can be packed into the same 32 bits storing the cell volume by sacrificing some unnecessary precision in this value. The cell volume is a floating point quantity always in the range  $[0, 1]$ . Therefore to pack a pointer and a cell volume into 32 bits it is simplest just to sum the pointer value and the cell volume together. Then to retrieve the pointer it is necessary only to truncate the packed result, and to retrieve the cell volume it is necessary only to subtract the retrieved pointer value from the packed result. The pointer indicates the location of the first geometry value,  $A$ , for that cell. The geometry values  $B$  and  $D$  are stored in the neighboring processors as in figure 5.3. The three values may be obtained by three successive router communication events, however this will triple the router overhead which for the `CM_get` instruction is relatively great. A better procedure is to temporarily modify the geometry table by letting the processors storing the  $A$  values get the  $B$  and  $D$  values from their neighbors using two successive NEWS communication events, and then the three values  $A$ ,  $B$ , and  $D$  can be obtained from a single processor with a single router communication event. Furthermore, if the number of interior and boundary cells is less than the number of router nodes for the geometry VP set, it is possible to arrange the second table such that each processor storing an  $A$  value is on a single router node therefore router node contention is minimized.

In the direct mapping the geometry table is not split, therefore there is a complete entry with  $A$ ,  $B$ ,  $D$ , and  $V$  for every cell in the geometry space (see figure 5.4). A reflected binary Gray code is used in mapping the table to the processors. This ensures that table entries are spread amongst all the router nodes thereby reducing router node contention when the table needs to be accessed. Note that with the direct mapping there is only a single communication event required to access the table. Therefore the overhead in starting the communication is paid only once, hence the communication cost tends to be lower for the direct mapping.

The direct mapping requires more storage than the indirect mapping because all the geometry cells which are not associated with a boundary must still have



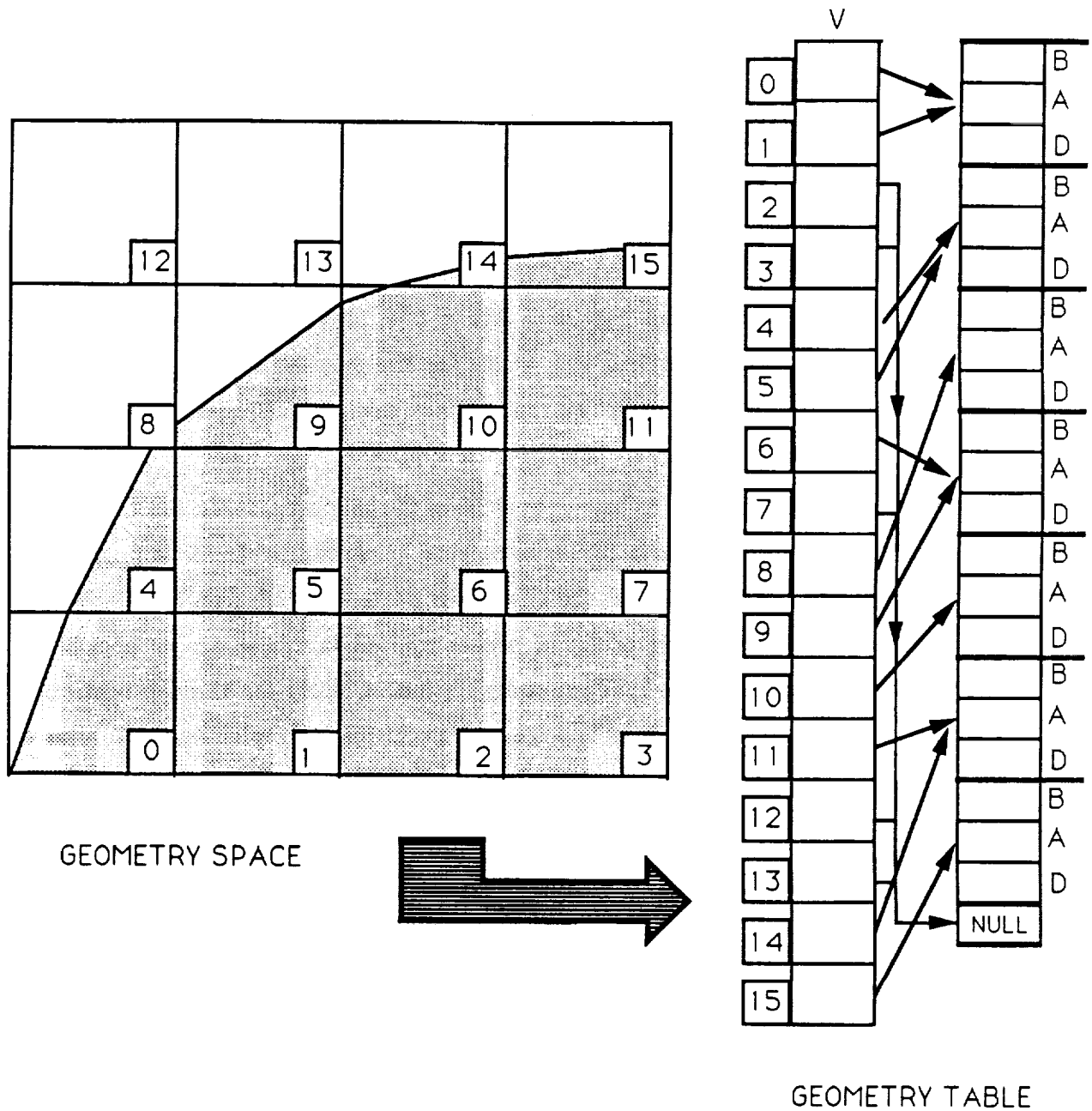


**Figure 5.3** Indirect mapping between geometry space and geometry table. For every cell in the geometry space there is an entry in the geometry table storing the cell volume  $V$  and a pointer to the storage location of the rest of the geometry values  $A$ ,  $B$ , and  $D$ .

space allocated for the  $A$ ,  $B$ , and  $D$  geometry values. However, the difference in

storage requirements is not as great as one would think because of the constraint the Connection Machine has on the minimum size VP set one can create. For example, the configuration installed at NASA Ames requires a minimum of 32768 (or 32k) virtual processors in a VP set when all 32768 physical processors are used. Consequently the smallest size table which can be stored must have at least 32k entries. For the two dimensional problems being considered the geometry space will usually consist of somewhat less than 32768 cells, therefore for the direct mapping the storage requirements can be met with  $32k \times 4 = 128k$  words. On the other hand the indirect mapping requires 32k words for the two tables, assuming they can be fit in a single VP set. Therefore the indirect mapping requires one quarter the amount of storage necessary for the direct mapping.

The above discussion serves to highlight some of the inadequacies in the Connection Machine architecture when it comes to storing small tables. In large part the impressive performance achieved on the Cray 2 in particle simulation calculations has been accomplished by using tables of pre-computed values wherever possible in order to avoid performing redundant computation. Clearly for the Connection Machine to compete there must exist adequate mechanisms for implementing similar table driven algorithms. Thus far the collision algorithm of Chapter 3 and the boundary conditions of this chapter have required table look up. Each case required careful attention to the manner of storage in order to minimize the cost of access. Each resulted in a very different manner of storage but common to both was a tradeoff of memory for communications performance. Consequently in both cases the storage requirements were greater than that demanded by the table.

The observations made in the preceding paragraph help substantiate a more general statement one can make about the Connection Machine, namely that memory requirements for algorithms implemented on the Connection Machine are generally greater than for the same algorithms on vector machines. This is due in part to the tradeoff between memory and communications but is more accurately prescribed to an inherent characteristic of the architecture. An example of this is manifest in the minimum table size requirement described above, but the implications are more general. Consider that the allocation of temporary space is

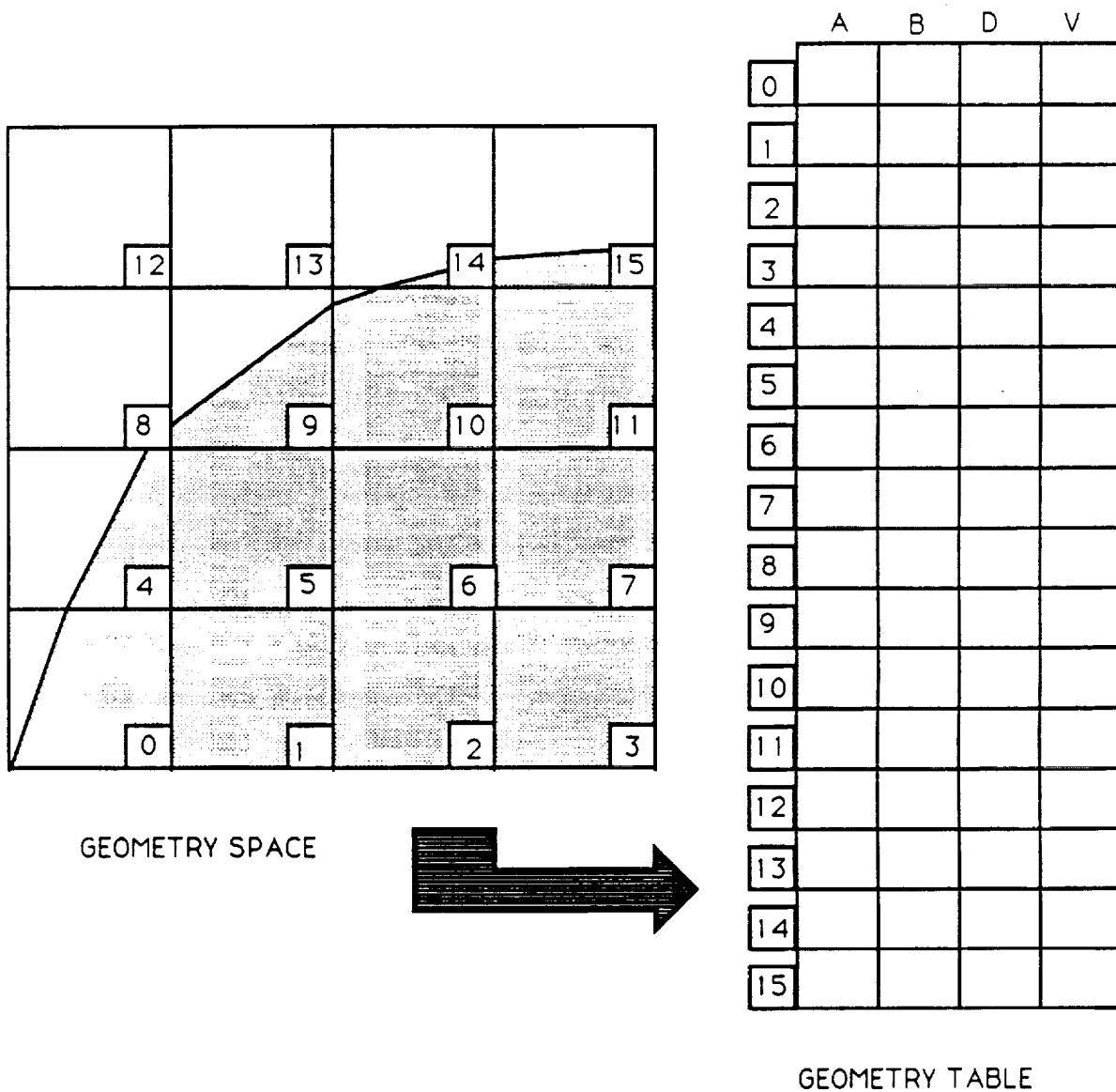


**Figure 5.4** Direct mapping between geometry space and geometry table. For every cell in the geometry space there is an entry in the geometry table storing the values *A*, *B*, *D*, and *V*. The geometry table is stored in its own VP set which, due to the minimum size restriction on VP sets, often will be much larger than the table. Table entries are spread amongst all the router nodes by use of a reflected binary Gray code mapping.

effectively equivalent to creating a table, therefore the minimum size temporary space which can be allocated is 32768 bits, in other words one bit allocated in each virtual processor of the smallest size VP set one can create. In reality the situation is worse because rarely can one use only a single bit of temporary space per processor and rarely is one operating in the minimum size VP set. In a particle simulation it is often necessary to allocate temporary space in the VP set storing the particles. This VP set may have over two million virtual processors in which case allocating a single word of memory in each processor leads to 2M words (that is 8 MB) of temporary space. Note that all this space must get allocated *even* if not all the processors are active for the calculation which requires the temporary space. This is due to the SIMD nature of the Connection Machine and cannot be avoided. All the processors in the active VP set must receive and be able to execute the instructions issued from the front end computer, therefore reference to memory locations within a processor must be identical for all the processors (since these must be part of the single instruction issued by the front end) consequently there can be only one stack pointer for all the processors in a VP set. The next section examines how these restrictions can be circumvented in some situations by spawning slave VP sets of smaller size.

#### **5.1.4 Master and Slave VP Sets**

Once the geometry space has been defined and the processors representing the particles within it have been identified, it seems the next logical step would be to have those processors get the geometry information from the geometry table and then carry out the necessary calculations. It is not immediately obvious why one would want to carry out the calculation with a different set of processors since that would introduce additional communication. However, this situation is analogous to sampling macroscopic quantities (see section 3.4) in that the total cost in communication can be reduced by initiating the communication from a smaller VP set. The reason for this has to do with the way instructions are carried out by the Connection Machine. Recall that instructions are issued from the front end and

sequenced to a set of virtual processors. Virtual processors are created from the physical processors by allocating physical processor memory in equal amounts for each virtual processor and then looping through the microcode of a given instruction once for each virtual processor. The important point to realize is that the loop is carried out even if the virtual processor is not active for the instruction. Therefore in general the cost of executing an instruction increases linearly with VP ratio regardless of the number of processors active. The most obvious exception to this rule is in the case of router communication where router network contention is reduced when less processors are sending messages, however from figure 2.3 it is clear that this has a second order effect on performance compared to reducing the size of the VP set. In the current situation we have isolated a relatively small number of processors in a very large VP set which need to get information from processors in a different VP set. Clearly there is a huge penalty to be paid if this operation is performed from the large VP set since most of the processors there will be inactive. The better solution is to create a separate VP set, which here will be called the *slave* VP set, just to accommodate the necessary data from the active processors and then perform these operations from there. The larger VP set for which the operations are to be performed naturally is called the *master* VP set. The slave VP set becomes a useful mechanism for improving performance only when there is a relatively large disparity between the VP ratio of the master and the slave VP sets. If this is the case then the cost of sending information from the master to the slave can be more than recovered.

Given the considerations of the preceding paragraph, the algorithm for computing the boundary interactions is as follows. A slave VP set just large enough to accommodate all the particles in the geometry space is created. The processors representing the particles in the geometry space then send their self-address and the cell index of their particle to the appropriate processor in the slave VP set. The sending processors here are in the master VP set, and the particle information in the master VP set is in the *master table*. The self-address of a master processor is actually the minimum required by the slave for it to proceed, however in the current context the next step for a slave would be to get the cell index from the master,

therefore it proves more efficient for the master to send both the self-address and the cell index in one package. With this information the slave processors can then proceed to get the geometry information from the geometry table. The pattern of communication here will depend on the method of storage for the geometry table, that is whether there is an indirect mapping or a direct mapping of the geometry table. The preceding section described the method of access in both cases. From the geometry information, specifically from the cell volume, a slave processor can determine if its particle is occupying a boundary or interior cell. Such particles must be checked to see if they have crossed into the body and must be reflected back into the flow. This requires the slave processors to get the position and velocity components from the master table and then apply equation (5.2). The manner of reflection depends on the type of surface being represented.

Three different types of surfaces can be represented corresponding to inviscid, isothermal, or adiabatic boundary conditions. The methods for simulating these types of surfaces are discussed in the next section therefore the details will not be described here. Essentially, for those particles which do undergo surface interaction the slave processors must get more information from the master table and possibly from the geometry table as well, perform some calculations, and then return the updated position and velocity information to the master table. The final operation which the slave processors must perform is getting the new cell volume for those particles which changed cells after reflection. This information along with the updated position and velocity for the reflected particles is returned to the master table. This ends the algorithm, the memory of the slave processors can now be deallocated and the slave VP set can be destroyed.

## **5.2 Models for Particle-Surface Interaction**

In this section three models for particle-surface interaction are discussed; they correspond to simulating inviscid, isothermal, and adiabatic boundary conditions.

### 5.2.1 Specular Reflection

The simplest surface interaction to model is specular reflection of a particle from a stationary surface. Specular reflection is defined such that the angle of incidence is equal to the angle of reflection, as in figure 5.5. No energy is exchanged between the particle and the surface nor is the tangential velocity of the particle affected, therefore this type of interaction is suitable for simulating inviscid boundary conditions. Typically only the wind tunnel walls are treated as inviscid but for validation purposes it is useful to compare simulation results to theory, in which case simple bodies (such as the two dimensional wedge) may also be treated as inviscid.

The only information necessary to perform the specular reflection of a particle from a plane surface is the definition of the plane itself. A particle  $i$  lying a distance  $d_n$  behind a plane with outward unit normal  $\mathbf{n}_s$  will be reflected as

$$\mathbf{x}'_i = \mathbf{x}_i - 2d_n\mathbf{n}_s. \quad (5.3)$$

The velocity will be reflected as

$$\mathbf{v}'_s = \mathbf{v}_i + 2(\mathbf{n}_s \cdot \mathbf{v}_i)\mathbf{n}_s. \quad (5.4)$$

Equations (5.3) and (5.4) can be generalized for the case of a non-stationary surface. Such a situation is of interest primarily for the development of general entrance and exit conditions in a wind tunnel simulation although it can also be of interest in the study of flow over a body in motion.

To generalize (5.4) it is necessary only to substitute the relative velocity  $\mathbf{v}_{rel,i}$  between the particle and the surface, therefore

$$\mathbf{v}'_s = \mathbf{v}_i + 2(\mathbf{n}_s \cdot \mathbf{v}_{rel,i})\mathbf{n}_s \quad (5.5)$$

where

$$\mathbf{v}_{rel,i} = \mathbf{v}_i - \mathbf{v}_s \quad (5.6)$$

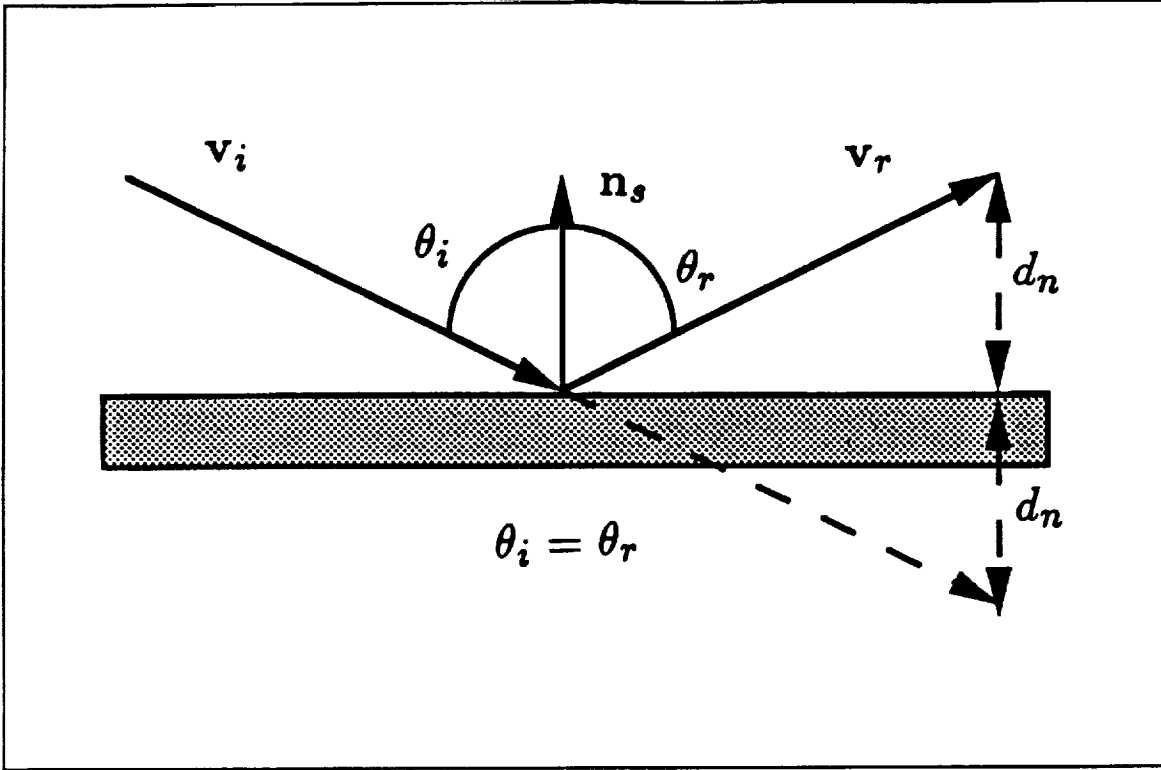


Figure 5.5 Specular reflection of a particle from a stationary plane.

and  $\mathbf{v}_s$  is the velocity of the surface.

The generalization of (5.3) is not quite as straightforward. It is necessary to consider the time step in two parts, that is the time before interaction and the time after interaction. The time before interaction,  $t_{bi}$  is just the time for the particle to have moved from its initial position to its intersection with the surface. Therefore

$$t_{bi} = \frac{\mathbf{n}_s \cdot (\mathbf{x}_s - \mathbf{x}_i)}{\mathbf{n}_s \cdot (\mathbf{v}_s - \mathbf{v}_i)} \quad (5.7)$$

where  $\mathbf{x}_s$  is any point on the surface. The new particle position must be given by advancing the old position for a time  $t_{bi}$  at the pre-interaction velocity  $\mathbf{v}_i$  and for time  $\Delta t - t_{bi}$  at the post-interaction velocity  $\mathbf{v}'_i$ . In other words,

$$\mathbf{x}'_i = \mathbf{x}_i + t_{bi}\mathbf{v}_i + (\Delta t - t_{bi})\mathbf{v}'_i \quad (5.8)$$

where  $\Delta t$  corresponds to a full time step. Combining with (5.7) this becomes



$$\mathbf{x}'_i = \mathbf{x}_i + \Delta t \mathbf{v}_s + 2\mathbf{n}_s \cdot (\Delta t(\mathbf{v}_i - \mathbf{v}_s) - (\mathbf{x}_i + \mathbf{x}_s))\mathbf{n}_s. \quad (5.9)$$

### 5.2.2 Diffuse Reflection With Surface-Driven Energy Exchange

The diffuse reflection of a particle from a surface represents a more realistic kind of surface interaction. A diffuse reflection is defined as one where the post-interaction velocity is independent of the pre-interaction velocity, consequently the post-interaction velocity must be sampled from some distribution. It can be proved theoretically (cf. Wenaas (1971)) that in equilibrium the diffuse scattering of particles from a surface must obey the cosine law. The cosine law states that particles striking a surface element will scatter with intensity proportional to  $\cos \theta_s$  regardless of the angle of incidence, where  $\theta_s$  is the scattering angle measured from the surface normal. Note that this law does not state that particles leave a surface in random equally weighted directions but rather the directions are weighted by a factor of  $\cos \theta_s$ . This is the result of biasing the equilibrium distribution to include only those particles which have crossed the plane represented by the surface. In other words, the cosine law can be arrived at by assuming that in thermal equilibrium the velocity distribution of particles *leaving* a surface is identical to that of particles *arriving* at the surface, both of which are distinct from the velocity distribution of the gas as a whole.

From the above discussion it is clear that the post-interaction velocity of a particle undergoing diffuse reflection can be arrived at by sampling from an equilibrium distribution and accepting only a result which directs the particle away from the surface. Alternatively, one can accept any sample from an equilibrium distribution but reverse all the components of a result which directs the particle back into the surface. The question remains as to the temperature of the equilibrium distribution to be sampled. If this value is fixed for all particle-surface interactions then the energy exchange between the particles and the surface can be considered surface-driven and the boundary condition is isothermal.

In the current context, the post-interaction velocity can be sampled directly from the thermalizer particles. As described in Chapter 3, particles which are not in the flow are kept in a separate reservoir, or thermalizer, and are allowed to collide amongst themselves. These thermalizer particles represent an equilibrium gas, therefore to sample a post-interaction velocity for diffuse scattering it is necessary only to use the velocity of a randomly selected thermalizer particle. The thermalizer is kept at the free stream temperature, consequently to simulate a surface at some arbitrary temperature it is necessary first to scale the thermalizer particle velocity by a constant factor equal to the square root of  $T_s/T_0$  where  $T_s$  is the surface temperature and  $T_0$  is the free stream temperature.

Unfortunately, there is no law similar to the cosine law for determining the post-interaction position of the particle. Currently the post-interaction particle position is defined by

$$\mathbf{x}'_i = \mathbf{x}_i - d_n \mathbf{n}_s \quad (5.10)$$

which is similar to equation (5.3) but always places the particle directly on the surface. Woronowicz and McDonald (1989) report some flow field sensitivity to the placement of the particle after boundary interaction, which is not unexpected given the direct influence this has on the boundary layer. Placing the particle on the surface is equivalent to assuming that the surface interaction time is on the order of a time step. This is not a good assumption and it is more likely that the surface interaction time is on the order of the collision time which is much less than a time step. The alternative then is to place the particle somewhere in the flow, consistent with assuming a short surface-interaction time. However this too is less than satisfactory. Consider that the post-interaction velocity must direct the particle away from the surface (a necessary restriction to satisfy the cosine law) therefore placing the particle away from the surface has the effect of creating a vacuum right at the surface which is also undesirable. The issue is far from resolved and is in an area which clearly deserves further investigation. Nonetheless (5.10) does seem to reproduce satisfactory results and is currently used for all diffuse reflections.

### 5.2.3 Diffuse Reflection With Gas-Driven Energy Exchange

The third type of surface which can be simulated is adiabatic and is defined as allowing no net heat flux across the boundary. The specularly reflecting surface is a very restricted example of an adiabatic boundary condition in that no energy is transferred into the surface, however the reflection is not diffuse. The more general case must have diffuse reflection and allow energy transfer into the surface on an individual basis but such that over many interactions there is no net energy transfer. The approach described in the previous section cannot be applied here because the surface temperature is not fixed or known *a priori*. The surface temperature is dependent on the state of the gas at the boundary, therefore the energy exchange between the particles and the surface can be considered gas-driven and requires a different approach to specify.

The approach taken here was first proposed by Woronowicz and McDonald (1989). In this method a *boundary particle* is created to represent the surface, then when particles interact with the surface they do so by undergoing a collision with this boundary particle. The collision is inelastic in the sense that the internal energies of the particles are allowed to participate in the energy exchange, however total energy is conserved over the collision. The surface is always in thermal equilibrium with the gas therefore the surface temperature will equal the gas temperature and there can be no heat flux into the surface. However the boundary particle will tend to acquire a net momentum from repeated collisions with flow particles which are always directed into the surface. This problem is alleviated by restricting the motion of the boundary particle to a cubical cell. This is accomplished simply by permuting the boundary particle velocity components after each collision and there is no need to trace the particle's position.

It is important to note that the model, as described thus far, allows only a single temperature for the entire surface represented by the boundary particle. In other words there is perfect thermal conductivity in the surface. Initial investigations with this model concentrated on the flow over a wedge and used a single particle to represent the whole wedge. It was found that the rear of the wedge acquired the

same temperature as the face and therefore had a stronger influence on the wake flow than ought to have been the case. The obvious solution for such a situation is to have two boundary particles, one for the face and one for the rear of the wedge. Since the flow over a wedge is conical the face will acquire a single temperature and a single boundary particle can be used to represent this surface. However, more general geometries cannot be represented as simply and in the most general case one would require a boundary particle for each cell of the surface. This is the model implemented on the Connection Machine.

On the Connection Machine there exists a boundary particle for every cell associated with the surface. The particle is monatomic therefore only the three translational velocities need to be stored. These are stored in the same VP set used to store the geometry information and again a binary reflected Gray code is used to ensure that the particles are spread evenly amongst all the router nodes for optimal communication. The boundary particle information is accessed by the slave VP set after the slave processors have determined which flow particles must undergo surface interaction. At this point the appropriate slave processors get the boundary particle information and perform a strictly elastic collision between the monatomic boundary particle and the flow particle. The updated boundary particle state is then returned to the geometry VP set. Note that all the particles in a particular cell that undergo surface interaction are made to collide with a boundary particle which is in the same state for each collision. After collision with the flow particles only one updated state is actually returned to the boundary particle, in other words only one surface interaction in a time step is allowed to change the state of the boundary particle. This imposes a small restriction on the influence a single surface interaction has on other surface interactions in that time step. For a given time step and in a given cell all the surface interactions are carried out independent of each other and the result of one interaction does not affect any other for that time step. Consequently the amount of energy exchange between the surface and the gas over one time step is more restricted than it would be if each surface interaction in a cell were carried out sequentially and thus allowed to influence the state of the surface for all succeeding interactions. However this is a small and therefore

acceptable restriction since the actual number of surface interactions in a cell is small and since the particles in a cell are all in a similar state. In fact gradients cannot be supported across a cell and the particles in a cell can be considered to be in thermal equilibrium therefore it is not strictly necessary to allow a dependence between particle-surface interactions within a time step.



## Chapter 6

# Active Flow Visualization Through the I/O Subsystems

The capability of transmitting at high bandwidth to I/O subsystems is a feature of the Connection Machine which allows the investigation of transient or unsteady flows. In particular, the DataVault can be used to save the solution throughout the transient or unsteady phase, and the frame buffer can be used to visualize the solution either in real time or as play back from the DataVault. The performance penalty in carrying out these operations during the calculation is minimal because the links to these I/O subsystems are of very high bandwidth. This chapter discusses the visualization technique employed with the particle simulation and various strategies for applying this technique in the investigation of transient flow phenomena. Finally, the extension of this technique to three dimensional flows is described.

### 6.1 Visualization Technique

#### 6.1.1 Mechanism for Visualization

The particle simulation method is particularly appealing to visualize because

the calculation is tied closely to the actual gas dynamics. The mechanism for flow visualization in real time and as play back is the same. Each particle is represented by a colored pixel in the display, therefore the motion of the particles is seen in the corresponding motion of the colored pixels.

This mechanism for visualization is unique in the quantity of information that can be assimilated by the viewer. Density in the flow is immediately visible through the concentration of painted pixels in the display. Similarly, the velocity field is visible in the motion of the painted pixels in the display. Therefore there is a direct correspondence between the number density and velocity in the flow and the painted pixel density and motion in the visualization. Furthermore, it is possible to concurrently visualize another thermodynamic variable, such as temperature or pressure, by mapping it to a color scale and applying this scale in painting the pixels. Such thermodynamic variables represent macroscopic flow quantities generated from the particle distributions within the cells, therefore within a cell a single color value is representative of all the particles. The color of a particle in the visualization corresponds then to the value of the macroscopic flow quantity in that region of the flow.

The limitation in this mechanism usually lies in the resolution of the display device. Typically one can expect no more than  $10^6$  pixels to be available for the display such that in a simulation space of  $256 \times 256$  cells one will have a resolution of 16 pixels per cell. In a simulation involving  $2.0 \times 10^6$  particles (currently the greatest number possible on the Connection Machine available through the Numerical Aerodynamics Simulation facility at NASA Ames, although one would expect this number to be as high as  $16 \times 10^6$  on a 64k processor machine with a memory upgrade) it becomes impossible to resolve the individual particles if all are to be displayed. Therefore it is necessary to display only a fraction of the particles in order to visualize their motion and concentration. By displaying every  $k^{th}$  particle in the list ( $k$  being some suitably large integer), one can still visualize the density and velocity field although not all the particles from the simulation are displayed.



### 6.1.2 Implementation of Visualization Mechanism

The implementation on the Connection Machine of this mechanism for flow visualization with a particle simulation makes use of the frame buffer. The frame buffer allows dynamic displays of size  $512 \times 512$  or  $1024 \times 1024$ . Naturally the greater resolution display will require a corresponding greater number of virtual processors, and therefore memory. The lower resolution display is useful when memory limitations rule out the greater resolution or when the visualization is to be recorded on video tape for play back at regular network television resolution (NTSC format).

The geometry is displayed on the overlay buffer. Since the geometry is static there usually is no need to redraw the overlay buffer during the visualization. Nonetheless redrawing the overlay buffer during the visualization normally is fast enough that it does not affect the animation of the flow. Therefore the overlay buffer can also be used to display changing statistics in the simulation. For example a dynamic "time bar" can be used to display the current time step or one may want to display other scalar information such as peak temperature in the flow, total heat loading on the body or lift and drag for the body. If the overlay buffer is to be used dynamically in such a manner then it is necessary to save the static portions to avoid recomputing the display. This is especially true when text is involved since fonts are bit mapped and font calculations are carried out on the front end at a tremendously slow rate by comparison.

The particles are displayed on the RGB (Red/Green/Blue) buffers. These can be configured as a single 24 bit color buffer or as three separate 8 bit color buffers. With the current technique 24 bit color is unnecessary since the eye is incapable of grasping such a broad palette of colors in a dynamically changing display of moving particles. Therefore it is better to employ 8 bit color thereby saving memory at a rate of 16 bits per pixel. For a static display 24 bit color may be useful for enhancing the visualization of density while letting all the particles be displayed. In such a case instead of using RGB values to map the colors one would use HLS (Hue/Lightness/Saturation) values, letting the hue and lightness determine the

color corresponding to the desired thermodynamic quantity for particles in a cell while letting the saturation give some idea of the number density. The color scale would then be two dimensional, with the mapping for the the displayed quantity given along one axis and the mapping for the density along the other.

With 8 bit color one has three separate color buffers for the display. It is possible to write to any of these three buffers, however only one buffer can be displayed at a time. Because changing the displayed buffer is always faster than writing to the buffer, animation is performed on most graphics systems by writing to an undisplayed buffer and switching with the displayed buffer once the writing is completed. This technique can be employed on the Connection Machine as well although, as was mentioned in describing the use of the overlay buffer, the writing to the buffer proceeds faster than the eye can respond therefore it is unnecessary to employ such a strategy.

Writing to the frame buffer is similar to communicating to a separate VP set. To display the particles in the frame buffer, the VP set storing the particle information must send an 8 bit color value to the frame buffer for every particle which is to be displayed. If only a fraction of all the particles are to be displayed, it is advantageous to use field aliasing (as discussed in Chapter 2) to reduce the VP ratio and speed the communication. If the color value is to correspond to a thermodynamic quantity, then that quantity must first have been sampled from the simulation and the result must have been mapped to an 8 bit integer in all processors which are to display their particle. Note that this additional calculation and communication takes less than 5% of the total computational time.

## **6.2 Visualization Strategies**

### **6.2.1 In Real Time**

In real time the technique described in the previous section is used for visualizing the calculation as it proceeds. This can be of tremendous use for debugging code

as well as for evaluating new geometries. As a debugging tool clearly it is useful for identifying how the data is becoming corrupted. Often bugs in the program are evident in the strange behavior of particles or unrealistic temperatures for the cells. This kind of information is immediately available from a real time visualization and can be used to identify the source of error.

In describing a new geometry it is necessary to ensure that particles do not leak through the body and that the body is having the desired effect on the flow. Any unexpected effect that the body definition may have on the flow becomes evident through the visualization. In applying the simulation method to a new geometry it is also necessary to make some estimate of how many time steps will be necessary to reach steady state. Again this is information that is immediately available from a real time visualization. In other words, one can see through the visualization when the shock structure has become fully developed and the flow has reached steady state.

### **6.2.2 Through Play Back**

The idea behind using play back visualization is both to speed up the display of information and to have a stored solution which can be viewed repetitively without repeating the initial calculation. The limitation one encounters is finding sufficient storage for the solution. If there were truly infinite storage devices, one would then store all the particle information for every time step and thus be able to completely recreate any aspect of the simulation in the play back. Unfortunately, at 28 bytes per particle (in two dimensions) and two million particles that requires 56 MB per time step or about 6 GB per 100 steps. Clearly this is unfeasible for visualizing transient flows over several thousand time steps.

An alternative is to store only the information sampled from the cells. At a minimum, one would store the number density, the  $u$  and  $v$  velocity components, and the translational temperature. This would require 16 bytes per cell or 1 MB per time step for a simulation with 64k cells. This is feasible in terms of the storage requirements, however the visualization now loses those appealing aspects described

in the first section. In other words, the visualization would now proceed in either of two ways. One would visualize the changing macroscopic quantities such as density or temperature by displaying those fields with a suitable color map, or one would visualize the changing velocity field using tracer particles in a manner analogous to the visualization techniques used with regular CFD solutions of transient flows. However, it is no longer possible to visualize both the thermodynamic quantities and the flow field simultaneously.

There are two alternative strategies one can use in order to retain the visualization technique described in the first section while using a feasible amount of storage. The first of these strategies is simply to save each image of the flow as it is created in the real time visualization. For a  $1024 \times 1024$  display this requires 1 MB per time step regardless of the number of particles or the number of cells employed. Although this scheme retains all the unique features of the particle simulation visualization technique it suffers from a lack of flexibility in the choice of displayed information. In other words, one has to decide ahead of time on the quantity to be displayed and the color map to be used. This requires running several smaller scale simulations with real time visualization to arrive at a suitable display for the full scale solution. If one later finds not all the necessary information has been captured, it becomes necessary to repeat the calculation.

A more robust scheme is to combine the two previous strategies, that is, saving the sampled information and saving the display. By eliminating redundancies in the information the storage requirements can be reduced to *less* than that necessary in applying either strategy individually. As a minimum one saves the sampled density, the temperature, and the flow speed for the cells. From the density and the temperature any other equilibrium thermodynamic quantity can be computed, and from the temperature and the flow speed the Mach number can be computed. For a grid of 64k cells these three quantities will require 768 kB of storage per time step. In addition to this, in order to visualize the particle motion in the flow just a bit map of the display is stored. Since the sampled flow information will be used to color the particles it becomes unnecessary to save the color used in the real time display. Storing a bit map of a  $1024 \times 1024$  display requires 128 kB, therefore in total

896 kB per time step are required with this scheme. To produce a display the bit map is used to identify the pixels which need to be painted, and the saved solution is used to select a color. This scheme has the advantage of saving the actual solution, as opposed to the displayed visualization. For this reason the scheme allows great flexibility in recreating the simulated flow. It is possible to visualize any desired quantity through an appropriate color map, therefore different reproductions of the simulated flow can be created in order to investigate the behavior of different quantities throughout the solution.

The design of a good color map is not a trivial matter. When the color is to be used to display a thermodynamic quantity it is necessary to know the range of variation for that quantity and ensure that there is good contrast between adjacent colors in the map throughout that range. The range of variation may change dramatically with free stream Mach number and a single universal color map is not possible. With the play back visualization one can tailor individual color maps for each displayed flow quantity to produce the best effect for the particular geometry and flow conditions being simulated.

### **6.3 Extension to Three Dimensions**

The discussion thus far has been restricted to the visualization of two dimensional flows. Eventually it is desired to apply this technique to three dimensional flows, therefore it is appropriate to address the question of the changes required in the visualization technique. It is clear that one could not simply display the entire flow as an isometric projection without adjusting the size of the displayed particles to reflect depth in the flow. In theory this would give a correct representation of a three dimensional flow, but in practice one would almost certainly find that the resolution of the display device would prove to be a limitation. The experience obtained in displaying two dimensional flows indicates that four pixels per particle is the coarsest resolution one can use without defeating the purpose behind using colored particles to visualize the solution. Even at a pixel per particle one has to

make compromises in the number of particles displayed, therefore the display device already is a limitation in the visualization of two dimensional flows.

It is evident that the technique can be applied only to the two dimensional planes making up a three dimensional flow. The issue then becomes how to convey the three dimensional information in a two dimensional medium. This could be best accomplished by allowing fast switches between planes in the simulation. In other words, the displayed plane could be allowed to change rapidly under user control thereby allowing the user to investigate the third dimension of the solution in whatever manner desired. In a two dimensional visualization user input is not necessary because people are accustomed to two dimensional displays and generally have similar responses to information conveyed in this manner. This is not true of three dimensional information where the response will vary greatly from person to person. Therefore it is important for the visualization of three dimensional information to be under the control of the viewer. In such a scheme it would be necessary to aid the viewer in grasping which plane is being displayed. For this purpose the overlay buffer could be used to display the entire three dimensional geometry in isometric projection while the particles corresponding to a two dimensional slice of this geometry would be displayed.

Naturally the storage requirements of a three dimensional flow visualization are much greater than for two dimensions. In three dimensional simulation with 64k cells in the two dimensional plane one would require 896 kB per plane per time step. With 50 planes in the simulated space one requires 44 MB per time step. Therefore storage limitations make it impossible to save a full transient solution, however the technique could be very useful for visualizing the steady state three dimensional solution. For the steady state one need save only the time averaged solution, not the transient solution at each time step. The steady state solution in this example would require 12.5 MB per sampled quantity. The bit map information for one time step would require an additional 5.3 MB. Therefore three sampled quantities and bit maps for 10 time steps would require only 91 MB of storage. The visualization would proceed by looping over the 10 bit maps to display the particle motion while using the saved solution to decide on a color for each particle. The user would

control which plane is displayed and what quantity is used to color the pixels. The entire 91 MB of information could be loaded into 16k processors so the visualization would proceed at a very fast rate entirely from the Connection Machine.





# Chapter 7

## Results

The algorithms presented in the previous chapters are now applied to several example problems in order both to validate the algorithms and evaluate the performance of their implementation on the Connection Machine. The first problem to be examined is the relaxation of the internal degrees of freedom in a diatomic gas. Results are compared to solutions computed with McDonald's code on the Cray 2. The second problem to be examined is the structure of a normal shock wave. Again results are compared to solutions computed by McDonald. Finally, a large two dimensional solution is presented for the flow field about a proposed geometry for the Hermes Space Shuttle to be built by the European Space Agency. This solution is used to demonstrate the capability of the method for solving hypersonic flow problems of practical engineering interest and is also used to evaluate the performance of the Connection Machine in comparison to the Cray 2 for a general two dimensional problem.

### 7.1 Relaxation of Internal Energy Modes

To test the the nonequilibrium temperature model, the relaxation of a diatomic gas to its equilibrium condition is examined. This simulation uses the adiabatic

box configuration with gas molecules initialized to a nonequilibrium state. The energy exchange resulting from collisions of the particles eventually relaxes the gas to equilibrium. In addition to providing a useful check on the nonequilibrium temperature model, this simulation provides a particularly severe test of the randomization algorithms incorporated to the merged ordered subsets sorting algorithm. The aim of these randomization algorithms is to make the deterministic "even-with-odd" pairing of collision candidates result in a statistically random and uncorrelated sample of colliding pairs. Since multiple collisions of the same pairs are effectively equivalent to a single collision, if the pairs in a sample are correlated to those of the previous sample then the effective collision frequency is reduced. The result manifests itself macroscopically as a reduced relaxation rate and produces an incorrect equilibrium division of energy between the various modes. The latter occurs because the temperature model assumes a particular energy distribution for the set of colliding particles and redistributes the collision energy based on this distribution. If the collision rate is incorrect then the set of colliding particles will also have an incorrect energy distribution and the correct equilibrium division of energy is not obtained.

Figure 7.1 presents the results for relaxation from three different initial temperatures and compares these to the same simulations performed by McDonald on the Cray 2. In all cases the agreement between the two is excellent. It should also be noted that these results are in agreement with results from DSMC calculations performed by Boyd for the same problem (McDonald (1990)). The collision numbers were fixed at  $Z_{rot} = 5$  and  $Z_{vib} = 50$ . The simulations employed a hard sphere interaction potential with diatomic molecules having two rotational degrees of freedom and a characteristic temperature for vibration corresponding to molecular nitrogen,  $\theta_{vib} = 3390^\circ K$ . The Connection Machine results are represented by the solid lines in the figure and the Cray 2 results are represented by the 'o' symbols.

The initial nonequilibrium condition was for all the energy to be in translation leaving no energy in rotation or vibration. Figure 7.1a is the result for an initial translational temperature of  $T_o = 273.15^\circ K$ . For such a low reference temperature one can expect essentially no excitation of vibrational states in the gas, and the

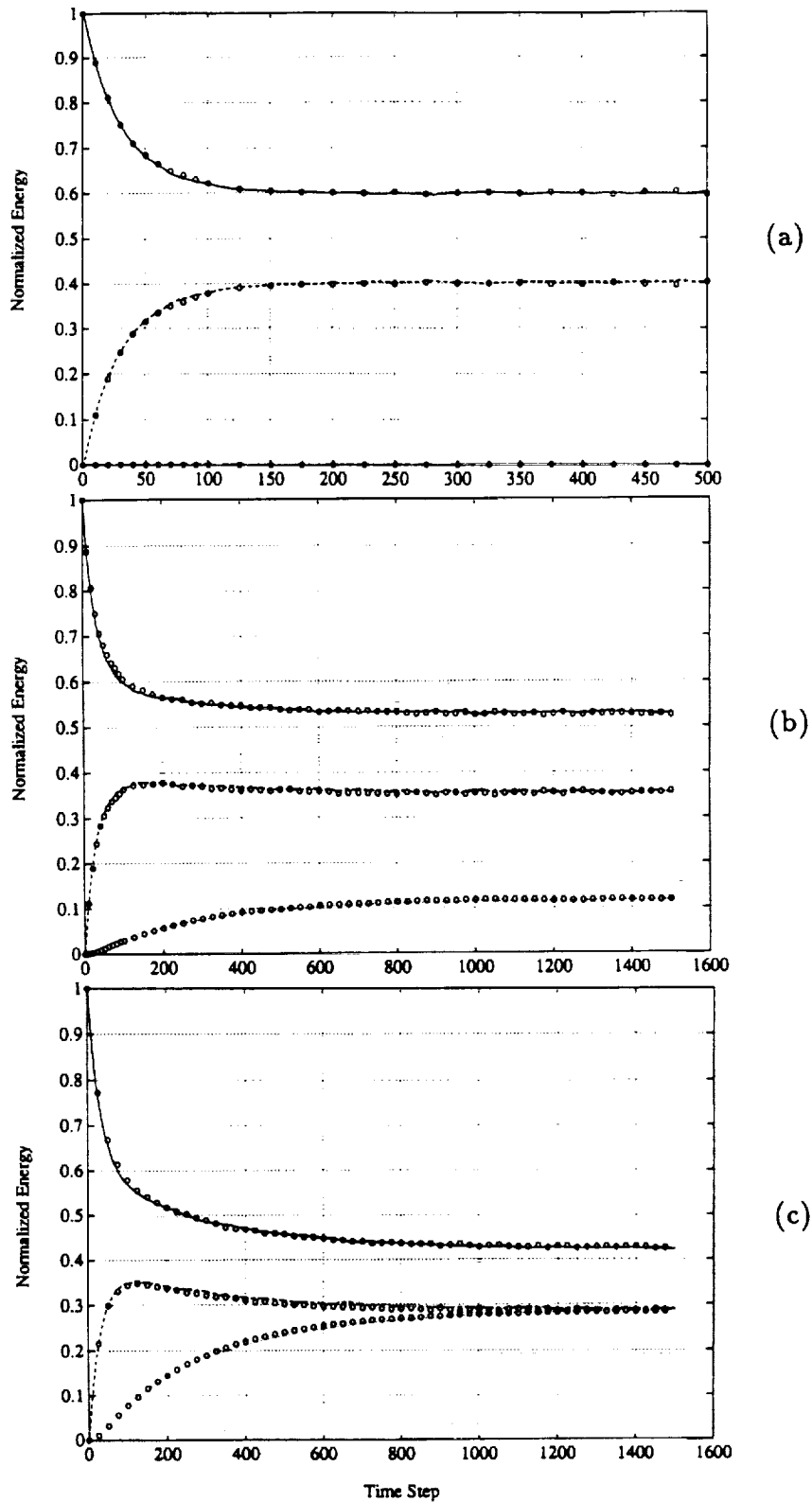


Figure 7.1 Relaxation of internal degrees of freedom in a diatomic gas with fully excited rotational energy and a characteristic temperature of vibration of  $3,390^{\circ}K$ . Results are for three initial gas temperatures with only translational energy present a)  $273.15^{\circ}K$ , b)  $3,390^{\circ}K$ , c)  $T \rightarrow \infty$ . Symbols are used for current results and lines represent the calculations by McDonald (1990). —  $E_{rot}$ ; - - -  $E_{tr}$ ; ···  $E_{vib}$

energy exchange is primarily between translational and rotational modes. For 3 translation degrees of freedom, 2 rotational degrees of freedom and no vibrational equivalent degrees of freedom one expects an equilibrium division of energy of 60% in translation and 40% in rotation, as is observed in the figure.

Figure 7.1b is the result for an initial translational temperature of  $T_o = 3390^\circ K$  which is exactly equal to the characteristic temperature of vibration. This represents a situation where the vibrational state is only partially excited. It is possible to calculate the theoretically expected equilibrium division of energy between the various modes by considering conservation of energy. Conservation of energy requires

$$e_{tr} + e_{rot} + e_{vib} = \frac{3}{2}RT_o. \quad (7.1)$$

Assuming translation and rotation are both fully excited and using equation (3.28) for vibration, then

$$\begin{aligned} e_{tr} &= \frac{3}{2}RT \\ e_{rot} &= \frac{2}{2}RT \\ e_{vib} &= \frac{R\theta_{vib}}{\exp(\theta_{vib}/T) - 1} \end{aligned} \quad (7.2)$$

Substituting (7.2) in (7.1) yields a transcendental equation in  $T$  which when solved numerically for this particular case results in a final equilibrium temperature of  $T = 1790^\circ K$ . This corresponds to an energy division of 53% in translation, 35% in rotation and 12% in vibration as is observed in the figure. Therefore the simulation is producing the correct equilibrium result.

Figure 7.1c is the result for an initial translational temperature approaching infinity such that the ratio  $\theta_{vib}/T$  approaches zero. This is the limiting case for which vibrational energy becomes fully excited with two full equivalent degrees of freedom. At equilibrium there is an equal division of rotational and vibrational energy as is observed in the figure. Evident in this figure also is the rotational

energy overshoot due to the great difference in the relaxation rates of vibration and rotation.

In all three cases the agreement with the Cray 2 results is excellent. This not only is a validation of the nonequilibrium temperature model as implemented on the Connection Machine but also is a validation of the randomization algorithms incorporated into the sorting. These results indicate that the simulation is creating and maintaining the correct distribution functions for the particles. The next section further validates the current implementation by examining the temperature and density profiles across a normal shock wave in an ideal diatomic gas.

## 7.2 Normal Shock Wave Structure

Accurately predicting the internal structure of a shock wave is a prerequisite of any valid particle simulation. The shock wave represents a region of highly nonequilibrium flow connecting two different equilibrium states. This is a much more complex problem to study than the relaxation of a gas because the molecules undergo convective processes in addition to diffusion. This also is an important test for a particle simulation since the shock wave problem represents an area where particle methods historically have provided the only accurate computational solutions. Continuum methods employing the Navier-Stokes equations produce incorrect results for the internal structure of a hypersonic shock wave and efforts at extending the continuum approach has focused on the solution of the Burnett equations. Only recently (Lumpkin, Chapman and Park, (1989)) have these been shown to provide reasonable solutions for shock wave profiles.

With the addition of bulk motion to the gas it becomes necessary to properly simulate entrance and exit conditions for the molecules. Proper entrance conditions are necessary for maintaining a uniform free stream, and a non-uniform free stream has an immediate and adverse effect on the shock wave. Proper exit conditions are equally important in order for the shock wave to remain stationary and allow time averaged solutions. A standing shock wave is only neutrally stable and the

stability problems encountered by experimentalists creating such a flow in a wind tunnel are also encountered in simulating this flow with a particle method. Owing to the difficulty in defining the exit conditions for a shock which excites vibrational modes, the results in this section are concerned only with rigid rotor particles with no vibrational energy. In the following section a closed end shock tube simulation is employed to study the vibrational relaxation behind a strong shock.

Figure 7.2 presents the normalized temperature and density profiles across a Mach 10 shock wave in an ideal diatomic gas and compares these to results from the same calculation performed on the Cray 2. The 'o' symbols represent results from the implementation on the Connection Machine and the solid lines represent results from the implementation on the Cray 2. The agreement between the two again is excellent. As with the relaxation results, these calculations have also been compared to DSMC calculations performed by Boyd and have shown excellent agreement. This calculation allowed only rotational nonequilibrium and assumed a rotational collision number  $Z_{rot} = 5$ . Values are normalized to the post-shock equilibrium state as given by the Rankine-Hugoniot jump conditions. Evident in the figure is the translational temperature overshoot due in part to the different relaxation times between rotation and translation. The faster translational relaxation causes the translational temperature rise to lead the rotational temperature rise and forces a translational temperature overshoot in order to conserve energy across the shock.

It is incorrect to assume that translation leads rotation solely because of the different relaxation times for these modes. Figure 7.3 presents the temperature and density profiles across a Mach 10 shock with the rotational collision number  $Z_{rot} = 1$ . Clearly evident in this figure is a lead in translation over rotation and the corresponding translational temperature overshoot. The reason for this lies in the transport process which causes the temperature shock to lead the density shock. Hot molecules from the high density region behind the shock migrate to the low density region before the shock. Because these molecules are few in number they have little effect on the density, however they have a great effect on the temperature since it is proportional to the variance of the velocity distribution, which in this low density region is defined on the basis of a relatively small number of molecules. It

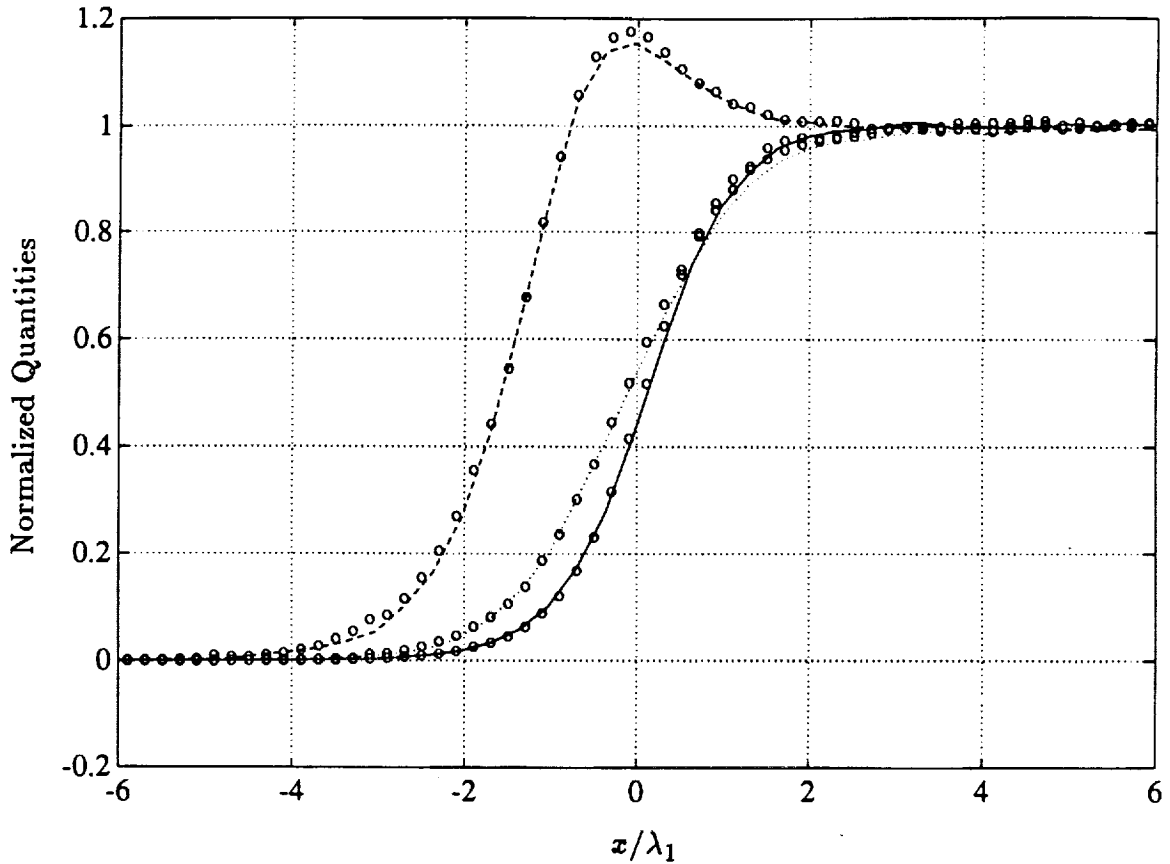
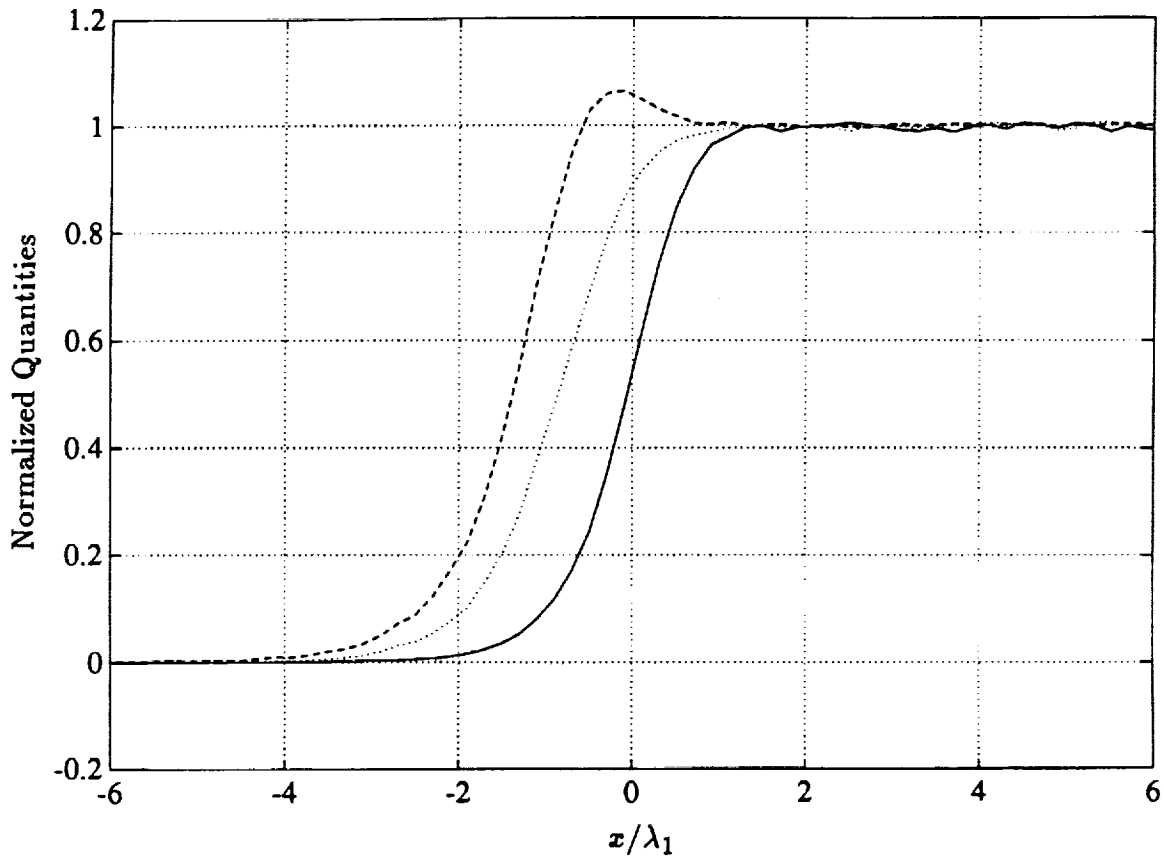


Figure 7.2 Shock wave structure at Mach 10 in a perfect diatomic gas with  $\gamma = 1.4$ . Symbols are used for current results and lines represent calculations made by McDonald (1990). —  $\rho$ ; - - -  $T_{tr}$ ; ···  $T_{tot}$ .

is for this reason that one sees the temperature shock leading the density shock. Now if one considers the situation where translation and rotation are allowed to relax at the same rate, the same transport process can be used to explain why the translational temperature should lead the rotational temperature. It is clear that those molecules which migrate furthest upstream will be the ones with the greatest translational energy. These same molecules will not necessarily have the greatest rotational energy as well, in fact the finite amount of energy available in a collision makes it more likely for molecules with a large amount of translational energy to have a disproportionately smaller amount of rotational energy. Therefore translational energy is more likely to be carried further upstream than rotational



**Figure 7.3** Shock wave structure at Mach 10 in a perfect diatomic gas with  $\gamma = 1.4$  and  $Z_{rot} = 1$ . Note the translational temperature overshoot exists even in this case where translation and rotation are allowed to relax at the same rate. —  $\rho$ ; - - -  $T_{tr}$ ; ···  $T_{rot}$ .

energy and the translational temperature rise leads the rotational temperature rise even when the two modes are allowed to relax at the same rate. On the basis of figures 7.2 and 7.3 one can conclude that the method is not only correct in its treatment of the nonequilibrium temperature relaxation but also in its simulation of the transport processes responsible for the nonequilibrium phenomena.

The results above were all carried out assuming a hard sphere potential for the molecules. Real gases exhibit somewhat softer potentials usually approximated by an inverse-power law. In order to test the ability of the simulation with respect to real gases, the shock wave structure for nitrogen was calculated for a range of Mach numbers and compared to the experimental results obtained by Alsmeyer (1976).



For all Mach numbers the agreement between the simulation and the experimental results was remarkably good.

Figure 7.4 presents the density profile for a Mach 10 shock in nitrogen, the solid line corresponds to the experimental results and the 'o' symbols correspond to the simulation results. The abscissa of figure 7.4 is non-dimensionalized by the hard sphere mean free path, this requires scaling the simulation mean free path as described by Bird (1983). Specifically,

$$\lambda_{HS} = \frac{24\lambda_{SIM}}{(7 - 2\omega)(5 - 2\omega)} \quad (7.3)$$

where  $\lambda_{HS}$  is the hard sphere mean free path,  $\lambda_{SIM}$  is the simulation mean free path and  $\omega$  is the exponent on the temperature dependence of viscosity with the assumed power law (i.e.  $\mu \propto T^\omega$ ). The simulation employed an inverse ninth-power molecule for nitrogen as suggested by Alsmeyer (1976) and shown by Lumpkin (1990) to accurately reflect the experimentally observed temperature dependence for the viscosity. This results in a viscosity proportional to  $T^{0.72}$ . A rotational collision number of 5 was used for this calculation. The excellent agreement observed between the experiment and the simulation for this and other Mach numbers serves as validation for the current method in the simulation of real gases.

### 7.3 Shock Reflection

Vibrational modes in a diatomic gas molecule become excited only once the temperature is of the order of the characteristic temperature of vibration for the molecule. Typically this is several thousand degrees, consequently experimental investigations of vibrationally excited gases have almost exclusively employed a shock tube since it is the simplest device capable of generating strong shocks with a high enthalpy. The relaxation zone following an incident shock can be investigated using optical techniques or, as demonstrated by Baganoff (1965), by monitoring the end wall pressure following the reflection of the incident shock. The reflection of a strong normal shock wave from a plane wall is a very complex process characterized

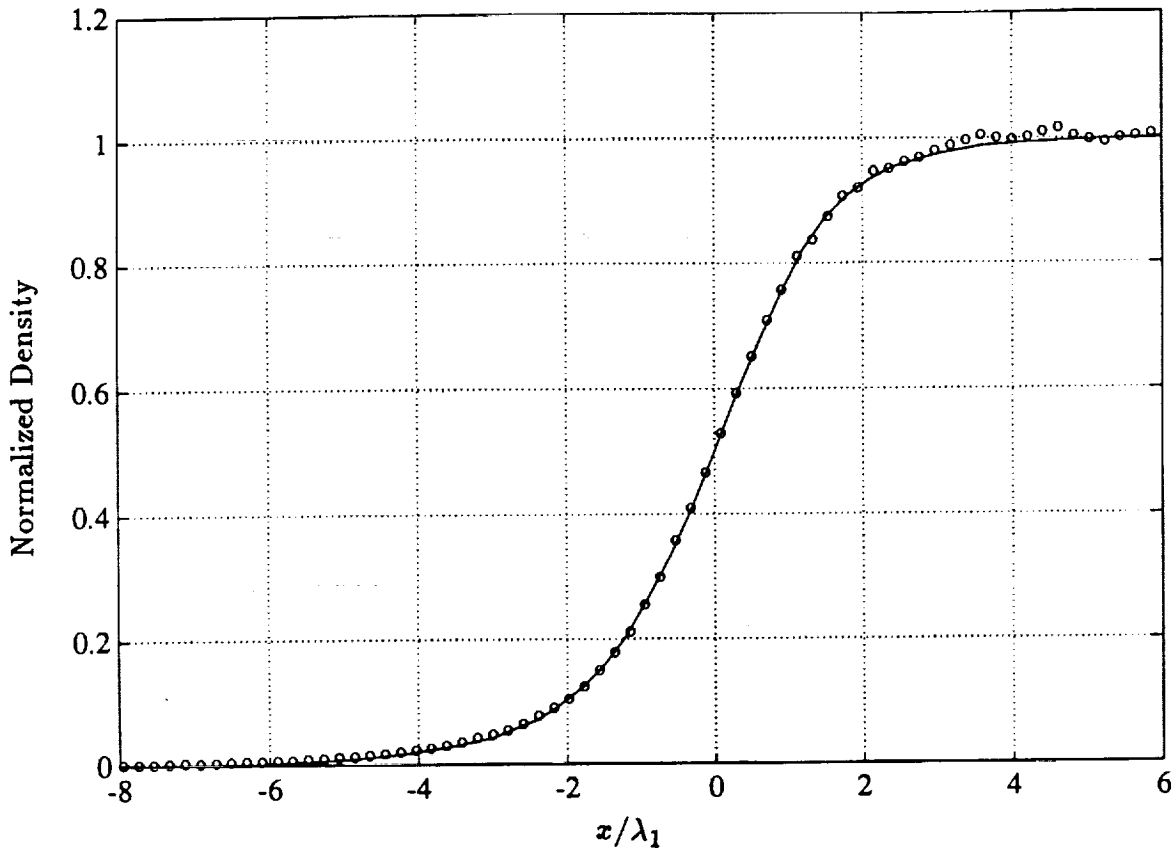


Figure 7.4 Shock wave structure at Mach 10 in nitrogen. Only the density profile is shown. An inverse ninth power potential with  $Z_{rot} = 5$  was employed in the simulation. Symbols are used for the simulation results, the solid line represents experimental results by Alsmeyer (1976).

by extreme pressures and temperatures in a non-uniform and highly nonequilibrium flow. For these reasons it was appealing to attempt a simulation of the shock reflection process as a means of further validating the method and, as well, as a means of uncovering the limitations of the internal energy model.

Two different simulations were carried out for this problem. In the first the end wall is assumed ideal and particles which strike the end wall are reflected specularly back into the flow. This simulates a perfect, adiabatic end wall which does not promote a boundary layer. In the second simulation the end wall is assumed to be isothermal with some degree of thermal accommodation. Particles which strike this wall are reflected back into the flow with energy corresponding to the wall

temperature. This type of boundary condition promotes a boundary layer at the wall and more accurately reflects the conditions under which experiments are carried out.

### 7.3.1 Ideal End Wall

The specularly reflecting boundary condition was discussed in Chapter 5. This type of boundary has the advantage of not introducing a boundary layer thus simplifying the interpretation of the results and allowing comparison with the inviscid theory.

The gas used for these simulations was carbon monoxide. The molecules were modelled similar to nitrogen, an inverse-power 9 potential was employed giving a viscosity temperature dependence of  $T^{0.72}$  which is a good approximation of the observed viscosity. Note that the use of a heteronuclear molecule (symmetry factor of 1) does not require any alteration of the rotational energy model since rotational energy is assumed always to be fully excited. The characteristic temperature of vibration of carbon monoxide is  $\theta_v = 3124^\circ K$ , and the vibrational relaxation time is given empirically by (Hanson (1971))

$$\log_{10}(P\tau, atm - sec) = 75.8T^{-1/3} - 10.16 \quad (7.4)$$

which has been validated up to  $6000^\circ K$ . The relaxation times in the simulation were fixed to give a rotational collision number of 5 and a vibrational collision number of 150. This is discussed more fully below.

Two sets of results employing an ideal end wall are presented here. The first set of results is used to demonstrate that the method is producing the correct frozen and equilibrium results in the gas. The second set of results is used to investigate the relaxation of the simulated gas between these two conditions in a situation where vibration is not fully excited by the incident shock and the exact equilibrium condition is difficult to predict. These conditions were chosen partly to allow comparison with the experimental results obtained by Hanson (1971) although because of the limitations of the implemented internal energy model a useful comparison becomes difficult to make.

The simulated shock tube had dimensions  $1022 \times 1$  and was initialized with 65000 particles at a temperature of  $300^\circ K$ . The Knudsen number for this initial gas condition based on the length of the shock tube was 0.0029. The piston was started at Mach 8.25 in order to create a Mach 10 shock wave incident on the end wall. After 9000 steps the number of particles was increased to  $2.1 \times 10^6$  through particle cloning. This technique allowed the simulation to quickly build up a respectable shock front and relaxation zone with a relatively small number of particles. Since the process of interest was the reflection of the shock from the end wall and the consequent motion of the reflected shock through the incident shock's relaxation zone, the maximum number of particles were employed for this part of the simulation.

Figure 7.5 presents the temperature and density profiles for the incident shock wave just before striking the end wall (the fluid motion is from left to right). There are about 2000 particles per cell ahead of the shock and about 14000 particles per cell behind the shock. This solution was time averaged for 5 steps over which the shock would have moved 0.25 cell widths. The effect of this slight shock motion during the time averaging interval is negligible. Values are normalized by the initial conditions (that is, the conditions ahead of the shock in this figure) and distance is measured from the end wall and normalized by the initial hard sphere mean free path (as given by equation (7.3)). The Rankine-Hugoniot equations for frozen conditions predict a temperature jump of 20.4 and a density jump of 5.7 for this Mach number. The translational temperature, which relaxes much faster than the rotational temperature, does reach its predicted frozen temperature jump before beginning to relax to its equilibrium value. The rotational temperature, however, does not reach its frozen jump value because of its slower relaxation time. The density is seen to rise quickly to its frozen jump value before beginning to relax to equilibrium. The equilibrium conditions for a shock wave at this Mach number with fully excited vibration correspond to a temperature rise of 15.9 and a density rise of 7.2 over the initial state. Because of the relatively low initial temperature ( $300^\circ K$ ) of the simulated gas, the shock wave in the simulation was not sufficiently strong to fully excite vibration. Consequently, the final equilibrium temperature is slightly

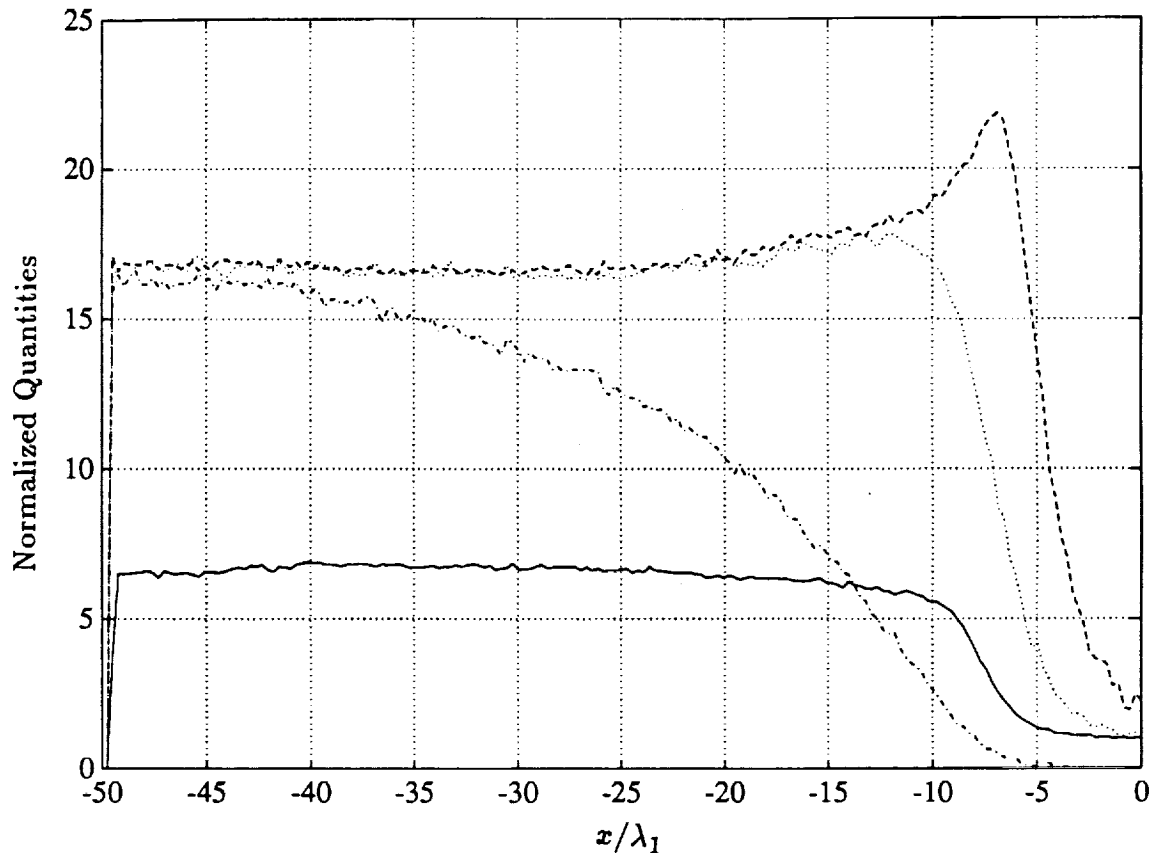


Figure 7.5 Temperature and density profiles of a Mach 10 shock wave in carbon monoxide just before striking the shock tube end wall. Values are normalized by the initial gas conditions. Flow is from left to right, distance is measured from the end wall in units of mean free path at the initial conditions. —  $\rho$ ; - - -  $T_{tr}$ ; ····  $T_{rot}$ ; - · - ·  $T_{vib}$ .

higher than predicted and, for this same reason, the final equilibrium density rise is slightly lower than predicted. The measured temperature and density rises are 16.8 and 6.7 respectively.

Figure 7.6 presents the temperature and density profiles for the gas in the shock tube some time after the incident shock wave has reflected from the end wall. At this instant the reflected shock wave is travelling upstream (from right to left) into the equilibrium region behind the incident shock wave. Again values have been normalized by the initial conditions and the solution was time averaged for 5 steps.

Because the gas ahead of the reflected shock has partially excited vibration, it is not possible to calculate the frozen and equilibrium conditions behind the

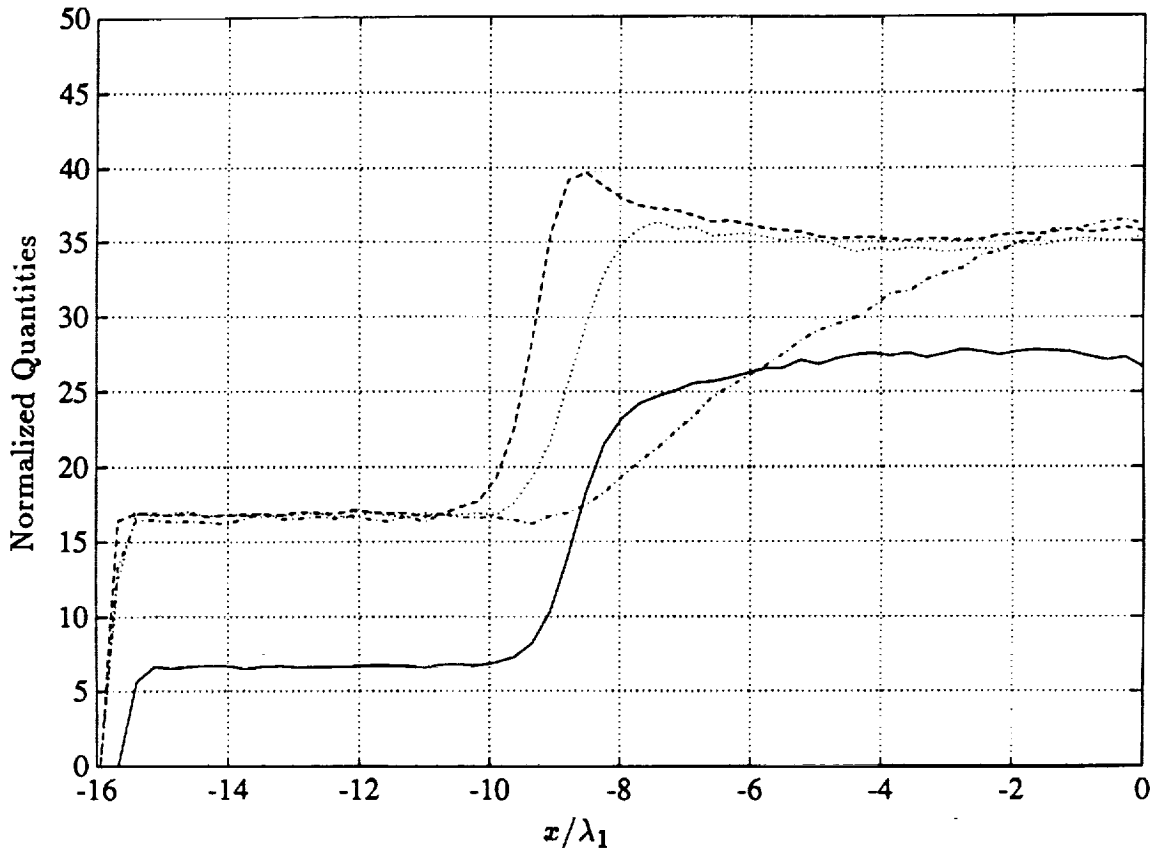


Figure 7.6 Temperature and density profiles in a shock tube when the initial shock wave has reflected from the end wall and is travelling upstream. The test gas is carbon monoxide. Values are normalised by the initial gas conditions. Flow is from right to left; distance is measured from the end wall in units of mean free path at the initial conditions. —  $\rho$ ; - - -  $T_{tr}$ ; ····  $T_{rot}$ ; - · - ·  $T_{vib}$ .

reflected shock based on the initial conditions of the gas. If vibration were fully excited by the incident shock the theoretical equilibrium temperature and density rise over the initial conditions would be 31.9 and 29.7 respectively. Since vibration is not fully excited by the incident shock, the final temperature and density rise are slightly higher and lower respectively. Since vibration is fully excited behind the reflected shock wave, one can calculate the final equilibrium conditions there using the observed equilibrium behind the incident shock. Doing this one predicts an equilibrium temperature rise of 34.8 and a density rise of 27.6 respectively. As can be seen from the figure these values are obtained to within a few per cent.

From figures 7.5 and 7.6 one can conclude that the simulation is reproducing the

correct frozen and equilibrium solutions for the gas. It is encouraging to see that the simulation has captured the correct shock behavior for both the incident and the reflected shock. The reflected shock is especially challenging not only because of the extreme conditions which it produces in the gas behind it but also because its behavior depends on the shape of the incident shock. Any errors generated in the incident shock will be multiplied in the reflected shock. Note that the solution has been generated employing only a uniform grid and that the problem is inherently transient allowing very little time averaging of the solution and making any grid fitting virtually impossible.

Having demonstrated the correct frozen and equilibrium behavior in the simulated gas, it is instructive to investigate the relaxation process between these two conditions. To do this it is most convenient to switch from a spatial to a temporal coordinate system. Therefore, rather than examine the spatial behavior of the gas at some instant in time we examine the temporal behavior of the gas at some fixed location in the shock tube—the end wall being the obvious candidate. Figure 7.7 presents the end wall density, translational temperature, and pressure histories. The density and temperature histories are the values measured in the last cell of the simulated shock tube, however the pressure history is the actual momentum flux into the end wall. Because the number of particles striking the end wall is much smaller than the number of particles in the cell next to the end wall, this last history is subject to greater statistical fluctuation and therefore is noisier than the histories measured from the cell. The values have been transformed in the same manner as the shock profiles of the previous section, that is the initial gas condition is mapped to zero and the final equilibrium condition is mapped to one. Finally, the histories have been time averaged over 10 steps; this was necessary primarily to smooth the end wall momentum flux history.

Not shown in figure 7.7 is the pressure calculated from the temperature and density measured at the end wall cell. This history was omitted primarily to avoid confusing the figure with too many curves especially since the pressure history follows the end wall momentum flux history rather closely. However there is an important difference between the two curves in that the rise in momentum flux

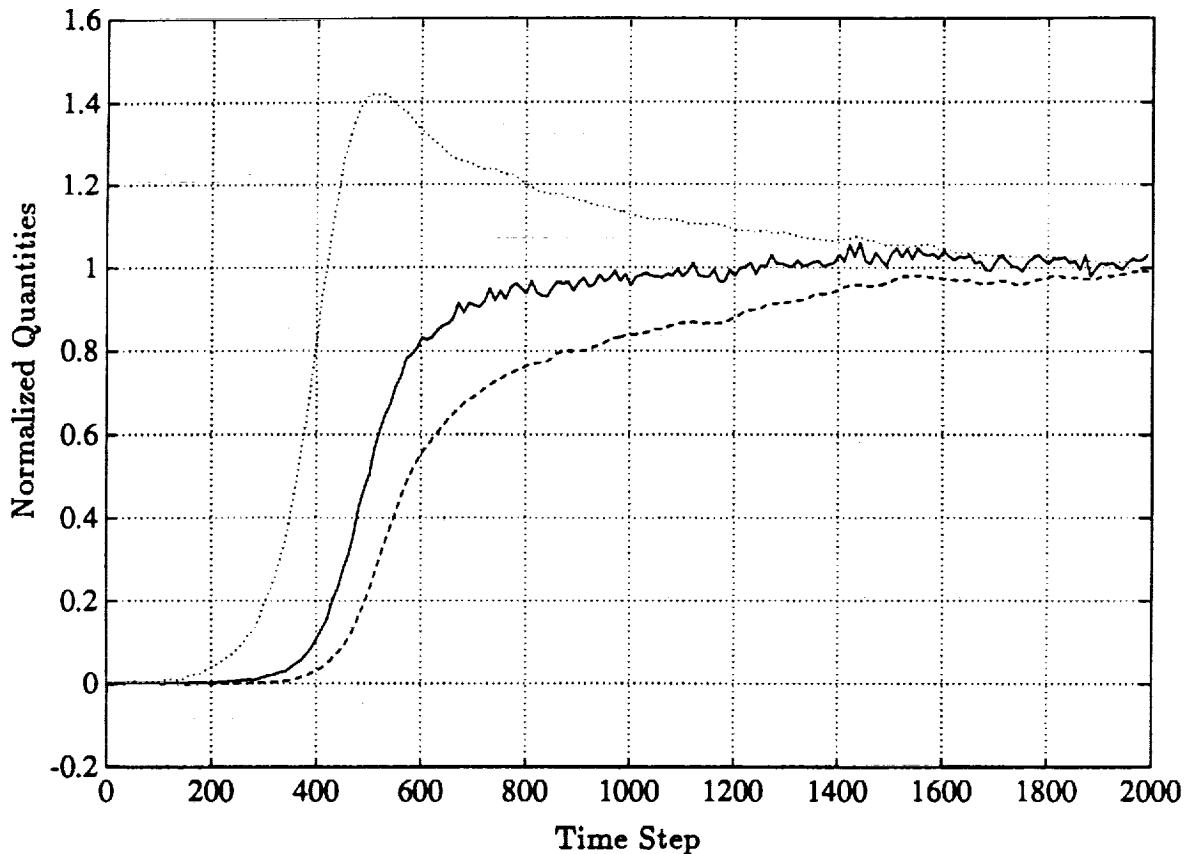


Figure 7.7 Temperature, density, and momentum flux histories at the end wall before and immediately following the reflection of the incident shock wave. The test gas is carbon monoxide. Values have been transformed such that the initial gas conditions map to zero and the final equilibrium conditions map to one. Time is measured in units of time steps in the simulation. One time step corresponds to  $4.5 \times 10^{-3}$  mean collision times at the initial gas conditions, or 0.241 ns for an initial gas temperature of  $300^\circ K$  and pressure 267 Pa (2 mm Hg). — momentum flux; --  $\rho$ ;  $\cdots T_{tr}$ .

leads the rise in pressure in the end wall cell. The reason for this is best understood by thinking of the pressure history as *lagging* the momentum flux history. Consider that the rise in temperature and density in the end wall cell are caused in sequence by the arrival of the incident shock and the passing of the reflected shock. However at the end wall itself these processes are occurring simultaneously, therefore one would expect the state measured in the end wall cell to react more slowly than that measured exactly at the end wall. Other than this small separation during the reflection process, the pressure and end wall momentum flux histories are identical.



Therefore one can conclude that the end wall cell is sufficiently small to capture all the gradients in the solution.

Unfortunately these results cannot be compared with experiment because the simulation assumes a constant vibrational collision number throughout the flow field. From equation (7.4), for an initial gas temperature of  $300^{\circ}K$ , one expects a vibrational collision number of 780 behind the incident shock and 46 behind the reflected shock. This order of magnitude difference between the two relaxation times means that in a real gas the relaxation zone behind the reflected shock is extremely short and one can assume equilibrium conditions are reached instantaneously. Consequently, the state of the gas behind the reflected shock is dependent only on the state of the gas ahead of the shock, therefore the relaxation behind the incident shock can be studied by monitoring the the conditions behind the reflected shock. In our simulated gas the relaxation times are equal on either side of the reflected shock, therefore the state of the gas at the end wall is a function both of the reflected shock's motion through the relaxation zone ahead of it and the reflected shock's own relaxation zone.

The use of a fixed vibrational collision number throughout the flow field is a major limitation of the current internal energy model. The reflected shock problem would be an ideal one to use in the study of more realistic models employing a variable collision number. Perhaps the simplest realistic approach would be to define a probability for vibrational energy exchange in a collision of the same form as is employed in the derivation of the Landau-Teller model. That is (cf. Hansen (1983)),

$$P_v \propto \exp(-g^*/g) \quad (7.5)$$

where  $P_v$  is the probability of vibrational energy exchange,  $g$  is the relative speed for the colliding molecules and  $g^*$  is a characteristic relative speed for the molecules. It is not clear at this time, however, that the current model for vibrational energy exchange would be consistent with such a scheme. Recall that the vibrational energy in obtained through the quantization of a Boltzmann distribution at the local gas

temperature. In the current model the rotational energy of the molecules is used to define this distribution. Because the decision to allow vibrational energy exchange is made independent of the colliding particles (that is, a fixed collision number is used), the rotational energy in the particles involved in vibrational energy exchange must represent a Boltzmann distribution at the local gas temperature. However, if the decision to allow vibrational energy exchange is made based on some function of the relative speed of the colliding particles, the distribution for the particles involved in such collisions becomes biased towards the higher energies (which is the purpose of incorporating a rule such as equation (7.5)) and the rotational energy of these particles can no longer be assumed to represent a Boltzmann distribution at the local gas temperature.

Certainly the idea of employing variable collision numbers in Monte Carlo simulations is not new. Davis, Dominy, Harvey and Macrossan (1983) describe a model for variable rotational collision number, and more recently Boyd (1989) presented a model for both variable rotational and vibrational collision numbers. For vibration Boyd used a form similar to equation (7.5) but including a factor to account for power law potentials (which the original Landau-Teller derivation neglects). However, these additional complexities seem to have little appreciable effect on most single shock calculations probably because single shock flows can be adequately modelled by a single relaxation time.

### 7.3.2 Isothermal End Wall

The results presented in this subsection were created by running the simulation under conditions identical to those employed in the ideal end wall results but with an isothermal end wall boundary condition. This gives a more accurate representation of the flow as encountered by experimentalists investigating the shock reflection process. The major difficulty with implementing such a boundary condition is in reproducing the correct collision frequency in the boundary layer created at the end wall. Consider that for the ideal end wall the temperature at the end wall can be as much as 40 times the initial gas temperature. The isothermal boundary fixes the

end wall temperature at the initial gas temperature, therefore the boundary layer is very cold compared to the gas behind the reflected shock. Consequently, the density through the boundary layer is very high and conditions within the boundary layer are more accurately represented by a continuum description of the gas.

For the results of this subsection the end wall was modelled as isothermal with a thermal accommodation coefficient of 0.9. The thermal accommodation coefficient,  $\alpha$ , is defined as (cf. Patterson (1956))

$$\alpha = \frac{E_i - E_r}{E_i - E_w} \quad (7.6)$$

where  $E_i$  is the translational energy of a particle incident on the wall,  $E_r$  is the translational energy of the particle reflected from the wall, and  $E_w$  is the "energy" of the wall, that is, the wall temperature converted into an equivalent energy.

The thermal accommodation coefficient is used to account for the observed difference between the temperature of particles emitted from the surface and the temperature of the surface. This difference is attributed to insufficient contact between the impinging molecules and the surface, and should not be confused with the temperature jump (cf. Patterson) which exists between a gas and a diffusely reflecting surface. The temperature jump is predicted by kinetic theory and is due to the temperature of particles impinging on the surface being higher than the temperature of the gas. Recall that the temperature of a gas is given by the variance of the velocity distribution of molecules in the gas. For a gas in equilibrium this distribution is a Maxwell-Boltzmann distribution and is different from the distribution for the molecules impinging on a surface. This latter distribution, for a gas in equilibrium, will be just the positive half of the Maxwell-Boltzmann distribution. Therefore the wall is continually robbing the gas next to it of the molecules from the positive half of the velocity distribution, hence the gas next to the wall is observed to have a lower temperature than the wall.

The use of a thermal accommodation coefficient is necessary for this problem because neither the required collision frequency nor the necessary density in the boundary layer can be sustained by the simulation. Consider that the mean free

path,  $\lambda$ , for molecules in a gas scales as

$$\frac{\lambda_2}{\lambda_1} = \left(\frac{n_1}{n_2}\right) \left(\frac{T_2}{T_1}\right)^{\omega-1/2} \quad (7.7)$$

where  $n$  is the number density,  $T$  is the temperature, and  $\omega$  is the exponent in the temperature dependence of the viscosity coefficient for the gas. At the end wall the temperature will remain constant given an isothermal boundary, therefore the mean free path will vary inversely with the density. Assuming the pressure remains constant through the boundary layer, then for a fully accommodating end wall where the temperature remains fixed at the initial gas condition the density rise at the end wall must equal the pressure rise. For the ideal end wall calculation of the previous subsection the pressure rise was about 950, therefore with a fully accommodating end wall the mean free path would be 1/950 of the initial gas mean free path and the number density should be 950 times the initial value. It becomes impossible to reproduce the correct collision frequency and the gas at the end wall cannot be fully thermalized. More importantly, the required density cannot be obtained from a shock tube which is 1022 cells in length. The observed simulation result is that the incident shock does not reflect from the end wall and all the incident gas is swallowed into the boundary layer.

By allowing incomplete thermal accommodation the wall influence is reduced since particles are allowed to retain some of the energy with which they impinge on the surface. Therefore the temperature of the gas at the end wall cell is not as severely constrained and the density rise through the boundary layer becomes manageable.

Figure 7.8 presents the density, temperature, and pressure profiles for the gas in the shock tube some time after the incident shock wave has reflected from the end wall. Note that the rotational temperature has been omitted in order to avoid cluttering the figure. At this instant the reflected shock wave is travelling upstream (from right to left) into the equilibrium region behind the incident shock wave. Values have been normalized by the initial conditions except for the pressure profile which has been normalized by a value ten times the initial pressure. The solution

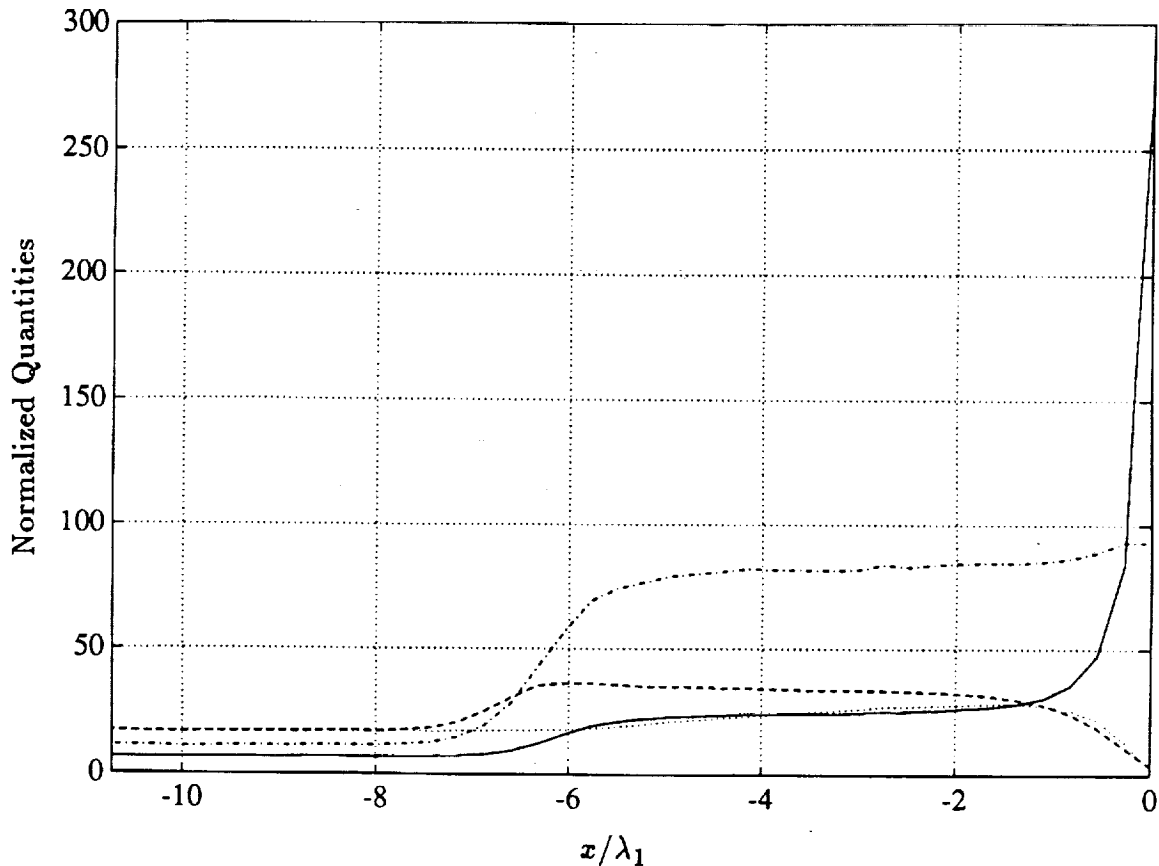


Figure 7.8 Temperature and density profiles in a shock tube when the initial shock wave has reflected from a cold, isothermal end wall and is travelling upstream. The test gas is carbon monoxide. Values are normalized by the initial gas conditions except for pressure which is normalized by a value equal to ten times the initial gas pressure. Flow is from right to left; distance is measured from the end wall in units of mean free path at the initial conditions. —  $\rho$ ; - - -  $T_{er}$ ; ····  $T_{eib}$ ; - · - ·  $p$ .

was time averaged over 5 steps.

The interesting feature in figure 7.8 is the presence of a boundary layer at the end wall. Clearly the flow external to the boundary layer is behaving in the manner predicted for the ideal end wall. However the cold end wall is cooling the gas over several cells and producing a very high density gradient through the boundary layer. An unexpected result is the slight perturbation in the pressure through the boundary layer. This is an error resulting from insufficient collisions of particles in this region. The gas is so dense and temperature so low that the required collision frequency

is not reproduced by the simulation. Consequently the hot particles from behind the reflected shock do not thermalize with the particles emergent from interaction with the end wall thus leading both to a higher temperature and to a higher density than would occur with complete thermalization. This was confirmed by running the simulation at double the initial gas Knudsen number such that the required collision frequency for the cells in the boundary layer was roughly halved. The gas conditions next to the end wall were still too close to continuum for the simulation to reproduce the necessary collision frequency, however the pressure perturbation did not occur until further into the boundary layer at the point where the probability of selection for the candidate collision pairs was exceeding unity.

Figure 7.9 presents the temperature, density, and pressure history at the end wall. As with figure 7.7, the density and temperature correspond to those sampled from the end wall cell whereas the pressure is the actual momentum flux into the end wall. In order to present all three histories in one figure it was necessary to perform some unusual scaling. The density is normalized by twice the initial density, the temperature is normalized by one tenth the initial temperature, and the pressure is normalized by ten times the initial pressure. Clearly the density and temperature histories are strongly affected by the cold end wall, however the pressure history is very similar to that of the ideal end wall. Note however that the pressure is upwards of 1200 times the initial value although the equilibrium pressure should be about 950 times the initial value. As discussed above, the hot particles from behind the reflected shock are not thermalizing with the particles emergent from the cold end wall. The end wall naturally is more sensitive to this error because the measured flux consists primarily of those hot particles directed towards the wall.

Perhaps the most important result from the isothermal end wall calculation for the shock reflection problem is the realization of the limits of the particle simulation method. Clearly the conditions in the boundary layer next to the end wall are well into the continuum regime where a particle simulation is hard pressed to provide meaningful results. The shock reflection problem is an extreme example of a more general difficulty which exists with the simulation of any hypersonic rarefied flow that develops a cold boundary layer. The cooling of the gas through the

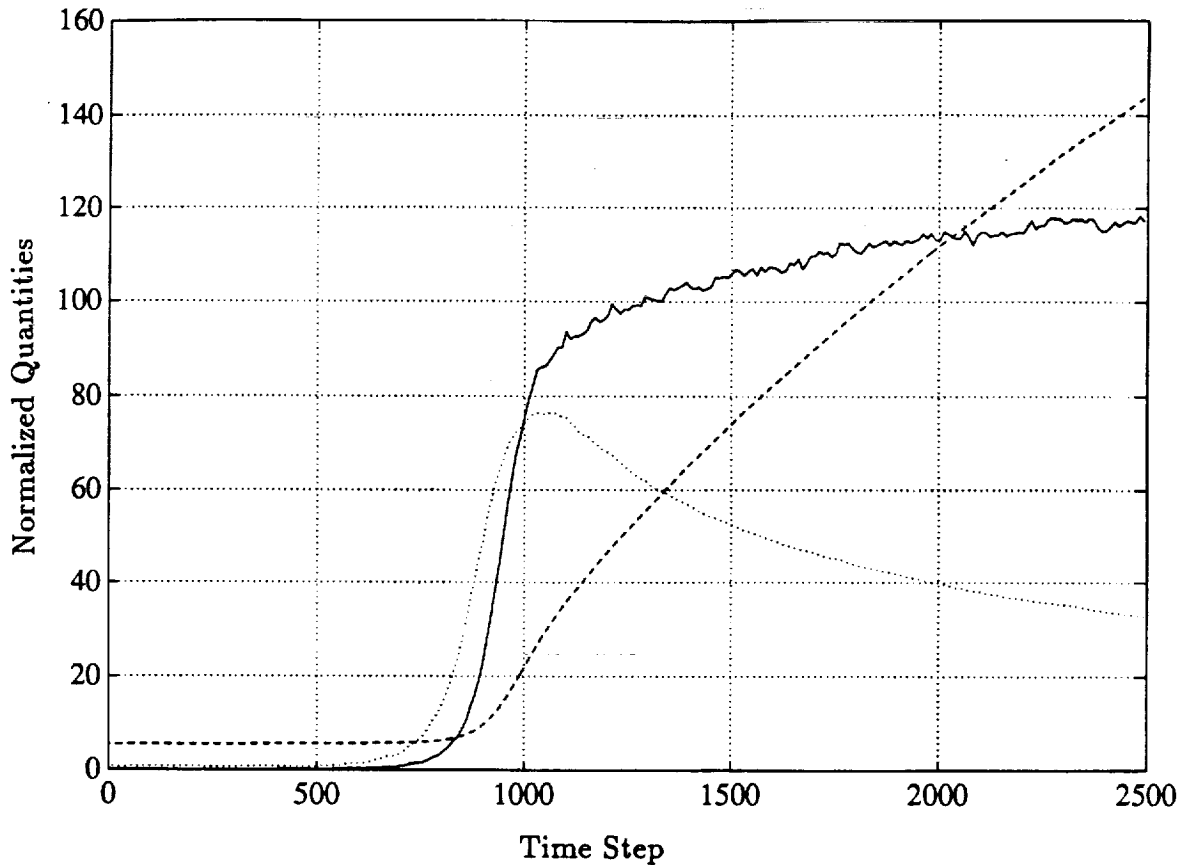


Figure 7.9 Density, temperature, and momentum flux histories for a cold, isothermal end wall. The test gas is carbon monoxide. Density is normalized by twice the initial value, temperature is normalized by one tenth the initial value, and momentum flux is normalized by 10 times the initial value. — momentum flux; - - -  $\rho$ ;  $\dots T_{tr}$ .

boundary layer may raise the density to values far greater than can result from shock compression thus requiring a larger investment of particles for the boundary layer than for the stagnation region of the flow. It would be more profitable to employ a less computationally intensive method for modelling the velocity distribution in the boundary layer such that more particles may be used elsewhere in the flow. Because of its one dimensional nature and well defined boundary layer, the shock reflection problem would be an ideal one for the development of such a hybrid scheme.

## 7.4 Double Ellipse in Hypersonic Flow

The previous sections have dealt with simple geometries and focused on very specific gas dynamic problems in order to demonstrate the capability of the method for properly simulating real gas flow phenomena. In this section the method is applied to a more complex geometry both to demonstrate the capability of simulating flows over general bodies and to compare the current implementation with the implementation of this method on the Cray 2.

The geometry of interest in this set of results is a double ellipse body similar to a proposed profile for the nose and cowl of the Hermes Space Shuttle. The geometry for this simulation was created by Feiereisen using the body generation scheme described in Feiereisen and McDonald (1989). The geometry in three dimensions consists of two intersecting ellipsoids extended by a truncated cylinder with a back plane. The two dimensional profile of this geometry was used for the simulation. The computational domain extends 180 cells in the  $x$  direction (the streamwise direction) and 250 cells in the  $y$  direction for a total of 45000 cells. The body is 90 cells in length and 50 cells in width at the back plate and is at a 30 degree angle of attack.

The free stream gas temperature for the calculation was  $13.5^\circ K$  and the body was at a fixed temperature of  $620^\circ K$ . Complete accommodation was assumed. The free stream mean free path was 0.105 mm and the free stream Mach number was 25. The Knudsen number, based on a body length of 0.076 m, was 0.0138 and the corresponding Reynolds number was 2700. A hard sphere interaction potential was assumed and no vibrational energy exchange was allowed. This was done in order to allow comparison with the Cray 2 calculation (Feiereisen (1990)) which employed this simplified model. The simulation was started with a total  $2.6 \times 10^5$  particles including the reservoir, and run for 1200 steps to clear the transient. This number was then raised to the maximum of  $2.1 \times 10^6$  through three clonings extended over a period of 100 steps to ensure any statistical dependencies from cloning were lost. The solution was then created by time averaging over 800 steps.

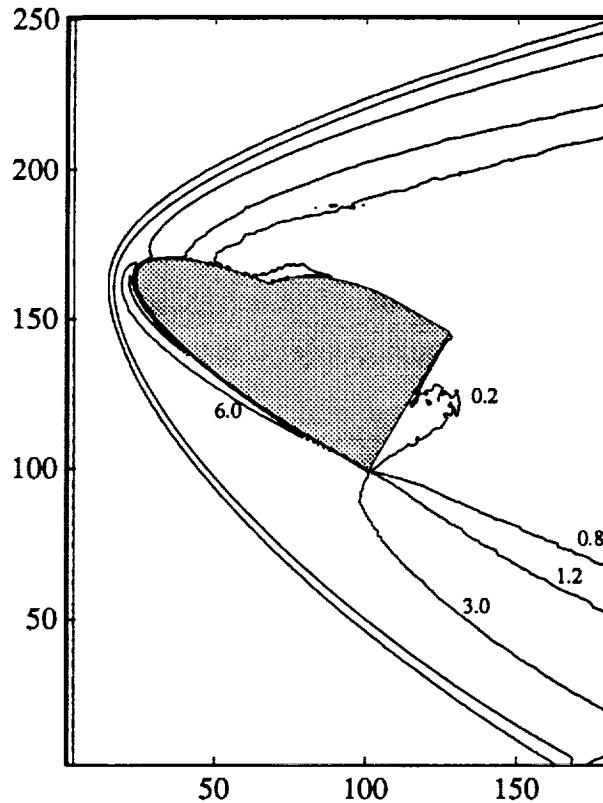
Figure 7.10 presents the density contours for the flow field. Values are



normalized by the free stream conditions. The relatively low Knudsen number of the flow puts it near the continuum regime hence the bow shock is very sharp and thin. Contours are mapped for normalized densities of 0.2, 0.8, 1.2, 3.0, 6.0, and 9.0. This last value is reached only near the surface of the body where the gas has been cooled by the isothermal wall. The effect of this boundary is more clearly evident in figure 7.11 which presents the density along the stagnation streamline. The o's in this figure correspond to the values calculated with the current code and the x's correspond to the values calculated by Feiereisen with the Cray 2 code. The stagnation point is at the right hand side of the figure. The stagnation density is 14 times the free stream density, and the boundary layer extends for about 3 cells from the surface. There is almost a merging of the shock and boundary layers. The agreement with Feiereisen's results is remarkably good.

Figure 7.12 presents the temperature contours for the flow field. Again values have been normalized by the free stream temperature and contours are mapped for normalized temperatures of 1.2, 20, 40, 60, 80, and 100. The effect of the second ellipse (the "cowl") is clearly evident in the flow field over the body. There is almost a second shock formed and there is a temperature rise due to the compressive effect there. The density field does not display this compression quite as clearly, largely because the flow is sufficiently rarefied in this region to wash out much of this effect. The temperature, being a higher order moment of the solution, is a much more responsive variable to observe.

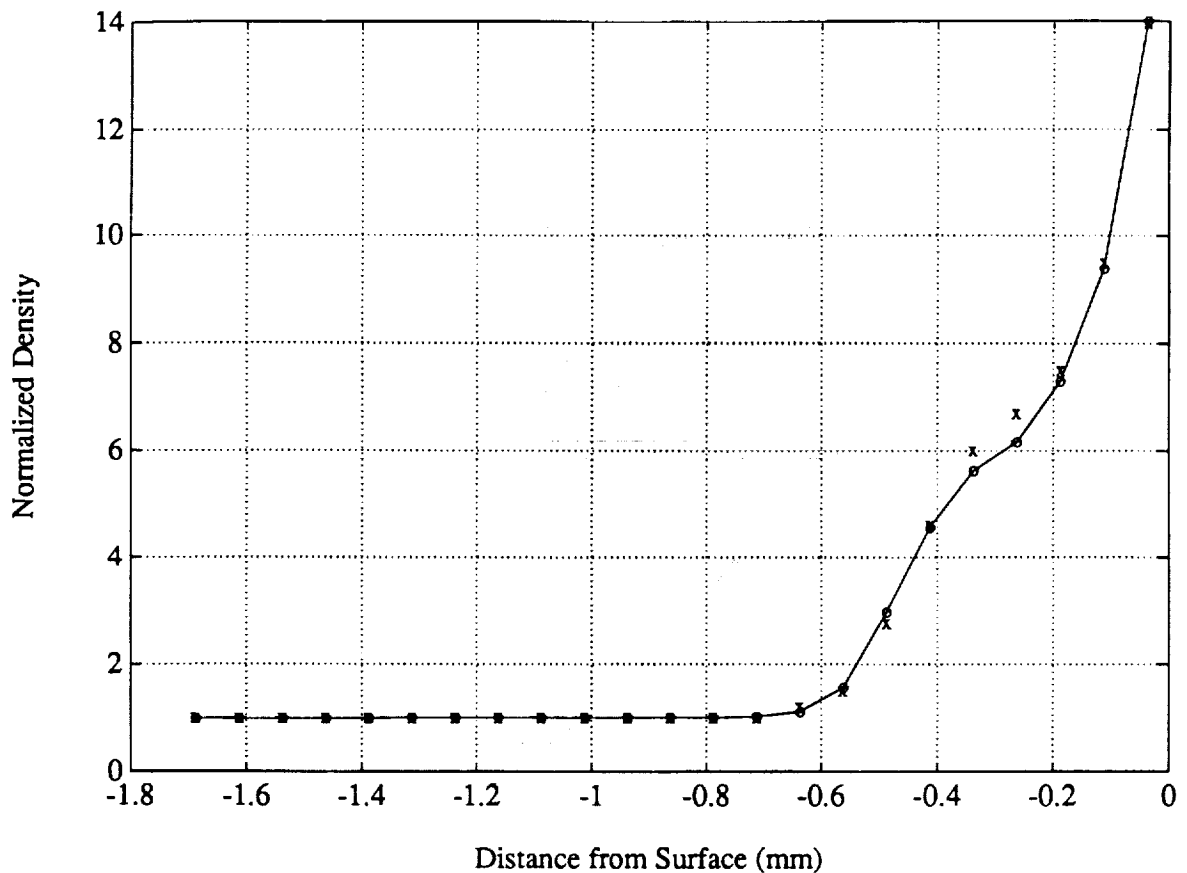
The cooling due to the body is also clearly evident in the figure. After being shocked to a high temperature the gas rapidly cools through a thermal boundary layer near the body. Figure 7.13 presents the temperature along the stagnation streamline. The peak temperature of  $1850^{\circ}K$  (140 times the free stream temperature) is reached about 5 mm from the surface of the body. Note that this is about half way through the bow shock defined by the density and this peak temperature corresponds to the characteristic translational temperature overshoot in a shock wave. The stagnation region in the flow is too small to compressively heat the gas behind the shock and the rapid drop in temperature following the peak is due both to the relaxation of the translational temperature after its overshoot



**Figure 7.10** Density contours in the Mach 25 flow over a double ellipse geometry. Contours are mapped for normalized densities of 0.2, 1.2, 3.0, 6.0, and 9.0. Values are normalized by the free stream conditions.

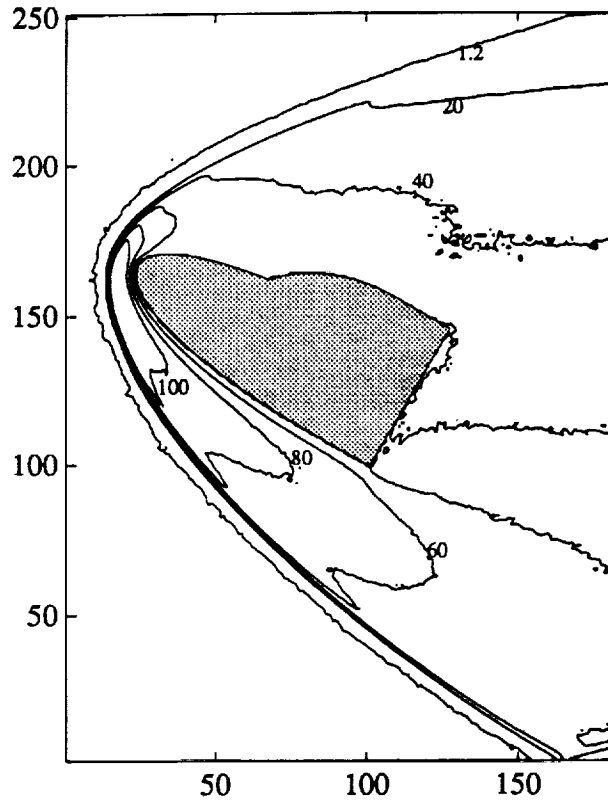
within the shock and to the cooling effect of the body. Note that Feiereisen's solution (the x's in figure 7.13) show a lower peak temperature corresponding to less overshoot in the translational temperature. Feiereisen's calculation employed the degree of freedom mixing collision algorithm which has an effective rotational collision number of about 2 whereas the current calculation employed the direction cosine decomposition collision algorithm with a rotational collision number of 5. This explains the difference in the computed temperature profiles through the bow shock. The agreement through the boundary layer is excellent.

Figure 7.14a presents the velocity field for this flow. The boundary layer is clearly evident as is the turning of the flow about the end of the body. The meeting



**Figure 7.11** Density along the stagnation streamline. Values are normalized by the free stream conditions. Solid line with 'o' symbols are used for the current results, 'x' symbols are used for the calculation by Feiereisen (1990).

of the flow over the body with that under the body normally would lead to a wake shock, however the extremely low densities in the wake for this flow preclude any evidence of such a shock. It is of interest to investigate more closely the “cusp” region where the nose and the cowl meet. Figure 7.14b is an expanded view of this region. The theory predicts a region of recirculation for such a geometry when the adverse pressure gradient from the cowl is sufficiently strong to force the boundary layer to separate. There is no evidence of separation in this figure, although there definitely is a growth in the boundary layer thickness after the cusp and the region right at the cusp is virtually stagnant. It is interesting to note from this figure that there is a small slip velocity at the surface. This is predicted by kinetic theory (cf.



**Figure 7.12** Temperature contours for Mach 25 flow over a double ellipse geometry. Contours are mapped for normalised temperatures of 1.2, 20, 40, 60, 80, and 100. Values are normalized by the free stream conditions.

Patterson (1956)) when the mean free path is of the same order as the boundary layer thickness. This slip velocity is due to the flux of particles incident on the surface. On average, molecules strike the surface with the momentum existing at one mean free path from the surface. If the mean free path is of the same order as the scale to which one is resolving the solution, then one expects to see this momentum in the flow. Therefore, although the diffuse reflection at the surface ensures that particles leaving the surface have no net momentum, the flux of particles onto the surface does have momentum which gives rise to a net velocity for the gas at the surface.

Finally, for completeness, figure 7.15 presents the velocity profile in the

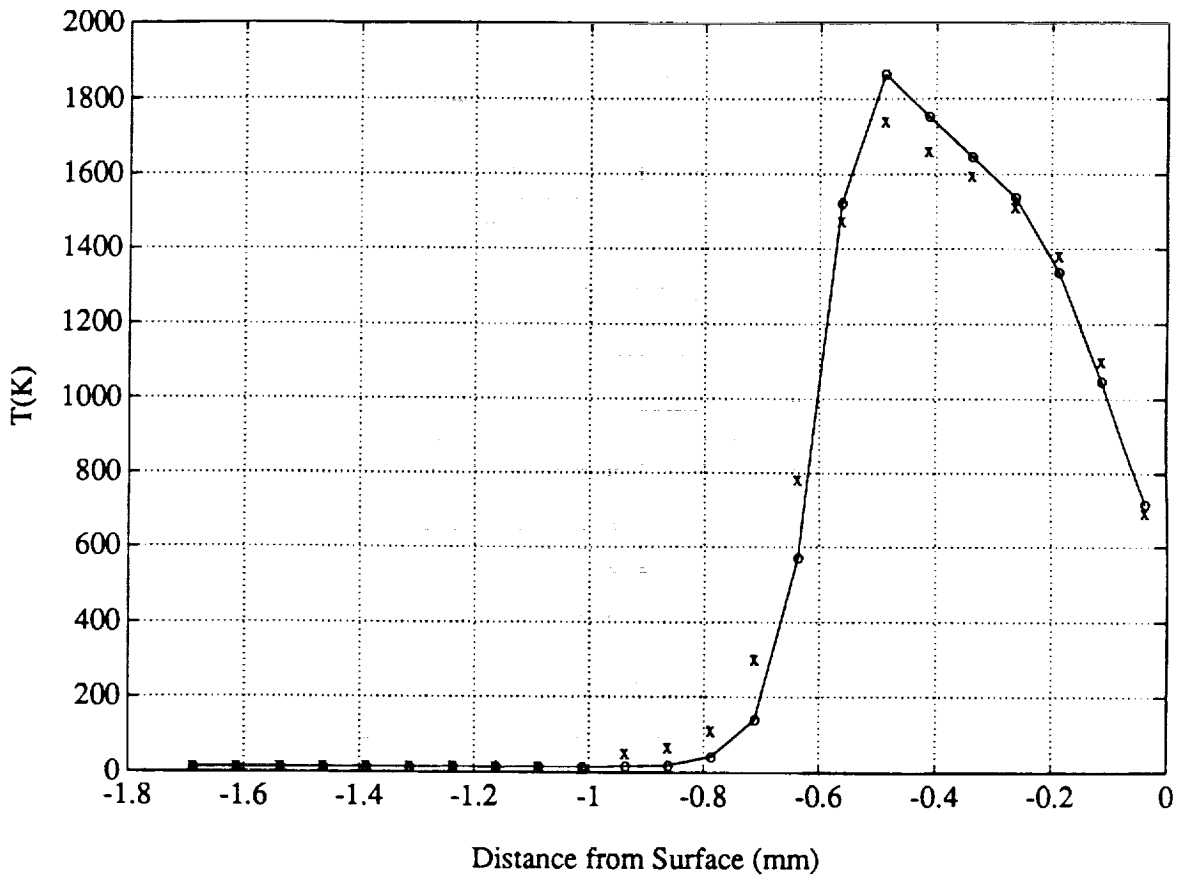
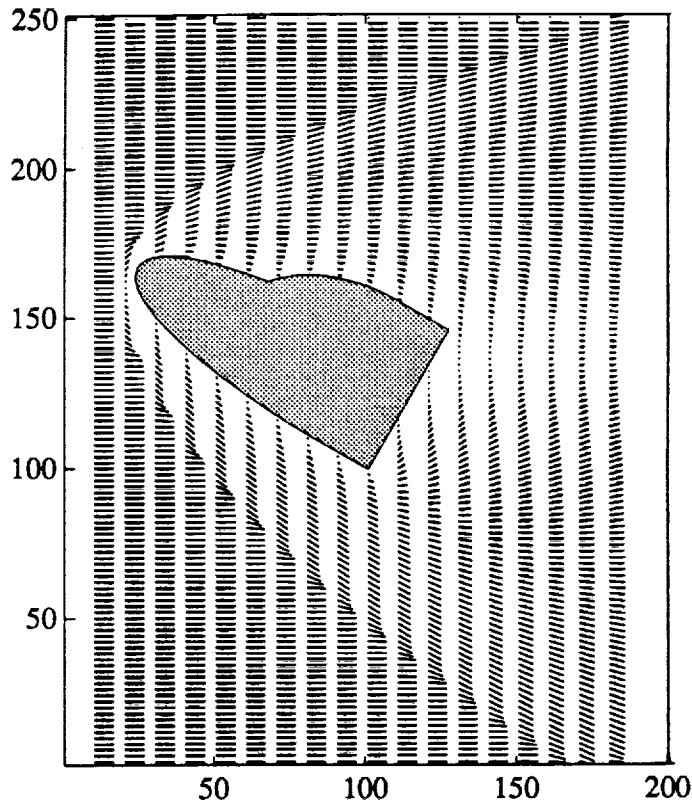


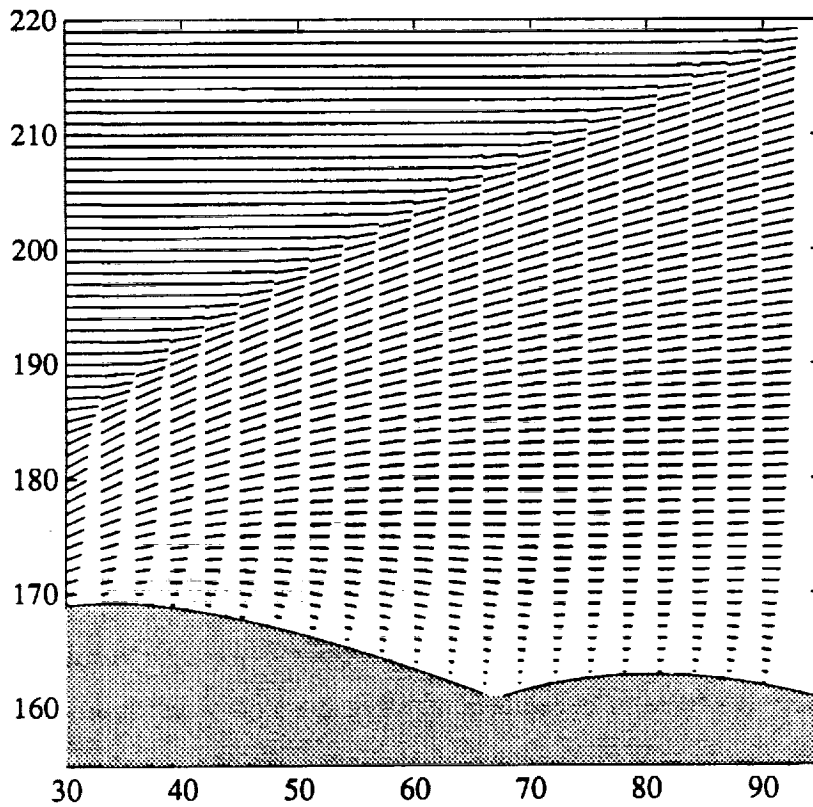
Figure 7.13 Temperature along the stagnation streamline. Values are given in degrees Kelvin. Solid line with 'o' symbols is used for the current results, 'x' symbols are used for the calculations by Feiereisen (1990).

stagnation streamline. Again the current results agree quite closely with those from the Cray 2 implementation. The slight differences which exist are probably attributable to the different collision algorithms employed. It should be noted that these Cray 2 calculations are somewhat of an anachronism and the latest implementation uses the direction cosine decomposition collision algorithm.

In conclusion, the implementation of the Stanford particle simulation method on the Connection Machine is capable of solving the flow field about a general two dimensional geometry to a high degree of accuracy. That the solution for the double ellipse geometry compares favorably with that calculated by the implementation of this method on the Cray 2 indicates there is consistency between the two



(a)



(b)

Figure 7.14 Velocity field for Mach 25 flow over a double ellipse geometry. a) The complete flow field. b) The flow field in the vicinity of the cusp where the two ellipses meet.

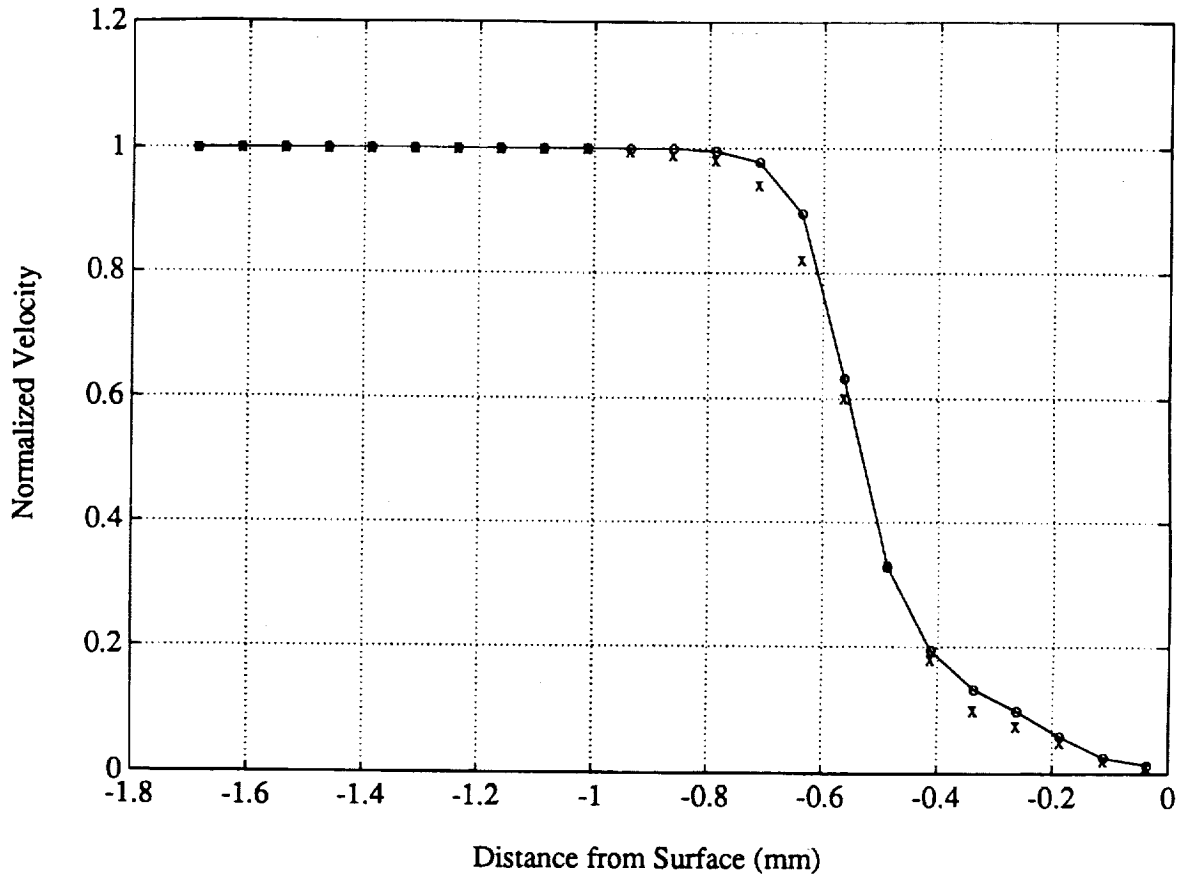


Figure 7.15 Velocity along the stagnation streamline. Values are normalized by the free stream conditions. Solid line with 'o' symbols is used for the current results, 'x' symbols are used for the calculations by Feiereisen (1990).

implementations. The results presented in the two previous sections serve not only to validate the current implementation but also the method in general. The next section will consider in some detail the performance of the Connection Machine with this method.

## 7.5 Performance

In Chapter 1 of this thesis the motivation for the research was described through the question: "What price for parallelism?" The answer to this question is given in this section. The first step towards answering this question is to consider the

distribution of computational time within the algorithm. This distribution is as follows:

- 1) move — 14%
- 2) rank — 40%
- 3) re-order — 26%
- 4) collisions — 7%
- 5) sampling — 13%

Within this breakdown, the rank and re-order represent two communications intensive events which have no equivalent in the vectorizable algorithm yet account for 66% of the computational time in the data parallel algorithm. This is time being spent on events which are necessitated by the parallel architecture and are not directly related to the computation required in a particle simulation. Therefore one can say quantitatively that the price for parallelism amounts to two thirds of the cost of the calculation.

It should be emphasized that this fraction remains constant when the calculation is scaled down to 16k or 8k physical processors. Therefore it is reasonable to expect that in scaling up to a greater number of processors this fraction will continue to remain constant. The property of scalability is extremely important in evaluating parallel architectures. In many of the MIMD architectures one often finds a less than linear speed up with increasing number of processors because the fraction of time spent on communication increases in going to more processors. That the cost of communication in the particle simulation is scaling linearly on the Connection Machine is a good indication that on future machines with more processors the performance of the simulation will improve linearly.

It is of interest also to see how the performance of the simulation scales with the number of virtual processors. Figure 7.16 presents the computational time as a function of virtual processor (VP) ratio. The values are normalized by the time at a VP ratio of 8, the lowest for which measurements were reasonable with the double ellipse problem of the previous section. Since the VP ratio is directly proportional to the number of particles in the simulation, one would expect the time to increase linearly with the VP ratio. The dashed line in the figure is an extrapolation of the



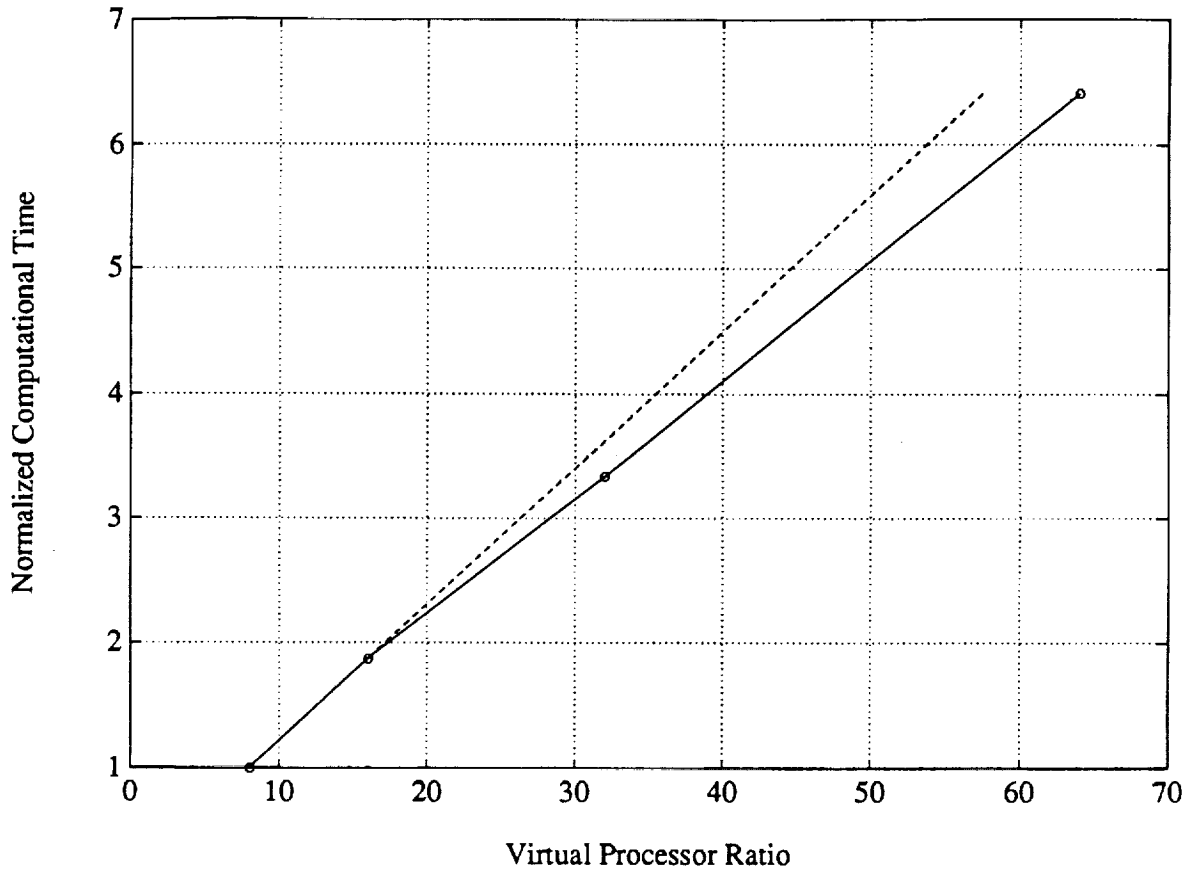


**Figure 7.16** Performance of the simulation as a function of virtual processor (VP) ratio. The dashed line gives the linear extrapolation of performance at VP ratios of 8 and 16. The actual performance is better than predicted by linear extrapolation because of the inefficiencies associated with lower VP ratios.

computational time based on the slope between the points for a VP ratio of 8 and a VP ratio of 16. This dashed line emphasizes that most efficient use of the machine is made at the higher VP ratios for the reasons outlined in Chapter 2.

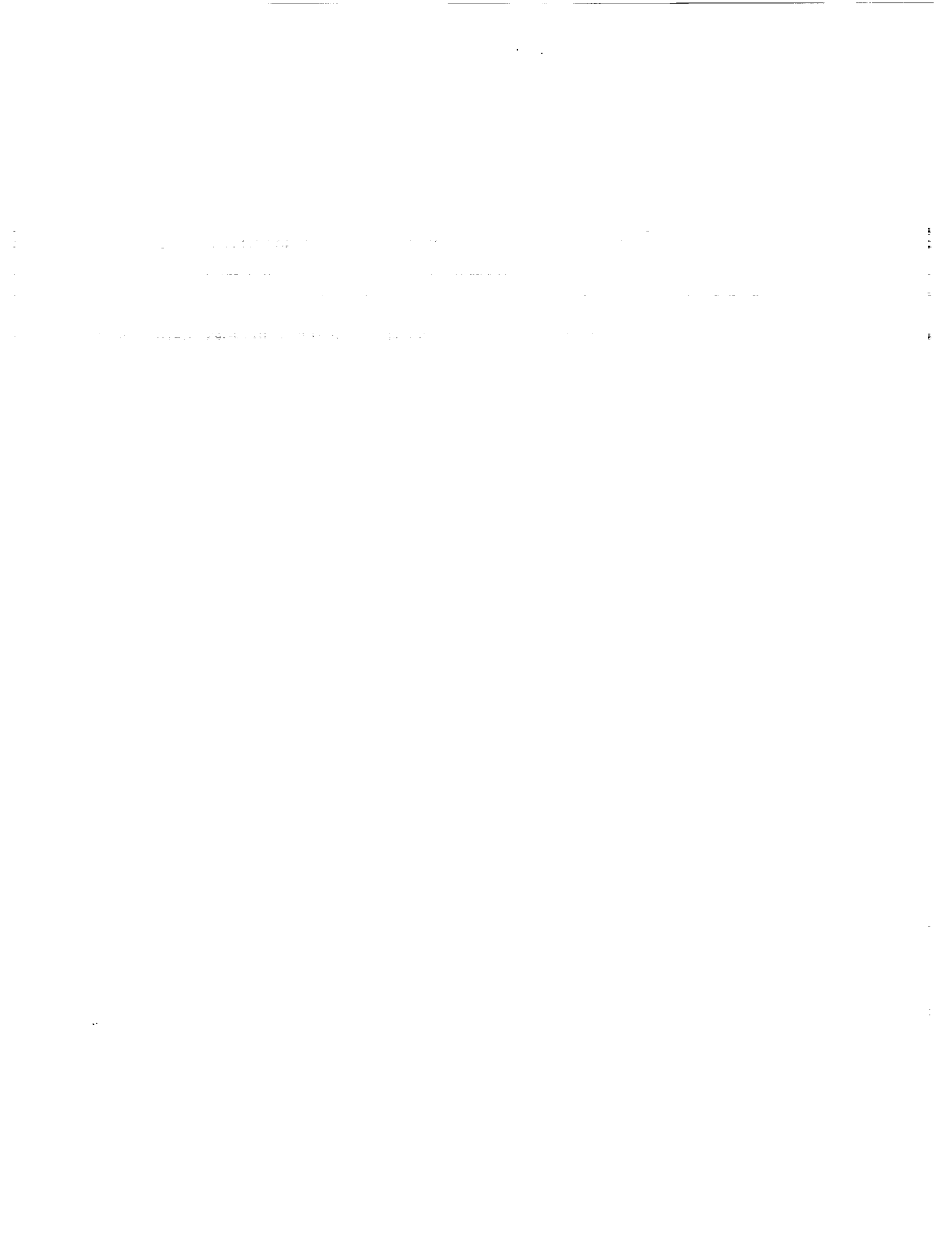
In order to determine if the 66% paid for parallelism is too steep a price, it is necessary to benchmark the performance of the simulation on the Connection Machine. The code used to generate the results of the previous section was written fully in C/Paris and run on the 32k processor Connection Machine Model 2 at the NASA Ames Research Center. The front end used to run this simulation was a DEC Vax 8800. The simulation employed 2048k virtual processors with a total of 256 MB of memory to simulate up to  $2.0 \times 10^6$  particles in the flow and a further  $10^5$

particles in the reservoir. To compare the performance of this implementation with that of a similar implementation on a different supercomputer it is useful to define a normalized time for the calculation given as the average time to advance one particle through one time step. Excluding the reservoir particles, for the calculation of the double ellipse that value is  $2.0\mu\text{sec}/\text{particle}/\text{timestep}$ . The same calculation fully vectorized on a single processor of the NAS Cray 2 took  $1.7\mu\text{sec}/\text{particle}/\text{timestep}$ . It should be noted that the Cray 2 calculation was three dimensional even though the double ellipse geometry is two dimensional. Nonetheless, it is apparent from this result that the 66% price of parallelism is being paid off through the great computational speed of the Connection Machine.

The final evaluation which needs to be made in judging the Connection Machine concerns the human effort required to program it. The discussion in section 2.1 on data parallel versus vectorizable algorithms is a good basis for this evaluation. Because the requirements for a data parallel algorithm are stricter than for a vectorizable algorithm, programming the Connection Machine is inherently more difficult than programming a vector computer. The current situation is probably worse than is implied by this statement because data parallel programming is relatively new and many of the algorithms which have been fully explored in vectorizable form have yet to be considered for data parallel form. Therefore one can expect that as a tradition of data parallel programming evolves there will develop a greater "intuition" for data parallel algorithms and many of the tasks which now are new and require some effort to conceptualize in data parallel form will have become routine and part of the data parallel diction.

Beyond the straight algorithmic considerations there is the question of how detailed a knowledge of the machine is required for efficient programming. From the discussion in section 2.4 and most of chapters 4 and 5 it should be abundantly evident that the promise of "general" communication is a myth for the Connection Machine. Although one can classify all communication which makes explicit use of the router as "general", it is incorrect to assume that all such communication comes at the same price. It is very difficult to make educated guesses at the particular cost for any communications event in a proposed algorithm; for the most part

all variations in an algorithm have to be implemented before an optimum can be selected. There is no well defined hierarchy of memory as exists in conventional computers because memory access times through the communications network are dependent on a large number of variables. Through experience it is possible to gain some intuition for the performance of communications but this certainly requires an effort which is unnecessary in programming conventional or even vector computers. Again part of the problem may be attributed to the infancy of this technology and in the future much of this effort may be unnecessary as the technology matures and languages and compilers for this architecture improve.



## Chapter 8

# Multiple Species and Chemistry

The work presented thus far has resulted in a particle simulation capable of simulating a single specie diatomic gas in hypersonic flow with no chemical reactions. This is the foundation upon which algorithms for simulating multiple species with chemical reactions can be built. This chapter outlines how these algorithms may best be implemented on the Connection Machine and identifies possible problems one may encounter in carrying out such work. It should be emphasized that none of the algorithms described in this chapter have been implemented on the Connection Machine and the purpose of this chapter is only to serve as a guide in this area.

### 8.1 Reaction Fundamentals

Atmospheric air subjected to hypersonic conditions can be modelled as a five species set composed of  $O_2$ ,  $N_2$ ,  $NO$ ,  $O$ , and  $N$ . There are 15 dissociation/recombination reactions and 4 exchange reactions associated with this set (Moss and Bird (1985)). In addition there are 15 allowable collision classes where a collision class is defined by any combination of two species. The collision selection rule for multiple species must account for the different number densities and the different sample sizes for each collision class within a given cell. Once a collision has

been decided upon the colliding pair must be tested to see if it will undergo reaction. Each reaction is characterized macroscopically with a reaction rate coefficient,  $k_f(T)$ , and a species concentration coefficient,  $K(T)$ , as fit by experiment. In a particle simulation, a distinct selection rule must be implemented for each reaction in order to reproduce the macroscopic reaction rate temperature-dependence. Pairs of particles which do not react undergo a regular thermal collision.

Dissociation reactions are characterized by the general equation



where  $AB$  is a diatomic molecule,  $A$  and  $B$  are monatomic particles, and  $X$  is a partner of any type. Only collisions with collision energy exceeding the threshold dissociation energy,  $E_d$ , are allowed to dissociate. Dissociation reactions are endothermic and the energy removed from the reactants would, in a real collision, be redistributed in the electron configuration of the products. In a particle simulation the electronic state of a particle is not usually modelled since it does not contribute energy in a collision. Consequently the dissociation energy must be removed from the system. Note, however, that the reverse reaction is exothermic therefore, at equilibrium, this energy is returned to the system at the same rate it is removed.

Exchange reactions are characterized by the general equation



where  $C$  is a monatomic particle. This reaction also requires the splitting of a molecule and therefore can only proceed if the collision energy exceeds the dissociation energy. However the reaction also results in the creation of a new diatomic molecule which allows the release of energy  $E_{d,ac}$ . That is, the dissociation energy for the reverse reaction must be returned to the system. Therefore the reaction requires energy  $\Delta E = E_d - E_{d,ac}$  to be removed from the reactants and redistributed as potential energy in the products.

Recombination is the reverse of dissociation; it is inherently a three-body process but can be modelled by two successive binary collisions. The first collision

requires two colliding atoms to form an unstable union characterized as a mutually orbiting pair. Therefore,



where  $(AB)$  is the orbital pair formed from atoms  $A$  and  $B$ . Orbiting pairs have a limited lifetime dependent upon the collision energy. If an orbital pair undergoes a collision within its lifetime it may then stabilize into a molecule thus completing the recombination process. This process is modelled by the equation



The dissociation energy,  $E_d$ , removed from the reactants in (8.1) must now be returned to the products of (8.4). If no stabilizing collision occurs during an orbital pair's lifetime then the pair is split into its free atoms.

## 8.2 Implementing Multiple Species

The first step towards chemical modelling in the simulation is to introduce the capability for simulating multiple species. The different species which may be encountered in simulating the flow of a gas may be broadly classified into three categories: monatomic particles, diatomic molecules, and orbital pairs. The last of these three is only encountered when modelling recombination reactions and will be discussed more fully in the section on chemistry. This section concerns itself only with the implementation of multiple species without chemical reactions.

The introduction of multiple species necessitates the specification of additional information concerning the different species. The actual number of species which are usually modelled is relatively small; hypersonic flows involving air are commonly modelled with a total of 5 different species, although the inclusion of recombination reactions requires an additional three species for the orbital pairs. This information is best stored in the front end computer, and the Connection Machine processors

representing the particles need only store a pointer to the appropriate table entry. The broadcast of information from the front end to the individual processors is very fast in comparison to either NEWS or general router communication. For the processors to get the species information from the front end it is necessary only to identify the processors representing particles of each species and copy the appropriate front end information into the processors. Information pertaining to a collision class may be stored in the same fashion. For the 8 species model there are 36 possible collision classes. This number is still small enough to make broadcasting from the front end a viable communications alternative for information which is strictly dependent only on the collision class. A problem arises when the necessary information is dependent not only on the collision class but also on the cell in the simulation, as with the determination of the collision class sample size discussed below.

If there is to be no chemical reaction the only additional information necessary for the calculation is the species mass and the collision cross section. The cross section is necessary in evaluating the probability of selection,  $P_s$ , for the candidate pairs. With multiple species, the probability of selection for collision of a particular candidate pair of particles, the first of specie  $a$  and the second of specie  $b$ , is given by (McDonald 1990)

$$P_s = \frac{n_a n_b}{(1 + \delta_{ab}) S_{ab}} \beta d_{ab}^2 g^{-\frac{4}{\alpha_{ab}}} g \Delta t \quad (8.5)$$

where  $n_a$  and  $n_b$  are the number densities for specie  $a$  and specie  $b$  respectively,  $\delta_{ab}$  is the Kronecker delta,  $S_{ab}$  is the sample size of candidate pairs in class  $ab$ ,  $\beta d_{ab}^2$  is the hard sphere collision cross section,  $g$  is the relative speed,  $\alpha_{ab}$  is the power defining the power-law interaction potential, and  $\Delta t$  is the time step.

The greatest difficulty one encounters when evaluating this expression is in determining the values of  $n_a$ ,  $n_b$  and  $S_{ab}$ . For the single specie case, the sample size is always  $n/2$  and determining  $n$  requires two scan instructions, that is, a `CM_enumerate` followed by a `CM_scan_with_copy`. The most straightforward approach for multiple species is to extend this directly, then for an 8 species model



one would require 16 scan instructions to determine the values of  $n_a$  and  $n_b$  and an additional 70 scan instructions to determine the value of  $S_{ab}$ . Note that these 70 scans would be across candidate pairs and could be carried out at half the VP ratio of the particles' VP set by using VP aliasing. Therefore they would be approximately equivalent to 35 scans at the higher VP ratio.

In practice a large fraction of all the collisions will fall into one of five classes. Specifically the three classes involving  $O_2$  and  $N_2$  are most common in the free stream and the two additional classes involving  $O$  and  $N_2$  are most common after the shock where most of the  $O_2$  molecules have dissociated. Therefore the 70 scan instructions necessary for determining  $S_{ab}$  may not be overly expensive since many of the collision classes are sparsely populated and hardware contention in the communications would be reduced. This sparsity may be used to some advantage in reducing the communications by employing a different algorithm for determining the sample sizes in the less common collision classes. In such an approach one first determines the sample sizes associated with the five most common collision classes by using the necessary scan instructions. Then to get the sample sizes for the remaining classes one employs a multi-grid algorithm similar to that described in Chapter 4. One creates a multi-grid with elements for each cell in the simulation and with a level for each remaining collision class. Therefore each remaining collision class is mapped to a level of the multi-grid and each cell in the simulation is mapped to an element in a level of the multi-grid. One processor from each candidate collision pair then uses the `CM_send_with_add` instruction to send a value of 1 to the appropriate grid element in its level. This results in each element in a particular level of the multi-grid storing the sample size for the collision class associated with that level. The same processor in the candidate pair then uses the `CM_get` instruction to get this value from the multi-grid. This algorithm takes advantage of the fact that the performance of general communication can improve dramatically with a reduction in router contention. Therefore this approach is suitable if it can be determined that over the whole flow field certain collision classes are greatly dominant leaving the remaining collision classes relatively sparse.

With the various factors comprising (8.5) made available, the probability of

selection is evaluated and the decision to collide a candidate pair is made. If there is no chemical reaction, then the next step is to carry out the appropriate collision mechanics. The introduction of three classes of particles necessitates the specification of three types of collision, specifically monatomic-monatomic, monatomic-diatomic, and diatomic-diatomic. Note that orbital pairs do not undergo collision as such and must either split into separate atoms or stabilize into diatomic molecules before undergoing collision. The mechanics of each of these three types of collisions are identical to those already implemented. The diatomic-diatomic collision mechanics are covered in Chapter 3; the monatomic-monatomic and the monatomic-diatomic collision mechanics correspond to the diatomic-diatomic collision mechanics with no exchange of internal energy. Therefore the introduction of multiple species does not require the specification of new collision mechanics; the collision mechanics already specified for the single specie diatomic particle simulation can be employed with only the introduction of the appropriate switch for the different particle classes.

### 8.3 Implementing Chemical Reactions

The addition of chemical reactions amongst the multiple species introduces no new communications problems. Once the decision to collide a pair has been made, the information necessary to decide on a reaction is strictly dependent on the species involved in the collision. This information can be stored in the front end and accessed very efficiently as described in the previous section. This is one of the few situations in the particle simulation algorithm where the amount of arithmetic computation is likely to exceed the communications. The probabilities which must be computed for deciding on a reaction are given by complicated expressions involving several transcendental functions potentially making this an ideal situation for the Connection Machine since it allows its floating point performance to be put to full use.

#### 8.3.1 Reaction Mechanics

The three types of reactions, dissociation, exchange, and recombination, were

described in the first section of this chapter. Figure (8.1) presents a flow chart for the collision process when these reactions are included (Haas (1990)). Note that recombination is modelled by a two step process therefore there are two branches in the flow chart for recombination. The mechanics associated with reactions are carried out only after a candidate pair has been accepted for collision. The selection rule for accepting candidate pairs has to be modified as described in the previous section to allow for multiple species.

Reaction types are identified on the basis of the participating particles. Dissociation reactions are allowed with all collisions of two diatomic particles or with half the collisions involving a diatomic and a monatomic particle. The other half of the collisions involving a diatomic and a monatomic particle may lead to exchange reactions. Collisions involving an orbital pair may lead to recombination reactions and collisions involving two monatomic particles always lead to the formation of an orbital pair, the first step in a recombination reaction. The calculation associated with each of these reactions must be carried out independently.

Dissociation reactions are allowed to occur with probability  $P_d$  given by (Haas (1990))

$$P_d = P_0 \left(1 - \frac{1}{\epsilon}\right) P_1 (\epsilon - 1) P_2 \quad (8.6)$$

where  $\epsilon$  is the ratio of the collision energy to the dissociation energy, and  $P_0$ ,  $P_1$  and  $P_2$  are constants dependent on the species. The collision energy must be known in all collisions and is calculated for all colliding pairs. The reaction constants are stored in the front end and broadcast to the processors. This probability is evaluated for all collisions which are allowed to lead to the dissociation of a colliding particle. The dissociation of a particle requires the creation of a new particle and the redistribution of the post-reaction energy. The creation and destruction of particles deserves special attention and the discussion of these processes is given in the following subsection.

The probability for the occurrence of an exchange reaction is of the same form as equation (8.6). Exchange reactions neither create nor destroy particles; the outcome

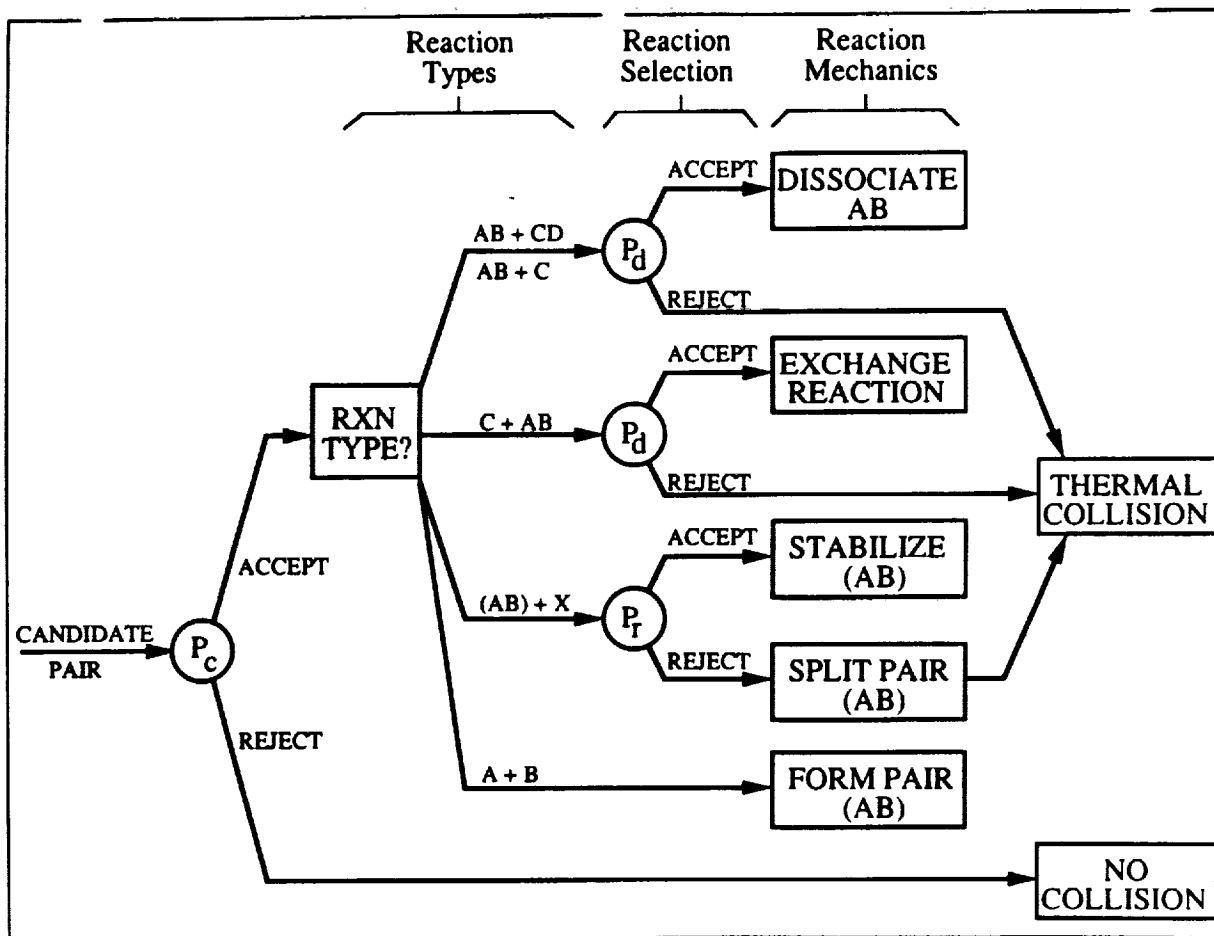


Figure 8.1 Flow chart for the collision process with the inclusion of chemical reactions. Four distinct reaction types are allowed based on the classes of particles participating in the collision. (Haas (1990))

is strictly a redistribution of energy and alteration of species. Exchange reactions are considered for half the collisions involving a monatomic and a diatomic particle thus leaving the other half of these types of collision to be considered for dissociative reactions. The split is made arbitrarily on the basis of the class of the first particle in the pair. If this particle is diatomic then the pair is considered for a dissociation reaction whereas if this particle is monatomic then the collision is considered for an exchange reaction.

The probability  $P_r$  for the occurrence of a recombination reaction is given by (Haas (1990))

$$P_r = P_3 \epsilon_{int,0}^{P_4} \epsilon_{int,1}^{P_5} \quad (8.7)$$

where  $\epsilon_{int,0}$  and  $\epsilon_{int,1}$  are the internal energies for the orbital pair and the collision partner respectively, and  $P_3, P_4$  and  $P_5$  are constants dependent on the species. The probability given by equation (8.7) is evaluated for all collisions which involve an orbital pair. If the partner is monatomic then the probability of reaction is based only on the internal energy of the orbital pair, in other words  $\epsilon_{int,1}$  is set to unity. If a collision leads to recombination then the orbital pair involved in the collision is stabilized to its diatomic equivalent. If recombination does not occur then the orbital pair is split into two monatomic particles of the species defining the pair. As with dissociation reactions, this requires the creation of a new particle. For reasons of efficiency it is best to create all new particles at the same time, therefore new particles resulting from split orbital pairs are created at the same time as new particles resulting from the dissociation of diatomic particles.

Any collisions involving two monatomic particles always lead to the creation of an orbital pair and the corresponding destruction of a particle. The creation of an orbital pair is the first step in a recombination reaction therefore it is not, strictly speaking, a fourth type of reaction. However, for the modelling of chemistry in a particle simulation it is convenient to view this process as a distinct reaction since it must be carried out separately from the other three processes.

### 8.3.2 Creation and Destruction of Particles

New particles are created from dissociation reactions and from failed recombination reactions. Particles for this purpose are available from the reservoir. Once all the reactions leading to the creation of a new particle have been identified, they are enumerated and the enumeration is used as an index into the reservoir. The appropriate state information is then sent to these reservoir particles to change them to their new state.

The creation of particles in this manner leaves the system of particles in a disordered state at the end of the time step. Consequently the merged ordered subsets sorting algorithm must be revised to allow for this situation. Since the new particles are, amongst themselves, in an ordered state, the sorting algorithm need be revised only to include the merging of an additional ordered system.

The destruction of particles involves the same process as the removal of particles which exit downstream of the simulation. These particles are simply converted to reservoir particles by changing their physical state and setting their cell index to point to the reservoir. Since this process is identical to the removal of exited particles, it proves most efficient to perform the two processes at the same time.

### 8.3.3 Estimated Cost

There are no apparent difficulties in extending the current implementation to include multiple species and chemistry. The greatest foreseeable cost will be in applying equation (8.5) to select pairs for collision. The straightforward application of (8.5) requires the equivalent of 51 scan instructions at the VP ratio of the particles' VP set. Since scans are about an order of magnitude faster than sends, the associated communications cost would be approximately equivalent to 5 send instructions. Therefore the amount of communications will probably be about equivalent to that associated with re-ordering the particle data, which currently takes 26% of the computational time (section 7.5). This, of course, is a very approximate estimate. The cost for the arithmetic computation is equally difficult to estimate but certainly will not exceed the cost of communication. Therefore a very conservative estimate on the total additional cost for simulating multiple species with chemistry is another 50% of the computational time.

# Chapter 9

## Concluding Remarks

### 9.1 Summary

Currently the fluid mechanics community is seeing a resurgence of interest in rarefied gas dynamics, a regime where computational methods often offer the only viable means of solving flow problems of practical interest. The method of direct particle simulation is one of the few methods, suitable to this regime, which provides accurate solutions at reasonable computational cost. Nonetheless, the expense associated with this method is such that solutions to engineering problems almost exclusively require the use of a supercomputer. The Stanford particle simulation (SPS) method has been developed to make the most efficient use of supercomputer architectures thereby allowing broader application of the direct particle simulation method.

It is largely accepted that future improvements in supercomputing performance will be in the direction of increased parallelism, and massively parallel architectures represent the research frontier in this direction. The massively parallel architecture of the Connection Machine has been successfully applied to a wide variety of scientific problems. The purpose of the current work has been to investigate the

suitability of this architecture, and this machine in particular, for the direct particle simulation of rarefied gas dynamic flows.

The work progressed in three stages. The first stage required the development of data parallel algorithms for particle simulation. Some of these algorithms were directly translatable from their vectorizable form, and these are described in Chapter 3. However several of the vectorizable algorithms could not be readily extended to data parallel form. These required new algorithms to be developed, and in particular, the sorting algorithms of Chapter 4 were an outcome of this effort.

The second stage involved optimizing the implemented algorithms to the Connection Machine architecture. This work required an intimate understanding of the communications network and resulted in the development of new communications algorithms. The master/slave algorithm of Chapter 5 was an important result of this effort. A related algorithm also is applied to the sampling of macroscopic flow quantities from the simulation and is described in section 3.4.

The third and final stage of the work required validating the implementation and gauging its performance. A large number of test calculations were performed and Chapter 7 presents the pertinent results. Thermal relaxation histories and the shock wave profiles are standard test calculations used to validate computational methods for rarefied gas dynamics. The reflected shock problem goes significantly further as a validation both of the implementation and the method. The results from that calculation also highlight some of the difficulties and inadequacies associated with direct particle simulation, especially as the continuum limit is approached. As further validation, the flow over a double ellipse was calculated and the results were compared to those from the implementation of the SPS method on the Cray 2. This calculation was also used to gauge the performance of the Connection Machine for direct particle simulation, and this is discussed in some detail in section 7.5.

## 9.2 Conclusions

An important result of this investigation has been a quantitative measure of



the performance of the Connection Machine for direct particle simulation. From this result it has been possible to conclude that the massively parallel architecture of the Connection Machine is quite suitable for this type of calculation. However, there are difficulties in taking full advantage of this architecture because of the lack of a broad based tradition of data parallel programming. An important outcome of this work has been new data parallel algorithms specifically of use for direct particle simulation but which also expand the data parallel diction.

.....

.....

.....

.....

.....

.....

.....

.....

.....

.....

.....

.....

.....

.....

.....

## References

- ALDOUS, D. and DIACONIS, P., *American Mathematical Monthly*, **93**, 333, (1986).
- ALSMEYER, H., *Journal of Fluid Mechanics*, **74**, 497, (1976).
- BAGANOFF, D., *Journal of Fluid Mechanics*, **23**, 209, (1965).
- BAGANOFF, D., *Simulation of Gas Motion by a Collection of Particles*, Proceedings of the IBM ACIS University Conference, Boston, Vol. II, p.304, (1987).
- BAGANOFF, D. and McDONALD, J.D., *A Collision-Selection Rule for a Particle Simulation Method Suited to Vector Computers*, To appear in *Physics of Fluids A*, (July 1990).
- BIRD, G.A., *Physics of Fluids*, **6**, 1518, (1963).
- BIRD, G.A., *Physics of Fluids*, **13**, 1172, (1970).
- BIRD, G.A., *Molecular Gas Dynamics*, Clarendon Press, Oxford, (1976).
- BIRD, G.A., *Monte-Carlo Simulation in an Engineering Context*, Invited paper 221, International Symposium on Rarefied Gas Dynamics, Charlottesville, Va., (1980).
- BIRD, G.A., *Physics of Fluids*, **26**, 3222, (1983).

- BIRD, G.A., *Perception of Numerical Methods in Rarefied Gasdynamics*, Invited paper, 16<sup>th</sup> International Symposium on Rarefied Gas Dynamics, Pasadena, Ca., (1989).
- BORGNAKKE, C. and LARSEN, P.S., *Journal of Computational Physics*, **18**, 405, (1975).
- BOYD, I.D., *Direct Simulation of Rotational and Vibrational Nonequilibrium*, AIAA-89-1880, (1989).
- BOYD, I.D., *Vectorization of a Monte Carlo Scheme*, Submitted to *Journal of Computational Physics*, (1990).
- BURNETT, D., *Proceedings of the London Mathematical Society*, **39**, 382, (1935).
- DAVIS, J., DOMINY, R.G., HARVEY, J.K. and MACROSSAN, M.N., *Journal of Fluid Mechanics*, **135**, 355, (1983).
- FEIEREISEN, W.J. and McDONALD, J.D., *Three Dimensional Discrete Particle Simulation of an AOTV*, AIAA-89-1711, (1989).
- FEIEREISEN, W.J., *An Assessment of "Shuffle Algorithm" Collision Mechanics for Particle Simulation*, 17<sup>th</sup> International Symposium on Rarefied Gas Dynamics, Aachen, Germany, (1990).
- FEIEREISEN, W.J., *The Hypersonic Double Ellipse in Rarefied Flow*, INRIA Workshop on Hypersonic Flows for Reentry Problems, Antibes, France, (1990).
- FISCKO, K. A., *Ph.D. Thesis*, Dept. of Aeronautics and Astronautics, Stanford University, (1989).
- FLYNN, M.J., *IEEE Trans. Computers*, **C-21** 9, 948, (1972).
- GOODMAN, F.O. and WACHMAN, H.Y., *Dynamics of Gas-Surface Scattering*, Academic Press, (1976).
- GUTTMAN, I., WILKS, S.S. and HUNTER, J.S., *Introductory Engineering Statistics*, John Wiley and Sons, Inc., Toronto, (1971).
- HAAS, B.L., *Fundamentals of Chemistry Modelling Applicable to a Vectorized Particle Simulation*, AIAA-90-1749, (1990).

- HANSEN, C.F., *Rate Processes in Gas Phase*, NASA Reference Publication 1090, (1983).
- HANSON, R.K., *AIAA Journal*, **9**, 1811, (1971).
- HILLIS, W.D. and STEELE, G.L., *Communications of the ACM*, **29**, 1170, (1986).
- HINSHELWOOD, C.N., *The Kinetics of Chemical Change*, Clarendon Press, Oxford, (1940).
- HURLBUT, F.C., *Gas/Surface Scatter Models for Satellite Applications*, AIAA Progress in Aeronautics and Astronautics, Vol. 103, pp. 98-119, (1986).
- KNUTH, D.E., *The Art of Computer Programming; Volume 2: Seminumerical Algorithms*, Addison Wesley Publishing Company, (1973).
- LORDI, J.A. and MATES, R.E., *Physics of Fluids*, **13**, 291, (1970).
- LUMPKIN, F.E., *Ph.D. Thesis*, Dept. of Aeronautics and Astronautics, Stanford University, (1990).
- LUMPKIN, F.E., CHAPMAN, D.R. and PARK, C., *A New Rotational Relaxation Model for Use In Hypersonic Computational Fluid Mechanics*, AIAA-89-1737, (1989).
- MCDONALD, J.D. and BAGANOFF, D., *Vectorization of a Particle Simulation Method for Hypersonic Rarefied Flow*, AIAA-88-2735, (1988).
- MCDONALD, J.D., *Ph.D. Thesis*, Dept. of Aeronautics and Astronautics, Stanford University, (1990).
- MELVILLE, W.K., *Journal of Fluid Mechanics*, **51**, 571, (1972).
- MOSS, J.N. and BIRD, G.A., *Direct Simulation of Transitional Flow for Hypersonic Reentry Conditions*, AIAA Progress in Aeronautics and Astronautics, Vol. 96, pp. 113-139, (1985).
- MYERS, D.W. and ADAMS, G.B., *Benchmarking and Performance Analysis of the CM-2*, Proceedings of the Conference on Scientific Applications of the Connection Machine, Moffet Field, Ca., (1988).

- NANBU, K., *Journal of the Physical Society of Japan*, **49**, 2042, (1980).
- PARKER, C., *Physics of Fluids*, **2**, 449, (1959).
- PATTERSON, G.N., *Molecular Flow of Gases*, John Wiley and Sons, Inc., New York, (1956).
- PLOSS, H., *Computing*, **38**, 101, (1987).
- PRYOR, D.V. and BURNS, P.J., *Vectorized Monte Carlo Molecular Aerodynamics Simulation of the Rayleigh Problem*, *Proceedings of Supercomputing '88*, Orlando, pp. 384-391, (1988).
- PULLIN, D.I., *Physics of Fluids*, **21**, 209, (1978).
- THINKING MACHINES CORP., *The Connection Machine System, Paris Release Notes*, Thinking Machines Corp., (1989).
- VINCENTI, W.G. and KRUGER, C.H., *Introduction to Physical Gas Dynamics*, John Wiley and Sons, Inc., New York, (1965).
- WENAAS, E.P., *Journal of Chemical Physics*, **54**, 376, (1971).
- WORONOWICZ, M.S. and McDONALD, J.D., *Application of a Vectorized Particle Simulation in High-Speed Near-Continuum Flow*, AIAA-89-1665, ( 1989).